ISTANBUL TECHNICAL UNIVERSITY ★ GRADUATE SCHOOL

EFFECTS OF SOLAR RADIATION AND NEUTRON, GAMMA MATERIAL INTEREACTION EFFECTS ON THE SOLAR CELLS/MODULES/PANELS

Ph.D. THESIS

İnal Begüm TURNA DEMİREL

Department of Physics Engineering

Physics Engineering Programme

DECEMBER 2021

ISTANBUL TECHNICAL UNIVERSITY ★ GRADUATE SCHOOL

EFFECTS OF SOLAR RADIATION AND NEUTRON, GAMMA MATERIAL INTEREACTION EFFECTS ON THE SOLAR CELLS/MODULES/PANELS

Ph.D. THESIS

İnal Begüm TURNA DEMİREL
(509162103)

Department of Physics Engineering

Physics Engineering Programme

Thesis Advisor: Assoc. Prof. Dr. Zuhal ER

DECEMBER 2021

İSTANBUL TEKNİK ÜNİVERSİTESİ ★ LİSANSÜSTÜ EĞİTİM ENSTİTÜSÜ

GÜNEŞ IŞINIMI VE NÖTRON, GAMA MALZEME ETKİLEŞİMİNİN GÜNEŞ HÜCRELERİ/MODÜLLERİ/ PANELLERİ ÜZERİNDEKİ ETKİLERİ

DOKTORA TEZİ

İnal Begüm TURNA DEMİREL
(509162103)

Fizik Mühendisliği Anabilim Dalı

Fizik Mühendisliği Programı

Tez Danışmanı: Doç. Dr. Zuhal ER

ARALIK 2021

İnal Begüm TURNA DEMİREL, a Ph.D. student of ITU Graduate School student ID 509162103, successfully defended the thesis entitled "EFFECTS OF SOLAR RADIATION AND NEUTRON, GAMMA MATERIAL INTEREACTION EFFECTS ON THE SOLAR CELLS/MODULES/PANELS", which she prepared after fulfilling the requirements specified in the associated legislations, before the jury whose signatures are below.

Thesis Advisor : **Assoc. Prof. Dr. Zuhal ER** ....
İstanbul Technical University

Jury Members : **Prof. Dr. Gönül ERYÜREK** ....
Istanbul Technical University

Prof. Dr. İskender AKKURT ....
Süleyman Demirel University

Prof. Dr. İskender Atilla REYHANCAN ....
Istanbul Technical University

Prof. Dr. Hakan ATEŞ ....
Gazi University

Date of Submission : 10.11.2021
Date of Defense : 17.12.2021

To my family,

FOREWORD

Even though I could not thank enough and find any expression for my gratitude, I would like to express my sincere thanks to my thesis supervisor Assoc. Prof. Dr. Zuhal ER for her endless support, mentoring and guidance, sharing her knowledge, experinece and vision with me and taught me to learn, and also giving opportunity to the scientific research.

I would like to express my grateful thanks to Prof. Dr. Gönül ERYÜREK and Prof. Dr. İskender AKKURT for their valuable guidance, suggestions and opinions, endless support during the periodical presentations of my thesis.

I could not thank enough Prof. Dr. Iskender AKKURT for allowing me to conduct my experiments in Isparta University Physics Department Laboratory. On the other hand, I would like to thank Assoc. Dr. Kadir GÜNOĞLU as he provides full support in the experiments.

I would like to thank laboratory members of the Turkish Standards Institute Energy Technology Laboratory (Ostim), with whom I could communicate thanks to the connections of the esteemed Assoc. Dr. Zuhal ER, for their support in carrying out the experiments.

My doctoral education process has not been a process involving only my studies. The contributions of my family and loved ones are very precious. I can't thank enough my only brother Korhan Anıl TURNA, who I grew up with, learned a lot from, who stood by me during my most difficult times and when I was afraid, and gave me strength.

I would like to express my gratitude to my dear father Mehmet Nail TURNA, my mentor, with whom I was able to move forward with what I could learn from his doctrine and discipline, my laboratory colleague with whom I learned together, who never spared the attention of his children at every stage of his children’s education life, who still does not lose hope that I will succeed in design geometry one day. I am grateful to my one and only mother, Neşe TURNA, who opened her home, life and heart, convinced me that I could succeed whenever I was depressed and fell, rushed to support me in my hardest times and cheered me up during my doctorate and all my other education processes. I would like to thank my one and only husband İsmail DEMİREL, who I grew up with, who showed me how to be calm and that everything would be alright, and bring peace to my every day. I would like to thank my one and only grandfather, İhsan KUTLU, who believes that I can achieve anything in life and who I know is watching me even though he can't see me giving this thesis. I would like to thank my one and only grandmother, Ömür KUTLU, who always supported me, motivated me, and did not spare her help and love. I would like to thank my aunt Rana KUTLU for her moral support in every academic and non-academic subject and always motivating me, and Murat Yiğit GÜVENKAYA, who was with me with her love.

I would like to thank my aunt Şeyma ÖZDİL, my mother-in-law Ünzile DEMİREL and my father-in-law Abdullah DEMİREL, who gave me spiritual strength with their prayers and good wishes. I would like to thank my brothers Şenol ÖZDİL, İlter ÖZDİL and their families who believed in me, gave me strength and motivated me. I would like to thank my sisters Özge TURNA, Gülçin ÖDEN, Gülay ŞAKAR and my aunt Ayla TURNA, who brought me joy with their conversations. I would like to thank my friends Gülay KARAKAYA, Seda ATASOY, Melis TAN, Oğuz GÜRCÜOĞLU, Hesaum, Hacire UĞUR and Onur KARAYALÇIN, for their help, motivations and support. I would like to thank all my teachers and friends who contributed to my success in this profession.

December 2021

Inal Begum TURNA DEMIREL
(Physicist)

TABLE OF CONTENTS

Page

ABBREVIATIONS

TEIAS	: Turkish Electricity Transmission Corporation
TSE	: Turkish Standards Institution
IEC	: International Electrotechnical Commission
ISO	: International Organization for Standardization
IRENA	: International Renewable Energy Agency
PV	: Photovoltaic
NREL	: National Renewable Energy Laboratory
EL	: Electroluminescence
IR	: Infrared
UV	: Ultraviolet
EVA	: Ethylene Vinyl Acetate
MDF	: Module Degradation Factor
STC	: Standard Test Condition (1000W/m^2 and 25°C)
NOCT	: Normal Operating Cell Temperature
SDM	: Single Diode Model
DDM	: Double Diode Model
CAMS	: Copernicus Atmosphere Monitoring Service
DHT	: Digital Temperature and Humidity
SD	: Secure Digital
GND	: Ground
SPI	: Serial Peripheral Interface
SCL	: Serial Bus Clock Line
SCK	: Serial Bus Data Line
SDA	: Serial Bus Data Line
MCU	: Microcontroller Unit
MISO	: Master Input Slave Output
MOSI	: Master Output Slave Input
CS	: Chip Select

SYMBOLS

q	: Electric charge (-1.602×10^{-19} C)
k	: Boltzmann constant (1.381×10^{-23} J/K)
G	: Solar radiation (W/m^2)
G_{STC}	: Solar radiation at STC(1000 W/m^2)
T_m	: Operation temperature of PV module/cell (K)
T_{amb}	: Ambient temperature (K)
T_{STC}	: Temperature at STC (298 K)
a_1	: The ideality factor of first diode
a_2	: The ideality factor of second diode
V	: Output voltage of PV cell (V)
$V_{oc,STC}$	: Open-circuit voltage of PV module/cell at STC (V)
V_{oc}	: Open-circuit voltage of PV module/cell (V)
V_{mp}	: Voltage at maximum power point (V)
V_D	: Diode voltage (V)
I_D	: Diode current (A)
V_{D1}	: Voltage of first diode (V)
I_{D1}	: Current of first diode (A)
V_{D2}	: Voltage of second diode (V)
I_{D2}	: Current of second diode (A)
I	: Output current of PV module (A)
$I_{sc,STC}$	: Short-circuit current of PV module at STC (A)
I_{sc}	: Short-circuit current of PV module/cell (A)
μ_{Isc}	: Temperature coefficient of short-circuit (%/°C)
μ_{Voc}	: Temperature coefficient of open-circuit (%/°C)
I_o	: Saturation current of PV module/cell (A)
I_{ph}	: Photocurrent of PV module/cell (A)
I_{sh}	: Current through shunt resistor (A)
I_m	: Current at maximum power point of PV module/cell (A)
P_{mp}	: Maximum power point (W)

N_s : Number of cells connected series in PV module/cell

N_p : Number of cells connected parallel in PV module/cell

R_s : Series resistance of PV module/cell (Ω)

R_{sh} : Shunt (parallel) resistance of PV module/cell (Ω)

LIST OF TABLES

Page

LIST OF FIGURES

Page

EFFECTS OF SOLAR RADIATION AND NEUTRON, GAMMA MATERIAL INTEREACTION EFFECTS ON THE SOLAR CELLS/MODULES/PANELS

SUMMARY

This thesis study covers the examination of the performance and degradation conditions of photovoltaic cells/modules/panels that convert solar radiation into electrical energy in case of exposure to solar radiation and nuclear factors (neutron and gamma irradiation) in laboratory and outdoor conditions. In this context, with the beginning of this thesis, first of all, the solar radiation for the province of Istanbul, where the performance and degradation experiments of photovoltaic devices will be carried out, was examined and presented to the literature. In these studies, statistical analysis methods were used to examine the accuracy of the models and the most suitable model was determined for the region to be studied. Afterwards, the working principles of the devices are examined and detailed on the basis of physical science in order to understand the effects of both natural conditions and nuclear effects that the photovoltaic cell/module/panels are exposed to on the device performance and to examine the decay structure.

There is a manufacturer's datasheet detailing the electrical characteristics of most of the produced photovoltaic cells/modules/panels at standard test condition (STC; 25℃ and 1000W/m2) and/or nominal operating cell temperature (NOCT; 20℃ and 800W/m2). By using the electrical characteristic data in this datasheet, performance and degradation modeling of photovoltaic cells/modules/panels can be performed theoretically. On the other hand, in some cases, the aforementioned data document may contain incomplete data, and even the data document of the produced device cannot be found at all. In this case, it becomes difficult to examine the performance of the device and to make performance predictions under different environmental conditions. Performance modeling of photovoltaic cells/modules/panels, which is one of the main objectives of this thesis; It was carried out by using the Single Diode Model (SDM), which is frequently used in the literature, and the Double Diode Model (DDM), which is rarely used in the literature, both in the absence of a datasheet or in the absence of a datasheet. The aforementioned theoretical study was firstly carried out by producing sub-models containing interconnected block structures on the MATLAB/Simulink platform and as a result of the merging of the sub-models, with the representation of the photovoltaic device. In the system; with the definition of the ambient conditions, which are the input data, the electrical characteristic output data that the photovoltaic device will show under these ambient conditions has been examined. Simulink study was performed for both SDM and DDM. There are electrical characteristic parameters of the photovoltaic device, which are not available in the manufacturer's datasheet, but have an important place in the evaluation of photovoltaic device performance. These parameters are; photocurrent, ideality factor, saturation current and resistance values. For performance and degradation evaluations, these parameters should be derived in line with the available data. By available data is meant manufacturer data sheet and/or experimental data. In cases where the manufacturer's datasheet is available, with the new photovoltaic device model created

on the Simulink platform, firstly the electrical characteristic parameters of the device are derived, and then the electrical data (current, voltage, power) produced by the photovoltaic device under the requested ambient conditions are turned into a program output for performance and degradation analysis. The slope method and/or the simplified open method were used in cases where the manufacturer's data sheet was missing. In this case, theoretical analyzes were carried out with the performance program created with a set of codes on MATLAB. These studies have been carried out for different photovoltaic type devices. Obtained results were compared with experimental data. Both the Simulink model and the MATLAB program result documents created with this doctoral thesis showed that; the theoretically produced performance result for the determined environmental conditions is more compatible with the experimental results carried out within the scope of this thesis in the Double Diode Model compared to the Single Diode Model.

As mentioned above, the performance evaluation of photovoltaic cells/modules/panels was also carried out experimentally within the scope of this thesis. The performance of 10W Monocrystalline and 7W Polycrystalline Photovoltaic Modules available in Zuhal ER's Laboratory at ITU Faculty of Arts and Sciences, Fluke Ti90_9Hz Thermal Camera also available within Zuhal ER's Laboratory, and some of the experiments were carried out with the Seaward PV200 Solar PV Test Device and Solar Survey 200R, which were purchased with the project support of the ITU Scientific Research Projects Unit, which is affiliated with the doctoral thesis, with the project number 41722. Performance and degradation effects of environmental factors on photovoltaic modules, which is one of the main objectives of this doctoral thesis, were determined with these devices. The electrical characteristics of the photovoltaic modules with the PV200 Solar PV Test Device and the solar radiation, ambient temperature, photovoltaic module surface temperature were determined with the Solar Survey 200R. It has been seen that the open circuit voltage has increased over time due to the overheating caused by the deterioration of the modules. On the other hand, the surface temperature of the photovoltaic module and extremely hot regions, which are indicators of degradation, were observed and determined with the Fluke Ti90_9Hz Thermal Camera. Performance and degradation evaluations of photovoltaic devices within five years were determined by the laboratory facilities of Zuhal Er, as well as the maximum power determination and performance experiments carried out at the Turkish Standards Institute (TSE). As a result of the experiments carried out at TSE, it was observed that the maximum power values obtained from the modules decreased with the effect of environmental conditions.

Experimental studies in addition to the above-mentioned modules, performance and degradation tests of a total of 20 modules, including 1.5W monocrystalline and polycrystalline photovoltaic modules, were carried out. As can be seen, the modules have very low power values compared to the modules mentioned above. The power measurement ranges of the Seaward PV200 Solar PV Test Device, which was purchased with the project support of ITU Scientific Research Projects Unit 41722, is between 5W and 15kW. Therefore, it could not be able to use in the electrical characteristic determination of 1.5W photovoltaic modules. In this case, measuring devices have been produced for the modules that are intended to be examined within the scope of the thesis. Arduino device, which is a microcontroller used in various projects and studies in recent years, has been used for the aforementioned purpose. On the other hand, sensors that determine current, voltage, ambient humidity and temperature are used. The communication protocol called SPI (Serial Peripheral

Interface) between the sensors and the Arduino, in other words, the data connection standard starts the operation of the data current sensor and the data flow is provided. Thus, the measurement is started with the Arduino signal and the obtained data is transferred to the SD card; it is recorded via the same communication protocol between the Arduino and the SD card module. Thus, electrical data is collected and recorded for each photovoltaic module. The code is processed on the Arduino in order to determine the initialization of the created measuring device, the operating range, the data collection frequency and the way the data is recorded and listed. Data are performed every five minutes and during the time the solar radiated module. On the other hand, solar radiation data is collected in line with latitude and longitude information via an online platform. Both solar radiation data and module electricity data were recorded and analyzed on both MATLAB and Excel platforms. The obtained results showed that the modules could not perform a full current-voltage curve as expected because they did not receive radiation at all hours of the day. Mostly, data is collected between the maximum power point and the open circuit voltage. On the other hand, it has been observed that modules of the same structure produce similar results. During these studies, since the system was exposed to the external environment, deteriorations such as dulling of the modules and wear at the junction of the cells were observed.

In addition to the determination of the effects of environmental factors on photovoltaic cells/modules/panels, neutron and gamma radiation effects are one of the other important objectives of this doctoral thesis. Neutron and gamma rays. Dr. It was held in Isparta, Süleyman Demirel University, Faculty of Arts and Sciences, with the support of İskender Akkurt. Modules that were not exposed to either solar radiation or neutron & gamma radiation before were exposed to gamma and neutron radiation in two sets. first set; two monocrystalline and 2 polycrystalline modules were exposed to gamma radiation for 30 days. second set; Two monocrystalline and 2 polycrystalline modules were exposed to neutron radiation for 15 days. Afterwards, electricity measurements were made under solar radiation like other modules. The results showed that the modules gave voltage values around the open circuit voltage. On the other hand, while fading occurred on the front surface of both sets of modules, deterioration occurred on the rear surface of the modules exposed only to neutron radiation.

GÜNEŞ IŞINIMI VE NÖTRON, GAMA MALZEME ETKİLEŞİMİNİN GÜNEŞ HÜCRELERİ/MODÜLLERİ/ PANELLERİ ÜZERİNDEKİ ETKİLERİ

ÖZET

Günümüzde fosil yakıt tüketimi, atmosferde karbondioksit gazının artışına, bu artış da ısının tutulmasına sebep olmuştur. Bu durum ise iklim değişikliğine diğer bir deyişle küresel ısınmaya yol açmıştır. Konu üzerinde çalışan birçok uzmanın da belirttiği gibi fosil yakıt tüketimini azaltılmalı ve hatta sıfıra indirmemiz gerekmektedir. Dolayısıyla, alternatif ve sürdürülebilir enerji kaynakları arayışı gündeme gelmiştir. En önemli alternatif enerji kaynaklarından biri ise güneş ve günümüzde başlıca çalışmalar ise güneşten elektrik üretimi alanındadır. Birçok alanda güneşten elektrik üretim sistemi etkinliğini sürdürmektedir. Örnek vermek gerekirse, binalar, taşıtlar, tarım arazileri, yollar, okyanus yüzeyi ile bütünleşik fotovoltaik sistemler, geniş araziler üzerinde kurulan fotovoltaik güneş santralleri. İlk kurulum maliyetlerinin yüksek olması, geniş alanlara ihtiyaç duyması, doğru akım ürettikleri için alternatif akıma dönüştürülmesi gerekliliği, güneş ışınım gücü ve süresine bağlı olması gibi sebepler sistemin dezavantajlarıdır. Öte yandan, kaynağının güneş olması avantajıyla hammadde maliyetinden muaftır, ses ve çevre kirliliği yapmayan, bataryalar ile üretilen elektrik depolanır ve istenilen zaman diliminde kullanılabilen, cihazların ömrünün kurulum maliyetini karşıladığı gibi birçok avantaja sahip bu sistemler için en önemli unsurlar yapılacak ön çalışma ve panel performansıdır. Bu durumda, sistemin kurulacağı bölgenin ışınım süre ve açıları, panel performansını ve ömrünü etkileyen çevresel faktörlerin irdelenmesi önem kazanmaktadır. Bu noktada fotovoltaik paneli iyi tanımak, hangi koşullarda nasıl tepki vereceğini önceden belirlemek önemlidir ki sistem zarara yol açmasın.

Bu tez çalışması, güneş ışınımını elektrik enerjisine dönüştüren fotovoltaik hücre/modül/panellerin güneş ışınımına ve nükleer faktörlere(nötron ve gama ışınımına) maruz kalma durumunda performans ve bozunum durumlarının laboratuvar ve dış ortam koşullarında irdelenmesini kapsamaktadır. Bu bağlamda, bu tez çalışmasının başlaması ile öncelikle fotovoltaik cihazların performans ve bozunum deneylerinin sürdürüleceği bölge olan İstanbul ili için güneş ışınımı irdelenmiş ve yapılan çalışmalar literatür sunulmuştur. Bu çalışmalarda modellerin doğruluğunun irdelenmesi için istatistiksel analiz metotları kullanılmış ve çalışılacak bölge için en uygun model tayin edilmiştir. Akabinde, fotovoltaik hücre/modül/panellerin gerek doğal koşullar gerekse nükleer etkilerin cihaz performansı üzerinde yol açtığı veya açacağı etkilerinin anlaşılabilmesi ve bozunum yapısının incelenebilmesi için cihazların çalışma prensipleri fizik bilimi bazında irdelenmiş ve detaylandırılmıştır.

Üretimi yapılan fotovoltaik hücre/modül/panellerin bir çoğunun elektrik karakteristiğinin standart test koşulunda (STC; 25°C ve 1000W/m2) ve/veya nominal çalışma hücre sıcaklığında (NOCT; 20°C ve 800W/m2) detaylandırıldığı üretici veri dokümanı mevcuttur. Bu föydeki elektrik karakteristik verilerin kullanılması ile teorik olarak fotovoltaik hücre/modül/panellerin performans ve bozunum modellemesi

gerçekleştirilebilmektedir. Öte yandan, bazı durumlarda bahsi geçen veri dokümanı eksik veri içerebilmekte, hatta üretilen cihaza ait veri dokümanı hiç bulunamamaktadır. Bu durumda cihazın performansının irdelenmesi ve farklı ortam koşullarında performans öngörüsü yapılması güçleşmektedir. Bu tez çalışmasının başlıca amaçlarından biri olan fotovoltaik hücre/modül/panellerin performans modellemesi; gerek veri dokümanı olduğu gerek ise veri dokümanı noksanlığında, literatürde sıklıkla kullanılan Tek Diyot Modeli (SDM) ve literatürde nadir kullanılan Çift Diyot Modeli (DDM) kullanılarak gerçekleştirilmiştir. Bahsi geçen teorik çalışma öncelikle MATLAB/Simulink platformunda birbirleriyle bağlantılı blok yapıları içeren alt modeller üretilerek ve alt modellerin birleşmesi sonucunda fotovoltaik cihazı temsili ile gerçekleştirilmiştir. Sistemde; girdi verisi olan ortam koşullarının tanımlanması ile fotovoltaik cihazın bu ortam koşullarında göstereceği elektrik karakteristik çıktı verisi olarak irdelenmiştir. Simulink çalışması hem SDM hem de DDM için gerçekleştirilmiştir. Üretici veri dokümanında mevcut bulunmayan fakat fotovoltaik cihaz performans irdelemesinde önemli yere sahip olan fotovoltaik cihaza ait elektrik karakteristik parametreler mevcuttur. Bu parametreler; fotoakım, idealite faktörü, doyma akımı ve direnç değerleridir. Performans ve bozunum değerlendirmeleri için bahsi geçen bu parametrelerin mevcut veriler doğrultusunda çıkartılması gerekmektedir. Mevcut verilerden kasıt ise üretici veri dokümanı ve/veya deneysel verilerdir. Üretici veri dokümanın mevcut olduğu durumlarda, Simulink platformunda oluşturulan yeni fotovoltaik cihaz modeli ile öncelikle cihaza ait elektrik karakteristik parametreler türetilmiş ve sonrasında istenilen ortam koşullarında fotovoltaik cihazın ürettiği elektrik verileri (akım, voltaj, güç) performans ve bozunum irdelemesi yapılmak üzere program çıktısı haline getirilmiştir. Üretici veri dokümanının noksan olduğu durumlarda eğim yöntemi ve/veya basitleştirilmiş açık yöntemi kullanılmıştır. Bu durumda, MATLAB üzerinde bir dizi kod ile oluşturulan performans programı ile teorik irdelemeler gerçekleştirilmiştir. Yapılan bu çalışmalar farklı fotovoltaik tip cihazlar için gerçekleştirilmiştir. Elde edilen sonuçlar deneysel veriler ile kıyaslanmıştır. Bu doktora tezi ile oluşturulan gerek Simulink modeli gerekse MATLAB programı sonuç dokümanları göstermiştir ki; belirlenen çevre koşulları için teorik üretilen performans sonucu Çift Diyot Modelinde, Tek Diyot Modeline kıyasla, yine bu tez kapsamında gerçekleştirilen deneysel sonuçlarla daha uyumludur.

Yukarıda bahsedildiği üzere, fotovoltaik hücre/modül/panellerin performans değerlendirmesi bu tez kapsamında deneysel olarak da gerçekleştirilmiş. İTÜ Fen Edebiyat Fakültesinde Zuhal ER'in Laboratuvarı bünyesinde mevcut olan 10W Monokristal ve 7W Polikristal Fotovoltaik Modüllerin performansı, yine Zuhal ER'in Laboratuvarı bünyesinde mevcut olan Fluke Ti90_9Hz Termal Kamera ve ayrıca bu doktora tezine bağlı İTÜ Bilimsel Araştırma Projeleri Biriminin 41722 numaralı proje desteği ile alınan Seaward PV200 Solar PV Test Cihazı ve Solar Survey 200R ile gerçekleştirilmiştir. Bu doktora tezinin başlıca amaçlarından biri olan çevresel faktörlerin fotovoltaik modüller üzerinde gerek performans gerekse bozunma ektileri bu cihazlar ile tayin edilmiştir. PV200 Solar PV Test Cihazı ile fotovoltaik modüllerin elektrik karakteristik özellikleri ve Solar Survey 200R ile güneş ışınımı, ortam sıcaklığı, fotovoltaik modül yüzey sıcaklığı tayin edilmiş, 2016 yılından bu yana laboratuvar bünyesinde bulunan fotovoltaik cihazların bozunmaları elektrik özellikleri bazından değerlendirilmiştir. Görülmüştür ki açık devre gerilimi zaman içerisinde modüllerin bozunması ile meydana gelen aşırı ısınmalar sebebiyle artmıştır. Öte yandan, Fluke Ti90_9Hz Termal Kamera ile fotovoltaik modül yüzey sıcaklığı ve bozunumların göstergesi olan aşırı sıcak bölgeler gözlemlenmiş ve tayinleri yapılmıştır. Fotovoltaik cihazların beş sene içerisinde performans ve bozunma değerlendirmeleri Zuhal Er'in laboratuvar olanaklarının yanı sıra Türk Standartları Enstitüsünde (TSE) gerçekleştirilen maksimum güç tayini ve performans deneyler ile de tayin edilmiştir. TSE'de yapılan deneyler sonucunda modüllerden elde edilen maksimum güç değerleri çevre koşullarının etkisiyle azaldığı gözlemlenmiştir.

Deneysel çalışmalar yukarı bahsi geçen modüllerin yanı sıra 1.5W monokristal ve polikristal fotovoltaik modül olmak üzere toplam 20 adet modülün de performans ve bozunum deneyleri gerçekleştirilmiştir. Görüleceği üzere modüller yukarıda bahsi geçen modüllere kıyasla oldukça düşük güç değerlerdedir. İTÜ Bilimsel Araştırma Projeleri Biriminin 41722 numaralı proje desteği ile alınan Seaward PV200 Solar PV Test Cihazının güç ölçüm aralığı 5W ile 15kW arasındadır. Dolayısıyla 1.5W olan fotovoltaik modüllerin elektrik karakteristik tayinlerinde kullanılmamıştır. Bu durumda, tez kapsamında irdelenmesi amaçlanan modüller için ölçüm cihazları üretilmiştir. Son yıllarda çeşitli projelerde ve çalışmalarda kullanılan bir mikro denetleyici olan Arduino cihazı bahsi geçen amaç doğrultusunda kullanılmıştır. Öte yandan, akım, voltaj, ortam nem ve sıcaklığı, tayin eden sensörler kullanılmıştır. Sensörler ile Arduino arasında SPI (Serial Peripheral Interface) adı verilen iletişim protokolü diğer bir değişle veri bağlantı standardı vasıtasıyla veri Akım sensörünün çalışmasının başlaması ve veri akışı sağlanmaktadır. Böylece Arduino sinyali ile ölçüme başlanır ve elde edilen veriler SD karta; Arduino ve SD kart modülü arasındaki yine aynı iletişim protokolü vasıtasıyla kaydedilmektedir. Böylece her bir fotovoltaik modüller için elektrik verisi toplanmakta ve kaydedilmektedir. Oluşturulan ölçüm cihazının başlatılmasını, çalışma aralığını, veri toplama sıklığını ve verilerin kaydedilip listelenme şeklini tayin etmek adına Arduino üzerine kod işlenmektedir. Veriler her beş dakikada bir ve güneş ışınımın hücreler üzerine düştüğü süre boyunca gerçekleştirilmektedir. Öte yandan, çevrimiçi bir platform üzerinden enlem ve boylam bilgileri doğrultusunda güneş ışınım verileri toplanmaktadır. Gerek güneş ışınım verileri gerekse modül elektrik verileri kaydedilerek hem MATLAB hem de Excel platformu üzerinde irdelenmiştir. Elde edilen sonuçlar göstermiştir ki modüller günün her saati ışınım almadığından dolayı beklenildiği üzere tam bir akım voltaj eğrisini gerçekleştirememişlerdir. Çoğunlukla, maksimum güç noktası ile açık devre gerilimi arasında veri toplanmıştır. Öte yandan, aynı yapıya ait modüllerin benzer sonuçlar çıkardığı gözlemlenmiştir. Yapılan bu çalışmalar boyunca sistem dış ortama maruz kaldığı için modüllerde matlaşma, hücreler bağlantı noktasında aşınma gibi bozunmalar gözlemlenmiştir.

Çevresel faktörlerin fotovoltaik hücre/modül/paneller üzerinde etkisinin tayininin yanı sıra nötron ve gama ışınımı etkileri bu doktora tezinin diğer önemli amaçlarından biridir. Nötron ve gama ışınımları Prof. Dr. İskender Akkurt desteği ile Isparta, Süleyman Demirel Üniversitesi Fen Edebiyat Fakültesinde gerçekleşmiştir. Daha önce ne güneş ışınımı ne de nötron & gama ışınımına maruz kalmamış modüller iki set halinde gama ve nötron ışınıma bırakılmıştır. İlk set; iki adet monokristal ve 2 adet polikristal modül 30 gün boyunca gama ışınımına maruz bırakılmıştır. İkinci set; iki adet monokristal ve 2 adet polikristal modül 15 gün boyunca nötron ışınımına maruz bırakılmıştır. Sonrasında, diğer modüller gibi güneş ışınımı altında elektrik ölçümleri yapılmıştır. Sonuçlar göstermiştir ki, modüller açık devre gerilimi çevresinde voltaj değerleri verdiği gözlemlenmiştir. Öte yandan, iki set modüller in de ön yüzeyinde solmalar meydana gelirken, sadece nötron ışınımına maruz kalan modüllerde arka yüzeyde de bozunmalar meydana gelmiştir.

1. INTRODUCTION

Sustainable energy sources, especially solar energy, become significantly important as the energy demand rise day by day. So world needs more solar energy facilities. The renewable energy shares 25,1% in 2011 and 36.6% in 2020 of the worlds electricity capacity. The renewable energy shares 36,1% in 2011 and 51,5% in 2020 of the Turkey's electricity capacity [1]. According to the Turkish Electricity Transmission Corporation (TEIAS) newly released May 2021 Installed Power Report; 9768 is the total number of installed power facility and 7862 number of it is the installed Solar Energy Plants in TURKEY. According to same report installed solar energy power is 7154 MW of total installed capacity with 97689,5MW where 14 % increase from the installed solar energy plants in 2020 [2] in which according to the TEIAS May 2020 Installed Power Report; 8778 is the total number of installed power facility with 91932,1MW capacity and 7080 number with 6152 MW of it is the installed Solar Energy Plants [3]. However, according to the TEIAS May 2019 Installed Power Report there is not much of increase of installed Solar Energy Plants where 7922 number with 89736,7MW is the total number of installed power facility and 6323 number with 5435,1 MW of it is the installed Solar Energy Plants compared to the increase globally [4]. The almost 12% increase in the solar photovoltaic plants installed capacity between 2019 with 5435,1 MW and 2020 with 6152 MW in Turkey is less compared the increase globally in which according to the report published at 2021 by International Renewable Energy Agency IRENA, the capacity statistics World's installed solar photovoltaic plants is 580760 MW in 2019 and 707495MW with almost 18% of increase [1].

The study published at 2019 [5] is a review of design, operation and maintenance of the photovoltaic. By design they revised component of the systems such as pv cells and their equivalent circuit design, and system design such as stand alone PV system or grid connected PV system. By operation they revised power quality, operation of hybrid systems and general operation. By maintenance they revised their performance and failure modes. The main importamcec of this review is to improve the performance and also considering the operational and maintenance costs decrease. One year later at 2020 Boretti and Castelletto [6] published a review about the performance trends of PV facilities considering mean value and standard deviation capacity factor over a year which affects the electricity cost. They considere 15 plants' construction cost that are established between 2014 and 2017. They result in that the cost data mostly missing and less relianble compared the energy production data. Therefore, they stated that accurate prediction of cost of PV facilities is not manageable compared to the performance evaluation of the facility.

At 2021 Ghosh and Yadav published a comprehensive review about PV technology of Future [7]. They present that almost twenty years ago within the laboratory conditions the efficiency of crystalline silicon photovoltaic cells reached 25%. Also they continue that although with hhigh technology the efficiency of crystalline silicon photovoltaic cells reached 26,6% since then. The increase of the efficiency of crystalline silicon photovoltaic cells are expecting to lower in long term.

In consideration of world's sustainable energy potential and investment statistics, Er Z. and Turna I.B., examined the utilization of the solar power. The solar power capacity of the entire world is overviewed and forecasts are made for the future. The position of photovoltaic technology is also discussed in the light of energy demand [8]. In order to, satisfy this need properly, with the least economic loss and maximum performance, the decision of the region for the facility to built and technology to use is crucial. Therefore, preliminary study which consists of understanding the solar radiation characteristics of the region. there are many studies relate to this issue. In conjunction with the importance of solar radiation evaluation, ER and Turna conducted a study at 2015 in which, solar radiation is evaluated for Turkey and 4 regions, 5 station in each region are selected. The monthly average global solar radiation on the horizontal surface models for Turkey in the literature are evaluated. The models are evaluated for each station by using the data gathered from Turkey Meteorology Station and results are examined by statistical analysis methods. The most applicable methods are selected for each region. New correlations are proposed to the literature as well [9]

This doctoral thesis study was intended to be built on the knowledge gained by completing the MS thesis under the supervision of previously. As in the MS thesis, the subject and idea of this PhD thesis was created by the consultant, under two objectives, to examine the decays of PV panels with various parameters and to examine the efficiency of the panels, and to use two different methodologies (experimental-simulation). One of the main purpose of this PhD thesis to evaluate performance of photovoltaic modules under different solar radiation conditions. Ergo, after M.Sc. and at the beginning of this PhD thesis in order to examine the panel performance, it was focused on Istanbul province in terms of solar radiation and two articles are published within this PhD thesis. The first one is published by Er Z., Turna I.B. and et. al. at 2017 about the mothly average daily global solar radiation. The evaluated models, that are selected from the literature, are examined due to the data for Istanbul where module performance experiments are conducted for this PhD thesis. The appropriate model for Istanbul is defined by the statistical analysis methods which are mean percentage error, mean absolute percentage error, mean bias error, root mean square error. It is seen that there is a significant agreement between the calculated and estimated results [10].

Besides, Er Z., Turna I.B. and et. al. published an article about the cloudless effect for hourly solar irradiance at 2018 [11]. The study is conducted for Istanbul Turkey. As it is stated in the study to define the position of the sun as important as to identify the relation between cloud and humidity. The May 2017 weather data is considered for Istanbul and global irradiance on horizontal surface with regard to cloud amount is defined. The study states that consideration of cloudless effect has significant impact on performance predictions.

Also again at 2018, Er Z. ve Turna I.B. published an article about solar radiation evalution that examines the 21 number of models for Turkey from the literature. For the decision of the most applicable model the north and south of Turkey are examined seperately. The three stations of each region are selected in order to decide more general model for both part. The t-statistical analysis, which give information about performance and accuracy of the model, is done for each station. As a result, it is seen that quadratic correlations are more applicable compared to other selected models [12].

In the literature reiew, Ahmad and Tiwari published a review about solar radiation models at international journal of energy and environment. The difference from studies that are mentioned above, they reviewed for models not only for a specific region but also large number of locations. They also evaluted these monthly average daily global solar radiation on horizontal surface correlation for New Delhi, with statistical analysis methods such as mean percentage error, root mean square error and mean bias error. The article states that the models are applicable for similar climatic conditions [13]

At 2014 Yao and et.al. evaluated solar radiation models for Shanghai, China. They compared monthly average daily global solar radiation models and daily global solar radiation models due to 42 years' meteorological data. The total number of 108 models are firstly divided into two group as monthly and daily global solar radiation. Then each group are subgrouped due to their correlation types. Models are evaluated with statistical analysis methods and showed which correlation type is more applicable for daily and monthly global solar radiation [14].

Besharat F. and et.al. published a review about gloabal solar radiation models. The review consists of models that are proposed for different regions around the world which have different atmospheric and geographic conditions. However, in this review the difference is that they collected emprical models chronologically and sort them due to the atmospheric conditions that are sunshine-based, cloud-based, temperature-based and othermeteorological parameter-based models. They evaluated all methods statistically for selected region which is Yazd city, Iran [15].

The studies mentioned above give investors and scientists information not only about the suitable region but also the photovoltaic panel type selection. The selection of the type of the photovoltaic panel is crucial to get the most possible performance. The solar radiation studies give us insight about the possible degradation forecasts of the photovoltaic facility. So, understanding the solar radiation and degradation characteristics of the photovoltaic panel technology is significantly important as it causes the power generation reduction.

Jordan D.C. and et.al. published an article named photovoltaic failure and degradation modes at 2017. The most comprehensible definition for term 'failure' is given by IEC 60050-191; as writers quated like, "the termination of the ability of an item to perform a required function.". The term failure has several usages, so they prefer to use 'degradation', for the change in the performance and appearance. The article listed the degradation modes of crystalline silicon with their severity rates. As a conclusion, it is stated that more types of degradation modes has seen in the modules at the hot and humin climates compared to moderate and desert climates [16].

Kumar M. and Kumar A. published a detailed review about performance assessment and degradation analysis of solar photovoltaic at 2017. They listed several degradation modes such as discoloration, corrosion, hot spots, delamination etc., their causes and consequences. They also listed the detection methods as visual inspection, I-V characteristics, ultrasonic inspection, infrared imaging, electroluminescence imaging, laser beam induced current [17].

The other study in the literature is done by Dhoke A., Sharma R., and Saha T.K., at 2018. They evaluate the effect of the degradation of module to the solar power plant. In the meantime, they stated the percentages of the degradation mode for silicon photovoltaic panel as 42% delamination, 19% breaking, 19% corrosion, 12% discoloration ve 8% ribbon crack as the study examines the levels of module degradation. It is stated that increase of degradation damage, cause decrease in the power generation of photovoltaic system [18].

Although the study published by Er Z. and et.al. give information about the performance of photovoltaic panel with respect to radiation and temperature effect, they also stated international standarts and testing of photovoltaic panels. They used a degraded panel. As they stated, although, there is low radiation and high wind speed during the examinations, the degraded solar cell act as load and cause increase in the module temperature and so the decrease in the open circuit voltage [19].

In the literature, there are several studies mentioned extraction of PV cell/module/panel(s) parameters [20]–[38]. Some of them use the manufacturer datasheet values or experimentally measured data from their system meanwhile some of them use both datasheet values and experimental results to extract unknown parameters which are series resistance, saturation current, ideality factor and photocurrent. After extraction of parameters, the performance of PV cell/module/panel(s) are examined.

Furthermore, there are several studies considers single diode [39]–[45] model meanwhile some others studied double diode model [39], [41], [46]–[51] to evaluate the performance of PV cell/module/panel(s). The literature summary is given in the table below and detailed table is given in the appendix part. The important part of performance modelling is to extract unknown parameter such as series resistance, saturation current, ideality factor and photocurrent, that are not given via manufacturer datasheet or could not found without examination of experimental data. In the literature some studies consider four unknown parameters and make some assumptions and some studies consider five unknown parameters [20]–[24], [27]–[31], [33], [36]–

[38], [52]–[57]. The extraction of unknown parameter is necessary to receive reliable PV cell/module/panel(s) performance results for both single and double diode model.

Table 1.1 : Literature studies.

Ref	Diode Model	# of Unknown Parameters	Extracted parameters
[58]	Single	5	R_s, R_sh, I_L, I_o, A
[59]	Single	6	R_s, R_sh, I_mpp, V_mpp, V_oc, I_sc
[60]	Single	1	P_mpp
[61]	Single	5	R_s, R_sh, I_L, I_o, A
[62]	Single	4&5	Rs, I_L, I_o,A & Rs, R_sh, I_L, I_o, A
[63]	Single	1	A
[64]	Single	5	R_s, R_sh, I_L, I_o, A
[32]	Single	5	R_s, R_sh, I_L, I_o, A
[21]	Single	5	R_s, R_sh, I_L, I_o, A
[66]	Single	1	A
[67]	Double	7	DDM: R_s, R_sh, I_L, I_o1, I_o2, A_1, A_2
[68]	Single	5	R_s, R_sh, I_L, I_o, A
[34]	Single	5	SDM: R_s, R_sh, I_L, I_o, A
[24]	Single	2	SDM: R_sh, A
[23]	Single	5	SDM: R_s, R_sh, I_L, I_o, A
[31]	Double	4	DDM: I_O, R_S, R_P, I_L
[69]	Single	5	R_s, R_sh, I_L, I_o, A
[38]	Single	2	SDM: R_s, R_sh
[43]	single	5	R_s, R_sh, I_ph, I_o, A
[53]	Single	4	SDM: R_s, R_sh, I_L, I_o
[40]	Single	6	Adjust, R_s, R_sh, I_L, I_o, A
[29]	Single	2	SDM: R_sh, A
[39]	Single + Double	5&7	DDM: R_s, R_sh, I_L, I_o1, I_o2, A_1,A_2 SDM: R_s, R_sh, I_L, I_o, A
[48]	Double	7	R_s, R_sh, I_L, I_o1, I_o2, A_1, A_2
[45]	Single	5	*5PM: R_s, R_sh, I_L, I_o, A

Table 1.1 (continued) : Literature studies.

Ref	Diode Model	# of Unknown Parameters	Extracted parameters
[49]	Single & Double	5&7	DDM: R_s, R_sh, I_L, I_o1, I_o2, A_1, A_2 SDM: R_s, R_sh, I_L, I_o, A
[37]	Single	4	R_s, I_L, I_o,A
[26]	Single	5	R_s, R_sh, I_L, I_o, A
[42]	Double	7	R_s, R_sh, I_L, I_o1, I_o2,A_1, A_2
[47]	Single & Double	5&7	DDM: R_s, R_sh, I_L, I_o1, I_o2, A_1, A_2 SDM: R_s, R_sh, I_L, I_o, A
[70]	Single	2	I_o, A
[35]	Single	5	R_s, R_sh, I_L, I_o, A
[50]	Single & Double	5&7	DDM: R_s, R_sh, I_L, I_o1, I_o2, A_1, A_2 SDM: R_s, R_sh, I_L, I_o, A
[41]	Single Double	5	R_s, R_sh, I_L, I_o, A
[72]	Single	5	SDM: R_s, R_sh, I_L, I_o, A
[51]	Single & Double	5&7	
[25]	Single	5	SDM: R_s, R_sh, I_L, I_o, A
[56]	Single & Double	5	R_s, R_sh, I_L, I_o,A
[22]	single	3	R_s, A, schottky-barrier height
[30]	Single	4	SDM: R_s, I_L, I_o, A
[28]	Single	4	SDM: R_s, R_sh, I_L, I_o
[55]	Single	5	
[73]	Single	5	R_s, R_sh, I_L, I_o, A
[74]	Double	7	DDM: R_s, R_sh, I_L, I_o1, I_o2, A_1, A_2
[75]	Single	5	SDM: R_s, R_sh, I_L, I_o, A
[57]	Double	5	DDM: R_s, R_sh, I_L, I_o1, I_o2,

The paper published in 2017, written by Fares and et. al. the PV panel characterisation is done according to the five parameter single diode model [71]. The characteristics of PV panel is evaluated via MATLAB Script similator. The electrical characteristics under standard test conditions are provided by the supplier which are open circuit voltage, short circuit current, voltage at maximum power and current at maximum power. However, in order to evaluate the performance of PV panel via five parameter model the resistance values, photocurrent, saturation current and ideality factor has to be known. The Wagner Method is used to extract the unknown values. Afterwards, they evaluated PV panel under different climatic conditions. They stated that the decrease in radiation make increase in short circuit current under stable temperature. Also the rise in temperature cause decrease in open circuit voltage at fixed radiation. They stated that the temperature affect on short circuit current is negligible. Then, the model results are compared with the manufacturer data which results in low root mean square error value implements similar results.

Theoretical PV performance single diode five parameter model via Matlab is compared with the results of DeSoto model and simulation software INSEL and PVsyst at different temperature and irradiation in the study by T. Ma, H. Yang, and L. Lu. They also compare the single diode five parameter model with experimental data received from 22 kWp grid-connected PV system and improve their model by considering soiling and aging factors [43].

Jain and et.al. contribute two studies to the literature one at 2004 [59] and other at 2006 [60]. In both studies they used Maple software and experimental data from other studies in the literature. In the first study six parameters series and parallel resistance, current and voltage at maximum power point, open circuit voltage and short circuit current are found by the use of experimental data of two solar cells by Lambert W function [59]. On the other hand, in the study at 2006 the series and parallel resistance, photocurrent, ideality factor and saturation current are received from data from other studies in the literature they cited. By Lambert W fuction they extracted maximum power value [60]. Different from the studies conducted from Jain and et.al. [59], [60], the study publish at 2009 by Jung and Guziewicz [65] present a analytic solution extract parameters by using Shottky diode equation which is similar with the single diode model and Lambert W function. The current voltage data of two different diodes is used to extract series resistance and ideality factor. Besides the study by Bayhan and Kavasoğlu [63] is also considers Lambert W function to calculate the diode ideality factor. They considered literature data of both resistance values and saturation current and also current voltage data of solar cell.

At 2011 Ishaque and Salam [68] used a different technique to extract unknown parameters of five parameter single diode model. Temperature and solar radiation dependence is considered and evaluated for different types of modules. The manufacturer's experimental data and datasheet are used to compare the computational model. The results show accurate results compared the experimental data and the dependence of temperature and solar radiation. On the other hand, at 2013 [69] study published that uses Analytic Method which is more common method is used to extract five parameter of the single diode model. They used free online database consist of various PV module and cell data to describe the current voltage data by analytic method. They also state in their study that commertial software PVsyst uses a simplified four parameters model and other commertial software TRNSYS uses the five parameters model. The reliability of model tested on the five PV panels with existing electrical data. The results show that considering G and T values at the model, show more accurate performance data.

The study by Liu and et. al., the theoretical evaluation they conducted consist of current voltage data at measured reference condition evaluated, the short circuit current and open circuit voltage are calculated, and last the performance of the PV panel at different splitting spectra [73].

In the literature there are also studies [21], [58], [66] consider numerical method for single diode model. In the study by Villalva [21], they aim to extract parameters by current voltage curve considering three points such as open circuit, maximum power, and short circuit. The difference from other studies is that they conduct two simulations based on single diode and two resistances, the other based on numerically solving the I–V equation of one current source. They extracted series and shunt resistance, photocurrent, saturation current and diode ideality factor. Likely the study by Chegaar and et.al. [58] also extracted five parameters however in this study they not only consider current voltage data but also slope of the current voltage curve. On the other hand, study published at 2010 [66] consider only extraction of diode ideality factor. The result of the study is that under constant voltage and temperature, diode ideality factor increases with the increase of current.

There are also other studies consider five parameters single diode model [35], [61], [62], [73]. The study by Celik and Acikgoz [62] and the study by Boutana and et.al. [35] conduct not only theoretical evaluation but also conduct experimental studies considering temperature and solar radiation effect. The study by Boutana and et.al [35] gave information about drawbacks of implicit method. The implicit method; a numerical method of extracting unknown parameters in which the initial value for the method is necessary. Therefore, the manufacturer datasheet information or experimental data is necessary. As for the study by Celik and Acikgoz [62], where the four parameters single diode model and five parameters single diode model. The results show that five parameters single diode model represent more accurate electric data compared to four parameters single diode model. Similar study conducted by Liu and et.al. at 2019 [73], however, they used different splitting films. By using those seven films they evaluated radiation effect. The calculated and measured datas are in good agreement. The study published at 2006 [61] also used five parameters single diode model however they compared the theoretical results with not experimental study but the results of previous studies in the literature which result in similar results.

At 2017 a study published [70] which uses different method from other studies. They consider Voc-Isc Method. The method used for not only extracting saturation current and diode ideality factor but also for degradation and quality assessment. The 36 Cell Multicrystalline Si Module and Monocrystalline Si Cell used for experimental studies to evaluate the validity of the model. They stated that after exposing solar radiation at outdoor conditions, saturation current and diode ideality factor increased. The increase in diode ideality factor is due to recombination in space charge region increase according to the study.

The study by Ibrahim and Anani illustrates the evaluation of the PV module parameters under different radiation and temperature conditions [72]. The various models for extracting of the unknown parameters for single diode model are evaluated. The reliability of the models are evaluated by the comparison of the model results and the manufacturer data sheet values. Overall, it is seen that the short circuit current value differs nonlinearly acccording to the variation of irradiance and changes slightly with the temperature. The behaviour of the photocurrent under varying temperature and radiation, is similar to the short circuit current. The models that considers the radiation and temperature effect on both the open circuit voltage and saturation current are much more reliable. At last they stated that the resistances changes more with radiation than temperature.

As module operating temperature has significant role in designing of a PV system, Segado and et.al. evaluated five existing model in the literature about the pretiction of the instantaneous and hourly module temperature [76]. Also, they proposed two model to the literature as well. The existing and proposed models are evaluated for four different PV technologies. The modules, on the other hand, are installed at the Universidad de Malaga at spain. There are also several sensors that collect meteorological and module data such as radiation, ambient temperature, module temperature, relative humidity, wind speed sensors. After predicted and observed module temperature data are taken, the validation of both existing and proposed models are done by statistical analysis methods. As a result, they stated that the thermal response of the instantaneous module temperature models to the meteorological changes is not urgent compared to hourly module temperature models.

Rizi and Abadi presented the five parameter single diode model via MATLAB-Simulink [77]. The effects of temperature, radiation, series resistance and shunt resistance are evaluated. At last they connect four PV modules in parallel to form an PV array. The PV array also simulated via MATLAB-Simulink. The results of the effect of radiation shows that the increase in the radiation, make rise in open circuit voltage, short circuit current, maximum power point. On the other hand, the incline in the temperature make decrease in open circuit voltage and maximum power point which is because of the increase in the saturation current. Meanwhile, they stated that the open circuit voltage stays almost same. On the other hand, they also evaluate the resistance and performance relation of PV cell. The results showed that the increase in the series resistance and the decrease in the shunt resistance cause reduction of output current of PV cell which is sign of the degradation of cell.

Double diode seven parameter model evaluated via numerical methods by the study published 2010 [67] The experimental data received from 6 identical monocrystalline PV module, each has 72 solar cells and 150W peak power and meteoreological data is also received from the experiment site. Data received and evaluated via LabView software.

The PV degradation rates are reviewed by Jordan and Kurtz and published by NREL (National Renewable Energy Laboratory) [78]. The results of several studies consist of different PV technologies such as Polycrystallinesilisium, cadmium telluride, copper indium gallium sellenide, monocrytalline silicon, multicrystalline silicon are examined under module and system consideration. The studies are examined under two different time span which are before and after 2000. The summary of those studies are listed according to number of data points, exposure time in years and degradation percentage by year.

The degradation analysis of a PV system under outdoor conditions via electrical parameters is done by Dhoke and Mengede [79]. The experiments are conducted at The University of Queensland, Australia. The degradation evaluation done by module degradation factor stated in the study which varies according to open circuit voltage and short circuit current. They stated that the change in the open circuit voltage is negligible. So, they examined the short circuit current. The degradation is seen as the series resistance is increased and caused decrease in short circuit current. At last, they stated that increase in degradation in other words decrease in current cause power generation and it also increase degradation with more speed.

As can be seen from the literature studies, outdoor testing plays a vital role in measuring the long-term behavior and lifetime of a PV panel or module. The reliability and lifetime of PV modules are highly dependent on the module construction and the climate in which it is installed. With the information gained during this thesis work, in order to provide an examination of the main PV durability and reliability.

Issues that contribute to power loss at both the array level and the module level are investigated. Namely: 1. Calculating the degradation rates of modules and arrays

2. Obtaining evidence confirming the absence/presence of potential induced

3. Emphasize durability and reliability specific to the “hot-dry” climate

4. Investigating the effects of solar radiation power and temperature on performance degradation

If the PV modules are removed from the field (or replaced) before the end of the warranty period due to any type of failure, including power outage beyond the warranty limit, these failures are classified as severe failures and this is called Reliability. On the other hand, if the performance of the PV modules degrades but still meets the warranty requirements, these losses can be classified as soft losses or dissipative losses and are called reability. Typically, product failures are categorized as infant failures, midlife failures, and wear-out failures.

The other main importance of this PhD thesis is to enlight the effects of not only environmental but also nuclear interaction on different types of solar photovoltaic cells/modules. The photovoltaic cells/modules degradation mechanism due to environmental and neutron & gamma irradiation is the scope of this thesis. The degradation evaluation of different type solar panels is the other purpose. Besides the evaluation of gamma irradiation and photovoltaic panel, interaction is one of the important aims of this thesis. The effects and consequences of neutron irradiation on the photovoltaic panel is also aimed to investigated. The mentioned neutron and gamma interaction and environmental evaluations are aimed to done by both experimentally and theoretically. The Radiation Protection Rules specify the duties and responsibilities of employers, licensees, workers and radiological safety officers. Atomic Energy Rules, legal authorities inspectors, workplace hygiene, safe use of machinery, employees, protective equipment, etc. is for. In this context, it is important to determine the compliance with the standards and to examine the working conditions under the standards, as well as to examine the possible accidents and the operation conditions under an extreme situation. Radiation can be defined as energy that comes from a source and travels in space and can penetrate various materials. Light, radio and microwaves are types of radiation called non-ionizing radiation, while ionizing radiation is produced by unstable atoms. Unstable atoms differ from stable atoms because unstable atoms have excess energy or mass, or both. As is known, types of electromagnetic radiation include sunlight, (cosmic radiation), x-gamma rays, radar and radio waves. The other form of radiation, known as particle radiation, is small fast-moving particles.

The form of radiation, which has both energy and mass (weight), includes alpha particles, beta particles, and neutrons. During the operation of photovoltaic solar cells, they can be exposed to radiation such as those used in space systems and satellites. Defects and electrical damage in solar cells collectively and result in significant degradation and the lifetime and performance of solar cells that correlated with the amount of radiation damage. To investigate the radiation defect for various gamma radiation doses, degradation of minority carrier lifetime, device properties may change. Importance of effective minority carrier lifetime for silicon solar energy The efficiency of the cell is reflected in its very significant influence on both the short-circuit current and the open-circuit voltage. Solar cells generally show a good spectral response to visible radiation. The wavelength region of the electromagnetic spectrum at 400-800 nm. In this thesis, how a solar cell responds to the selection of narrow radiation bands - spectral characteristic - and its behavior when exposed to neutron irradiation is observed with expected results. Details on radioactivity are presented in section 2.2.

In the literature, there has been several study related to degradation of solar photovoltaic system due to environmental and atmospheric conditions. Most part of literature studies consider the terrestrial radiations which are radiations that passes the atmosphere and reaches the ground. However, there are applications of photovoltaic panels that are used to generate electricity for the sattelites which are exposed to the extraterrastrial radiations such as cosmic radiations. In this point, the particle interactions with photovoltaic panels are unique and need to evaluated.

In the literature, there are also many studies related to neutron and gamma interaction with matters that are used also in some material parts of solar energy technologies. However, there are few studies related to neutron and gamma interaction with photovoltaic panels which are only consider the change in the electrical characteristics. So, the degradation of irradiated different types of photovoltaic cells are unique and need to be examined as well.

Besides, recently, the solar photovoltaic facility is established on the area of chernobyl nuclear accident. Although years have passed from the accident date, the impact of that accident on the photovoltaic panels is unknown and need to be understood. As nuclear studies can not be ignored, there might be a need for hybrid energy system of solar energy and nuclear power. Hence, at that point the interaction mechanism and the degradation relation should be known.

The hypothesis that the thesis is built on is there is not only environmental impacts but also neutron and gamma irradiation effects on photovoltaic cells/modules/panels and the degradation consequences due to those irradiations. The contribution of experimental results by this PhD thesis will gave new aspect to the literature about interaction and degradation mechanisms in different circumstances.

The studies from the literature about the 0n1, γ material interaction effects on the solar cells/modules/panels considers either 0n1 irradiation [80]–[86] or γ irradiation [87]–

[91], but very few of those studies evaluate both irradiations [92]–[98]. The experimental and measurement procedures of the studies in the literature are examined.

Simic and et.al. published an article at 2013 about neutron irradiation effects on solar cells, photodiodes and phototransistors. They considered only the current voltage characteristics. The examined samples are the monocrystalline silicon solar panel with the maximumpower voltage 4.0V, maximum power current 100.0 mA, four types of silicon PIN photodiodes which is diode that consist p-type, n-type and undoped intrinsic semiconductor, two types of silicon NPN phototransistors. The samples are irradiated by the certain amount of dose in the air temperature at 21 C and relative humidity is 40% to 70%. The digital multimeter is used for to define current-voltage characteristics which are measured in certain illumination for each sample such as 10W/m2 for phototransistor, 4.32W/m2 for solar panels, and 0.45W/m2 for the other phototransistors and all photodiodes. Although neutron irradiation affected the solar cell at least and the phototransistors at most, they all show the similar response; neutron irradiation decreased their photocurrent and by the annealing process photocurrent of devices are increased. The article states that although with the increased neutron irradiation, by the annealing process solar cell's current voltage characteristics are become almost near to the characteristics that has seen at before irradiation [99].

At 2014 Tobnaghi D.M. and et.al. published an article name "Effect of gamma radiation on the aged mono-crystalline silicon Solar cells". They irradiated gamma on the 15 sample of monocrystalline silicon solar cells. They examined the electrical characteristics of solar cells such as short circuit current, open circuit voltage, current at the maximum power point, voltage at the maximum power point, fill factor, efficiency. Solar cells are divided into 5 groups and irradiated with 1.23MeV 60Co gamma source with dose of 50 krad, 100 krad, 500 krad, 1000 krad, 2000 krad for each group respectively and illuminated at standart test conditions. Electrical characteristics of all samples are measured before and after irradiation. The results show that the diffusion length and minority charge carrier lifetime decreased. By this decrease shunt resistance increased and cause the decrease in short circuit current, maximum power point, fill factor, eficiency, open circuit current. Overall, the solar cell group that is under irradiated with lowest dose of gamma ray recovered the most [90].

Nikolic D., and Vasic-Milovanovic A. compared the neutron and gamma irradiation impacts on only one type of solar panels which has maximum power voltage 4.0V, maximum power current 100.0mA. They examined the electrical characteristics of solar cells such as short circuit current, open circuit voltage, current at the maximum power point, voltage at the maximum power point, fill factor, efficiency. The evaluations are done before the irradiation, immediately after irradiation and one month after the irradiation. Panels are divided into two groups and irradiated at 21 C and relative humidity of 40% to 70%. First group is irradiated with an energy that is sufficient for the creation of electron hole pairs which is 1.25MeV and with Co60 gamma source with dose rate of 100Gy/h at a distance of 15cm. Second group is irradiated with neutron and gamma with 241Am-Be source and dose of 229.71mGy. Gamma and neutron irradiation decrease the electristic characteristics such as short circuit current, fill factor, eficiency, open circuit current. Although shunt resistance increased with both neutron and gamma irradiation, series resistance decreased with neutron irradiation and increased with gamma irradiation [94].

In the literature, there are also other studies that irradiate particles on the photovoltaic devices rather than neutron or gamma irradiations. Perny and et. al. examined the Xe-Ions irradiations on c-Si and a-SiC device [100]. Meanwhile, Zhang and et.al. evaluated degradation mechanism of electron irradiated metamorphic tri-junction solar cells at 2016 [101]. The most recent study is done by Aierken A. and et.al., at 2018. They use test cells as metamorphic GaInP/GaInAs/Ge triple junction solar cells and irradiated with protons [102].

The other purpose of this PhD thesis is to evaluate the performance of the photovoltaic cell/module/panel and examine the degradation caused by natural and nuclear sources. The studies have conducted with regard to the aims and time schedule of this thesis. The performance evaluation is conducted via experiment devices and computational studies. The theoretical performance analysis is done with regard to equivalent circuit of photovoltaic technology by single diode model and double diode model. Also, experimental data is collected via Arduino sets and the solar radiation, ambient temperature, cloud opacity, wind direction and wind speed were received from online database. Besides, the theoretical evaluation is conducted via MATLAB the theory of performance evaluation considering the extraction of unknown parameters is explained and evaluated via MATLAB.

Besides, the neutron and gamma irradiation experiments are conducted and the performance of irradiated solar cells are evaluated. Experimental data received from Seaward PV200 Solar PV Test Equipment which is bought by the budget of research project supported by ITU Scientific Research Projects Unit (BAP) and the thermal images have also collected via the existing experiment device Fluke Ti90_9Hz Thermal Imager within the Zuhal ER's Laboratory at ITU Faculty of Arts and Sciences.

2. METHODOLOGY

As this thesis is aimed, the method has been applied under two main headings (experimental and simulation) to examine the efficiency and degradation of modules and panels according to various parameters. At this point, experimental considerations are also in itself; Regarding the investigation of the parameters affecting the module efficiency and the interaction of gamma / neutron radiations with the material, it has been examined under two sub-headings.

2.1 Photovoltaic (PV) Cell/Module/Panel

As presented in the previous section, there are many studies in the literature on PV cell modeling and analysis, and research continues rapidly. Based on equivalent circuit designed with single diode and resistors for PV cell model), two diodes and resistor (s) models are studied in the literature.

PV module is formed as a result of connection of PV cells which are represented as p-n junction diodes in solar cell equivalent electrical circuit is illustrated in the figure below. In Fig.2.1(a) the single diode model and in Fig 2.1(b) the connection of cells to form a module are illustrated.

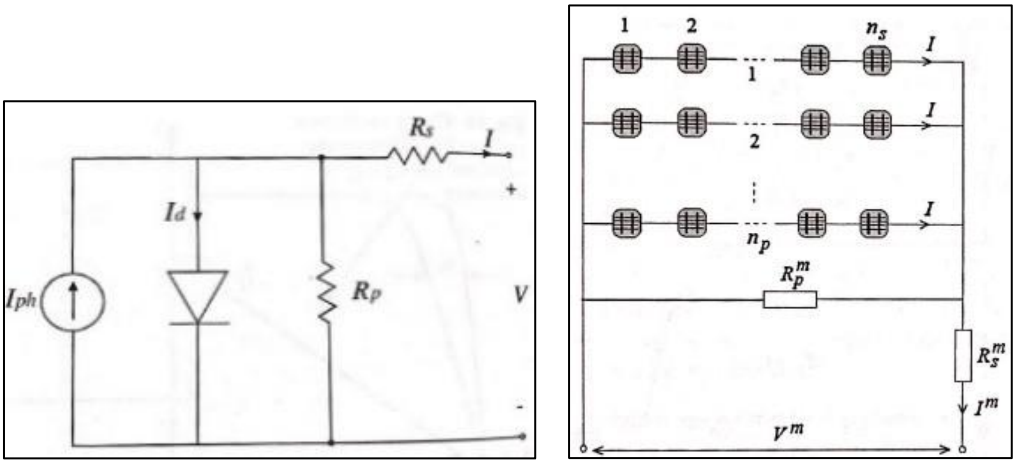

(a) **(b)**

Figure 2.1 : (a) Equivalent electrical circuit of a single diode solar cell **(b)**Illustration of connection of solar cells to form a module [102],[103].

PV cell/module allows current in one direction while blocks in the opposite direction as it is considered as pn junction [103]. The pn junction formed by connection of p type and n type semiconductors. The p type semiconductor has the majority charge carrier as holes and minority charge carriers as electrons where the doped material gains electrons and so make bond. The n type semiconductor has the majority charge carrier as electrons and minority charge carriers as holes where the doped material gave out electrons and so make bond. The figure below illustrates p-type and n type semiconductor separately. The blue dots refer as holes and red dot refer as electrons. The minus illustrates acceptor ion that gains electrons to make the bound and positive illustrates donor ion that gave out electrons to make the bound. The figures are drawn via AutoCAD by the knowledge gained from education of Delft University of Technology [105].

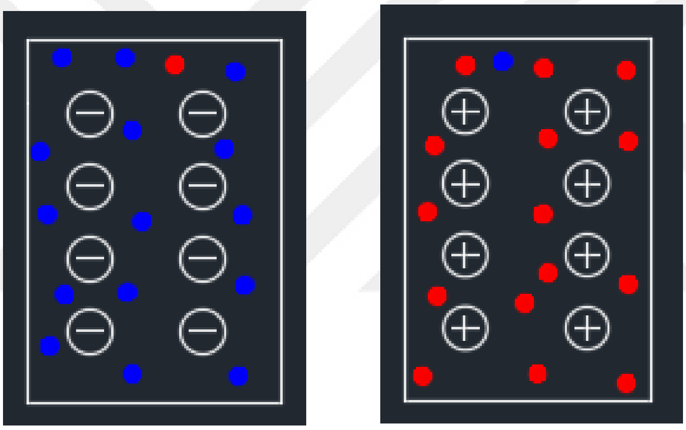

(a) **(b)**

Figure 2.2 : (a) The p type semiconductor and **(b)** n type semiconductor [105].

The connection of p and n type semiconductors form pn junction result in forming internal electric field where none of the majority and minority charge carriers exists. There are two transport mechanisms that are diffusion and drift. The diffusion is controlled by density gradient and works on majority charge carriers. Drift is controlled by electric field and works on minority charge carriers.

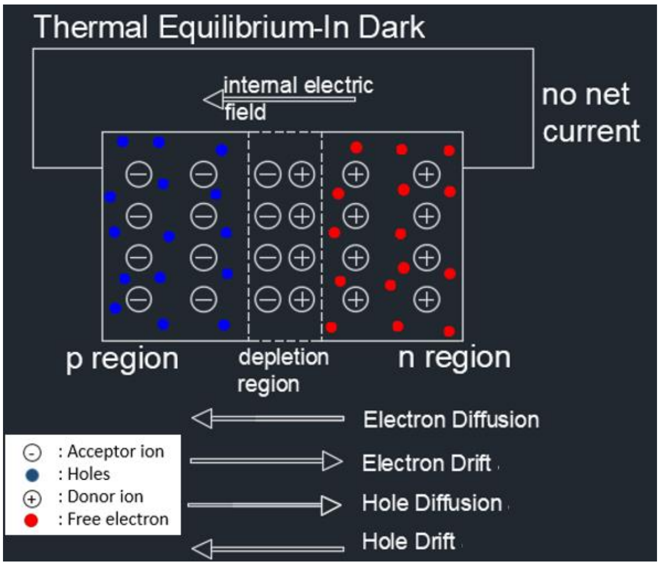

Figure 2.3 : PN Junction in Thermal Equilibrium [105]**.**

In thermal equilibrium there are no radiation or applied voltage. The drift and diffuse mechanisms are in balance and there is not any current generated as shown in AutoCAD drawing above. When p and n type connected; the majority charge carrier electrons of n region diffuse from n region to p region because of the density gradient and meanwhile the minority charge carrier holes of n region drifts from n region to p region because of the electric field. On the contrary, when p and n type connected; the majority charge carrier holes of p region diffuse from p region to n region because of the density gradient and meanwhile the minority charge carrier electrons of p region drifts from p region to n region because of the electric field.

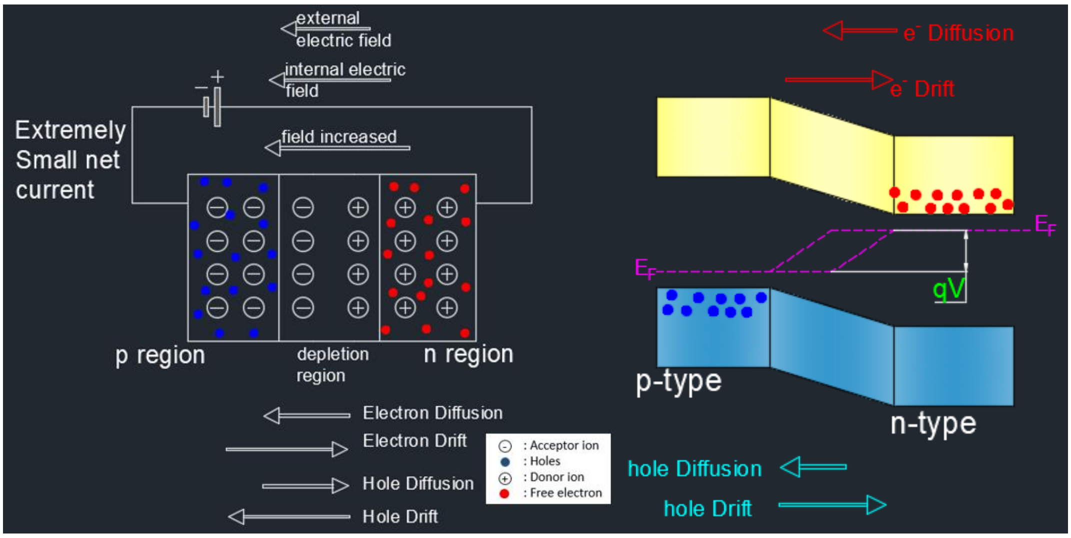

Figure 2.4 : Reverse Bias PN Junction in Dark [105]**.**

On the other hand, if pn junction connected to voltage supply there will be forward or reverse bias will have generated. In forward bias, a voltage supply is connected to pn junction where higher electric potential interval of the voltage supply is connected to the p region and lower electric potential interval of the voltage supply is connected to the n region. In reverse bias, a voltage supply is connected to pn junction where higher electric potential interval of the voltage supply is connected to the n region and lower electric potential interval of the voltage supply is connected to the p region.

If reverse bias is applied, an external electric field occur in the same direction of existing internal electric field and cause reduction of electric field so depletion zone enlarges. Drift is controlled by electric field and limited by the number of minority charge carriers so electrons in p region and holes in n region. Drift electrons generate almost zero current. Also by the increase of depletion region, the current density related to diffusion decreased. In reverse bias the drift mechanism is overrule diffusion mechanism. The current generated in dark at reverse bias is called reverse saturation current which is also called leakage current as reverse saturation current is extremely small.

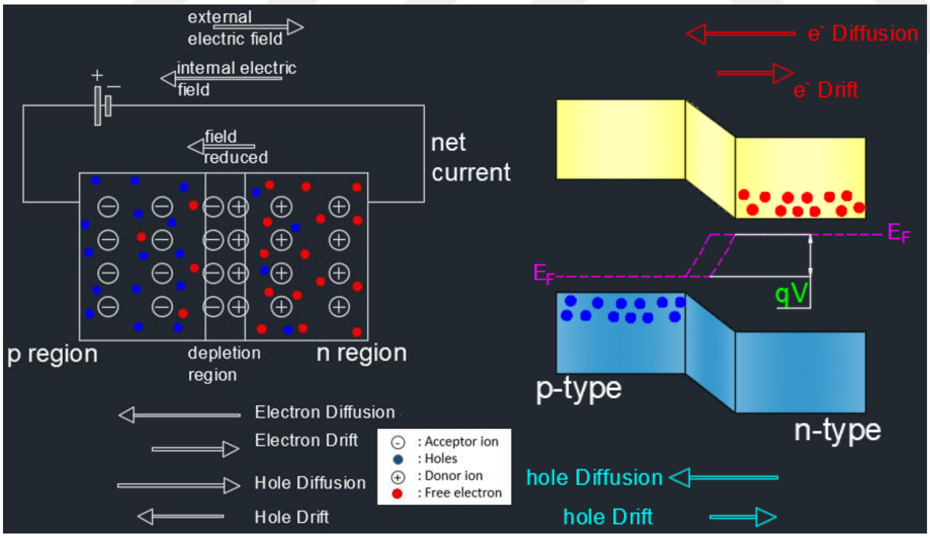

Figure 2.5 : Forward Bias PN Junction in Dark [105].

If we apply forward bias in dark, an external electric field occur in the opposite direction of existing internal electric field and cause reduction of electric field so depletion zone narrows. Diffusion of electrons and hole is more compared to the drift mechanism. In forward bias, electrons diffuse from n region to p region within pn junction and leave pn junction at p region, continue traveling through circuit and reach n region of pn junction by ending recombination of hole. The current generated in dark at forward bias is called saturation current.

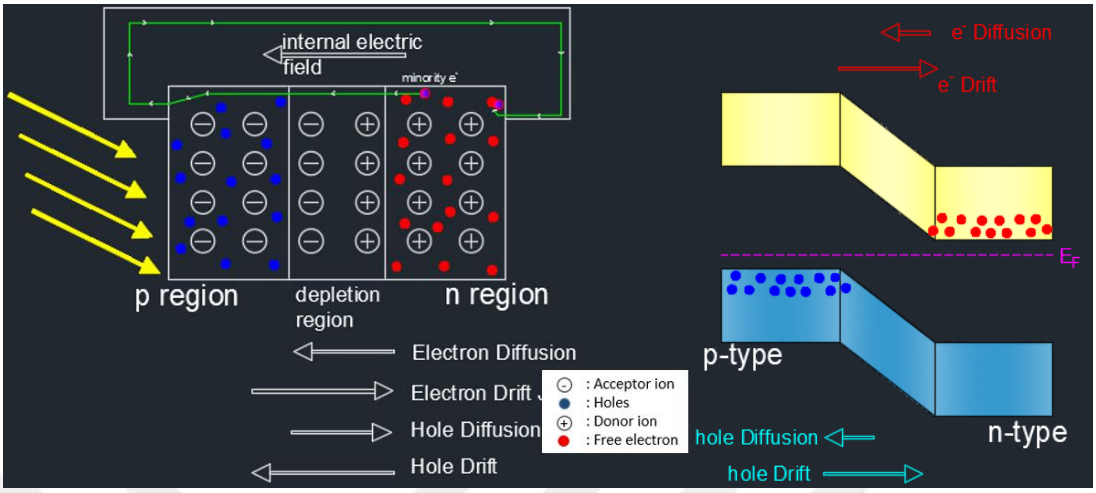

Figure 2.6 : PN Junction under radiation [105].

Consider pn junction is exposed to radiation. The photoelectric effect is occurred which result in, generation of electron-hole pairs due to light absorption, later electrons and holes separated and at last collection of electrons and holes recombined after minority charge carrier traveled through the circuit. Consider pn junction that light is absorbed by n region of the junction result in generation of electron-hole pair. Light absorption increase minority charge carrier so holes in n region. Density of minority charge carriers increases so drift mechanism become more effective that diffuse transport mechanism. Therefore, pn junction generates current which is called photocurrent and is large compared to forward bias.

It is mentioned above that current generated when pn junction forward biased and radiated. Eventhough extremely small there is also current occurred in reversed biased pn junction.When the pn junction so PV cell is not illuminated, it generates saturation current at the forward bias and reverse saturation current at reverse biased which is also called leakage current as reverse saturation current is extremely small.Besides when the PV cell is radiated, it generates photocurrent[104].To analyze generated current and other parameters such as open circuit voltage, power at maximum point, related to pn junction so PV cell, there are PV cell models with equivalent circuit of PV cell.Applying a solar cell model to analyze / examine solar cells makes the studies systematic. The cell models are single diode moel with two resistances and double diode model with two resistances as illustrated below. The circuits are drawn via online circuit simulation platform named as circuitlab [106].

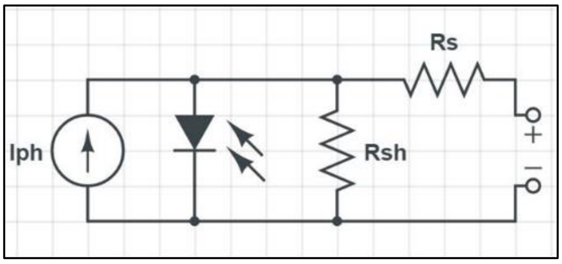

(a)

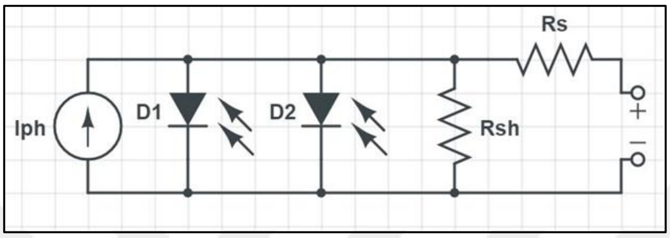

(b)

Figure 2.7 : Equivalent circuit design for **(a)** single diode model **(b)** double diode model.

At this point, modeling a solar cell will involve examining current voltage (I-V) and power voltage (P-V) properties with the help of fundamental equations. The most popular analysis approach is to draw the equivalent circuit and examine the output voltage and current relationships in terms of various parameters such ascurrent when there is no voltage, voltage when there is no current, slope at open circuit and short circuit point which is detailed in the following. An example of I-V and P-V graph and also key points such as open circuit voltage, short circuit current, current and voltage at maximum power point, maximum power is illustrated by the figure below.

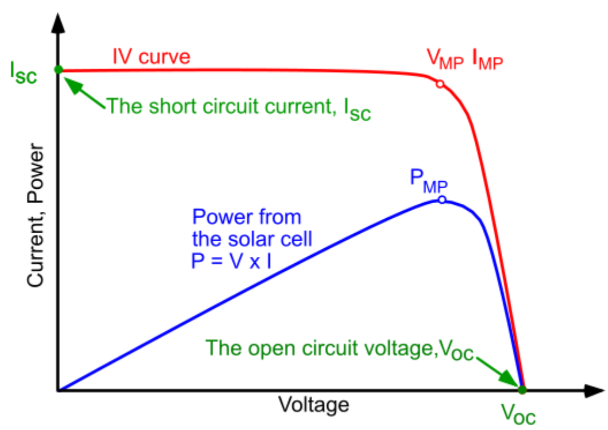

Figure 2.8 : Key points I-V and P-V graphs [107].

The output current of a PV cell for ideal single diode model is depends on photocurrent, current through shunt resistance, saturation and reverse saturation current. On the other hand, in order to define the performance of the PV cell, the relations between the voltage and both current and power are examined within this study. The current-voltage and power-voltage graphs, give information such as the PV cells' maximum operation power which is the preferred performance point, when the cell consumes and produces power [19]. When PV cell is open circuited as in the figure below, it does not generate current, but there exist again an electric field, or voltage. The voltage created by an illuminated solar cell under open-circuit conditions is called the open-circuit voltage. Open circuit voltage basicly depends on saturation current, photogenerated current and temperature.

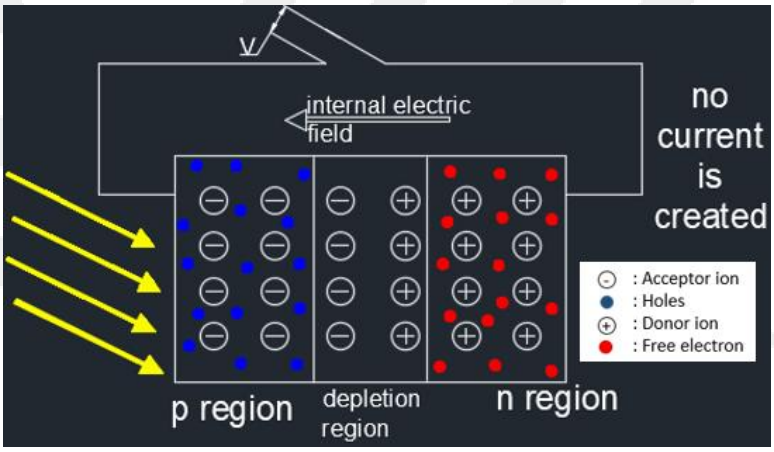

Figure 2.9 : Open Circuited PV cell points I-V and P-V graphs [105].

On the other hand, by closing the switch in the figure, by an electrical circuit, the contact at the p type semiconductor with that of the n type semiconductor are connected which in other words PV cell is short-circuited. In this condition, the radiated PV cell produces only an electrical current which is called the short-circuit current of a solar cell. Short circuit current basicly depends on the area of the cell, intensity of the light, absorption and reflection properties of the cell and minority charge carrier lifetime. Both short circuit current and open circuit voltage changes according to the bandgap which is explained in the following. The short circuit current is the maximum current and open circuit voltage is the maximum voltage value of the cell and yet at those points the power generated by cell is zero. From P-V graph the extreme point gives the maximum power and also the corresponding voltage. Also by using the voltage at maximum power point, the current at maximum point can be found.

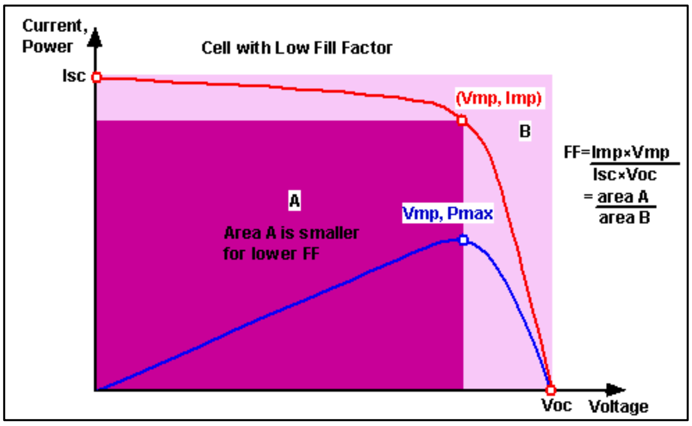

Figure 2.10 : Fill Factor illustration via I-V and P-V graphs [108].

Besides, the quality of the cell in other words fill factor can be received from the I-V and P-V graphs as well. As in the figure below, fill factor is the ratio between the area of the rectangle formed by voltage and current at maximum power point and the origin, and the area of the rectangle formed by open circuit voltage, short circuit current and origin. This ratio will result in one as maximum value which will not be equal to one. However, as close as to one the fill factor so the quality of the cell increases. Besides, fill factor value lower with the increase with series and the decrease with shunt resistances which are illustrated in the equivalent circuit design.

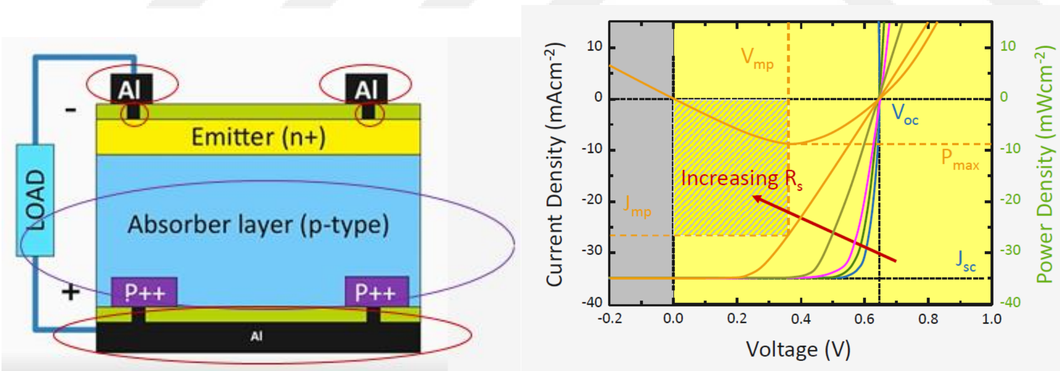

(a) **(b)**

Figure 2.11 : (a) Series resistance of solar cell and **(b)** relation of I-V graph [105].

Series resistance is expected to be low in order solar cell not to lose voltage over it and for higher fill factor. The current passing the semiconductor materials can experience resistance. The interface between the semiconductor material and the metal contacts, besides only metal contacts itselves are resistors as well and that are symbolized by series resistance in the equivalent circuit design. The series resistance received from the slope at open circuit voltage in I-V graph. By the increase of the series resistance which is not wanted, the slope and maximum power that cell produce will decrease so the fill factor.

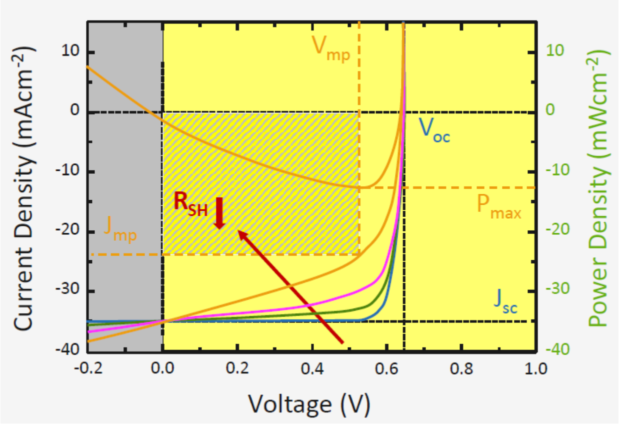

Figure 2.12 : Shunt resistance of solar cell and relation of I-V graph [105].

In the solar cells there are alternative paths for generated photocurrent, which result in losses, called as defects and represented by shunt (parallel) resistance in the equivalent circuit design. By the decrease of shunt resistance, photocurrent find more alternative paths so this will decrease the maximum power and fill factor. Also decrease in shunt reistance observed in I-V graph as the slope at open circuit voltage increases as shown in the figure above. For diode model, the series resistance expected to be as small as possible, meanwhile the shunt resistance is expected to be as large as possible for low performance loss and high fill factor.

Such in practical usage, the performance is also detected and compared via the efficiency correlation as given below. In general description the efficiency is the ratio between output and input power. In here the input power refers as the power of the radiation and the output power refers as the maximum power of solar cell. The losses such as inverter, battery, cable are neglected.

$$\eta = \frac{P_{max}}{P_{in}} = \frac{V_{oc} I_{sc} FF}{P_{rad}} \tag{2.1}$$

In the outdoor conditions, the change in the solar radiance and the temperature of the module value affects both open circuit voltage and short-circuit current values, so the efficiency. Previously mentioned, bandgap where electrons or holes do not exist, is one of the factors that effect open circuit voltage so the efficiency.

In semiconductor material, for instance solar cell, in order to generate current an external source is necessary such as solar radiation, voltage source. Solar radiation can exite electron and start the electric current. However, not all wavelength so energy of solar radiation can cause generation of current. The photon energy which is hc/λ, should be equal or greater than bandgap energy.

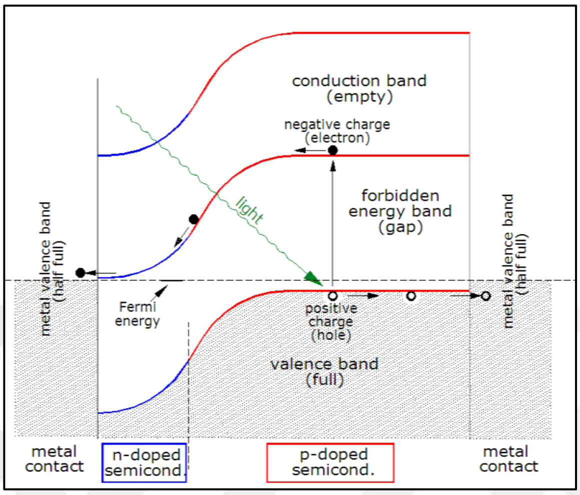

Figure 2.13 : Simple diagram of solar cell [109] [105]**.**

On the other hand, Shockley and Quisser mentioned about an upper theoretical limit for the efficiency of an ideal solar cell and called as detailed balance limit [110]. In order to define the maximum open circuit voltage for an ideal solar PV cell the detailed balance limit can be used. Kirk mentioned three different case for defining open circuit voltage that are case one for a perfect backside mirror, case two for an air-exposed backside which is also called as bifaicial configuration, and case three for a parasitically absorbing backside substrate [111].In this PhD thesis the first case with a perfect backside mirror is considered, in which the open circuit voltage is given as;

$$V_{oc} = \frac{E_g}{q} - \frac{kT}{q} \ln \frac{2\pi E_g^2 kT}{h^3 c^2 J_{ph}} \tag{2.2}$$

$$\eta = \frac{I_{sc} V_{oc} FF}{\Phi_{light}} \tag{2.3}$$

where T is the cell temperature. As if efficiency is given in the eq.3 that is inversely proportional with flux of light and proportional with open circuit voltage which is given in the eq.2.2. Efficiency is in the dependence of bandgap energy as it effects open circuit voltage.

2.2 Radioactivity, Irradiation and Efficiency of Solar Module

The smallest unit of matter, atom; has atomic nucleus at the center of the matter consists of proton and neutron. Some nuclei have excess energy which result in unstability of the nucleus. Therefore, unstable nuclei loss energy by electromagnetic radiation and emitting elementary particles such as neutron and proton. This radiation process is called radioactivity, those atom and nucleus is called radioactive atom and radionuclide. Unstable nuclei transform into other nuclei by radiating without being under any external influence. The decay rate of radionuclide is activity with SI unit of Becquerel (Bq). The time period that radionuclide to reduce upto half of its initial amount is called halflife.The radioactive decay of unstable nuclei might be alpha decay in which alpha particles with two neutrons and protons are radiated so the unstable nuclei decrease by two protons and neutrons and become stable, beta decay is the conversion of excess neutron in the nucleus into proton also other beta decay is positron which the conversion of excess proton in the nucleus into neutron,electron capture in which combination of proton and electron result in X ray is radiated. Apart from those there is also gamma decay and neutron emission might occur. The excess energy of nucleus losses via gamma decay which mostly form after other decays such as alpha or beta decay. Neutron emission occurs excess of neutron in the nuclei.

Radiation can be classified either its ionizing ability or its form as particle or wave. The radiation can be classified into two groups as radiating as wave form such as radio waves, visible, X- rays and gamma rays, and radiating as particle form such as alpha, beta and neutron radiation. The particle form of radiation can be subclassify as charged particles such as beta, alpha, proton and uncharged particles such as photons as gamma and x rays, neutrons, neutrino.

In order to detect the radiation, the matter-radiation interaction need to be observed. When considering the interaction, the radiation can be classified into two groups as ionizing and non-ionizing radiation. Non-ionizing radiation is electromagnetic radiation such as radio waves whose energy of the photon is from 1.24 μeVto 124 x10-15eV, ultraviolet whose energy of the photon is 124 eV – 3.3 eV, infrared whose energy of the photon is 1.7 eV – 1.24 meV, micro-waves whose energy of the photon is 1.24 meV – 1.24 μeV and visible whose energy of the photon is 3.3 eV – 1.7 eV.

Ionizing radiation can be classified within itself as particle radiation as alpha, beta and neutron, and electromagnetic radiation as X- rays and gamma rays.

Besides, radiation and irradiation interaction with matter is important for the PhD thesis, especially solar radiation, gamma irradiation and neutronirradiation interaction. To avoid confusion, the difference between radiation and irradiation should be defined. Radiation and irradaition is energy, generated via and fall onto a surface respectively [112].

Gamma irradiation classified as uncharged particle means it does not experience Coulomb Force and also can penetrate through matter more long distances compared to the charged particles. So while interacting with matter; high energy gamma irradiation cause pair production which is the conversion of gamma irradiation into positron and electron while passing near the nucleus of the matter, low energy gamma irradiation causes photoelectric effect which is the conversion of gamma irradiation into electron; photoelectron, after collision with the electron of the target atom by converting total energy of the gamma irradiation to electron. Besides, gamma irradiation can cause compton scattering which is loss of energy and change in direction of the gamma irradiation over elastic collision with electron. By the result of Compton scattering, contrary to others, gamma irradiation does not transform total energy to particle.

Neutrons can be classified according to their energy, such as neutron with energy greater than 100 MeV is high energy neutron, neutron with energy greater than 100-200 keV smaller than 10-20MeV is fast neutron, neutron with energy greater than 0,1eV smaller than 100 keV is epithermal neutron, neutron with energy almost equal to 1/40 eV is thermal/slow neutron, neutron with energy in the order of meV and μeV is cold/ultracold neutron. The neutron interaction with matter can be classified into two groups as scattered via nucleus in which direction and speed stays same after collision, and as absorbed via nucleus result in emission of radiation and fission where nucleus split into smaller nuclei. For scattered procedure, there might occur two collisions; elastic and inelastic collision. In elastic collision, neutron interacts with atom nucleus and result in scattering for both neutron and nucleus in different directions. In inelastic collision, neutron interacts with atom nucleus and result in scattering of neutron from nucleus and radiation of gamma ray. For absorption procedure, if thermal/slow neutron interacts with nucleus, it is absorbed and gamma rays irradiated. When neutron with energy between 0,1eV and 100 keV interacts with nucleus result in emission of charged particles such as proton, alpha. Thermal neutrons, interacts with nucleus and as a result the nucleus split into nuclei and energy.

Energy emitted via Sun is solar radiation which is reflected by atmosphere, clouds and from ground surface, absorbed by atmosphere, clouds and at ground surface. Apart from absorbtion and reflection, not all photons emitted via Sun converted in to electricity by solar cells. The visible, ultravioletand near infrared are able to contribute to power production, whereas radio waves, microwaves and most infrared photons will not. The Sun rays are defined as direct, diffuse and global solar radiation. Direct solar radiation is the Sun rays received to a surface perpendicular meanwhile diffuse solar radiation is scattered Sun rays after passing through atmosphere. Global solar radiation (H in W/m^2) is the total radiation that covers both diffuse and direct radiation. The correlation for monthly average daily global solar radiation on horizontal surface is given in below.

$$H = H_0\left[a + b\left(\frac{S}{S_0}\right)\right] \tag{2.4}$$

As it is seen, monthly average daily global solar radiation on horizontal surface depends on the monthly average daily extraterrestrial radiation H0, average daily sunshine S and average maximum possible daily sunshine duration S0. The correlation constants a and b vary according to considered region.

Photon energy is evaluated within this PhD thesis as photon emitted from a source which is irradiation and photon absorbed by a surface which is radiation as explained previously. However, flux definition is similar for both situations. Flux (Φ in number of rays per second. $meter^2$) is the ratio between power density (H in Watt/$meter^2$) and photon energy (E in Joules).

Generation of current occurs when energy of the photon is greater than bandgap energy of the pn junction. The energy of the photon is inversely proportional with the wavelength of the photon. The origin of this energy can either be solar radiation or gamma and neutron irradiation.

Efficiency of solar cell is the ratio between maximum power and power of radiation. To find the efficiency of solar radiated solar cell; power of radiation is the surface area (m^2) of solar cell product by solar radiation H with SI unit of W/m^2.Solar radiation or in other words power density H is proportional with the photon flux Φ and inversely proportional with the wavelength λ of the solar radiation.

$$\eta = \frac{P_{max}}{P_{rad}} = \frac{V_{oc} I_{sc} FF}{HA} \tag{2.5}$$

$$H(W/m^2) = \Phi \mathrm{E} = \Phi \frac{hc}{\lambda} \tag{2.6}$$

where;

h is the Planck's constant with the value of 6,62606957 x 10^{-34} $m^2 kg/s$

c is the speed of light in vacuum value of $3x10^8$m/s

On the hand, to find the efficiency of irradiated solar cell; power of radiation is the surface area (m^2) of solar cell product by irradiation H with SI unit of W/m^2. The irradiation power density H which is given with the equation below, is proportional with the photon flux Φ($m^{-2}s^{-1}$) and the photon energy E (joule).

$$H(W/m^2) = \Phi qE \tag{2.7}$$

$$\Phi = \frac{S}{4\pi d^2} \tag{2.8}$$

For neutron or gamma irradiated solar cell, flux Φ (n/cm^2/s) is proportional with emission rate S (n/s) and inversely proportional with the square of distance from the source d (cm). the flux correlation is given as in the above.

2.3 Degradation

As the time passes, the PV module/panel(s)' efficiencies that related to the effort made in relation to the output attained start to decrease according to environmental reasons such as solar irradiance, temperature, snow loads, dirt. The decrease in the 'performance' that relates to the output achieved is related to the degradation of the module. However, degradationshould not confused with failure which is defined as "the termination of the ability of an item to perform a required function."by IEC within the standard of IEC 60050-191) [113].

Besides, Kumar and Kumar mentioned reliability and durability of PV module [17]. Accordingly, reliabily of the PV is the capacity of PV to perform conversion of solar radiation to electric current for a defined time plan which measured according to the rate of failure. Also, durability is measured during time as degradation rate and decrease in performance step by step. Durability is achievement of expected performance of PV within a specific time period.

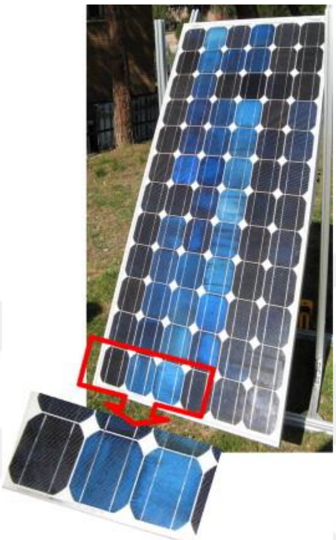

Figure 2.14 : Example of Discoloration; caused by deterioration of anti-reflective coating [114].

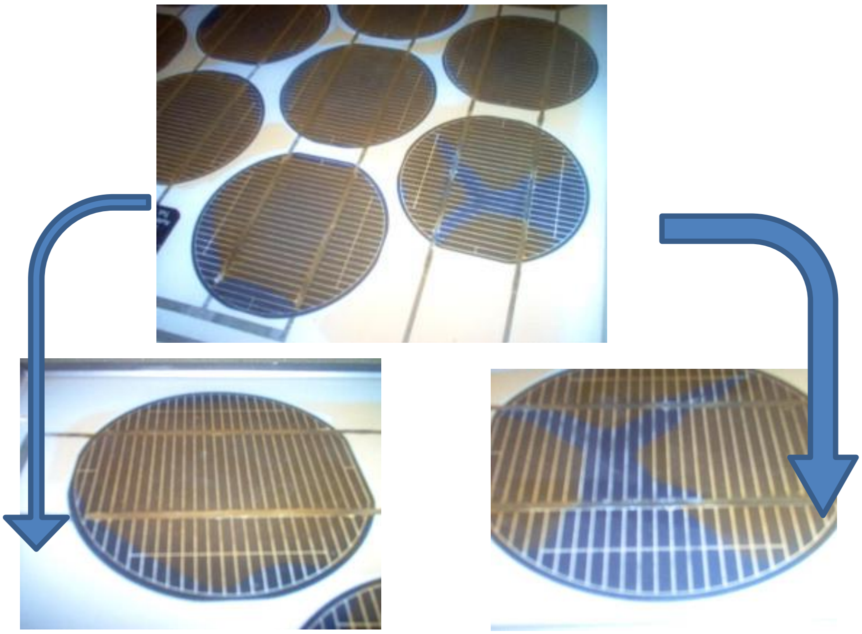

Figure 2.15 : Examples of Discoloration; browning occur caused by humidity after twenty years of operation[115].

There are several degradation modes such as discoloration, delamination, hot point, corrosion. Encapsulant quality, high temperature at location, dry heat, high UV radiation, humidity, chemical products that are four different silver salts (Silver Phosphate, Silver Sulphide, Silver Carbonate, Silver Acetate) and available on the front surface metallization as crystallites, insufficient adhesion between the cells and glass material make damage on the PV panel surface by browning and yellowing and on the grid fingers which is called as discoloration [16]–[18]. The visual examples of discoloration due to change in anti reflective coating and humidity are given in the figure above. This degradation type cause reduces the sunlight approaching the PV panels. Visual inspection and electrical characterization (I-V Characteristics) are used to detect discoloration.

Figure 2.16 : Corrosion of bus bar of twenty years operated PV module [115].

The degradation mode, corrosion causes, the moisture that penetrates in the PV panel through the laminated edge or back sheet, which result in reduction of the electrical resistance of the material and the loss of adhesion between metallic frame and cells. The visual example of corrosion is given in the figure above. Corrosion is detected by visual inspection and electrical characterization (I-V Characteristics).By time, the performance degradate by increasing the leakage current [16]–[18].The leakage current defined as without passing through load current passes base layer to emmitter layer and illustrated with a figure in the study of Nehme and et.al.[116]as given below.

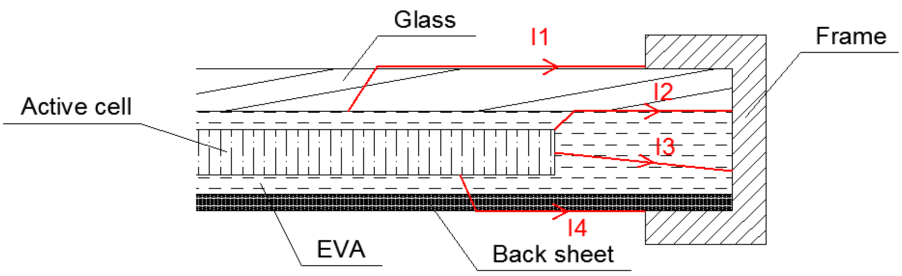

Figure 2.17 : Leakage current illustration in PV [116].

As shown leakage current can follow four different routes. Current goes through; glass and water molecules on the surface in the first route I1, electrons or ions in the second route I2, excapsulated layer EVAin the third route I3, back contact in the fourth route I4. They also states that leakage current increase with the increase of relative humidity, panel lifetime, panel voltage, temperature [116].

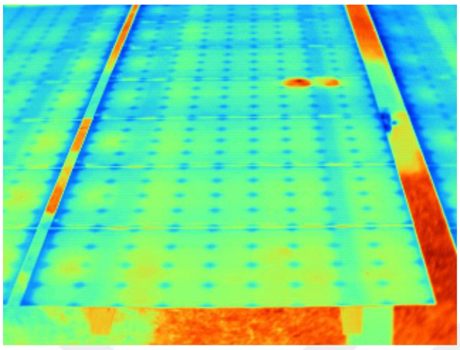

(a)

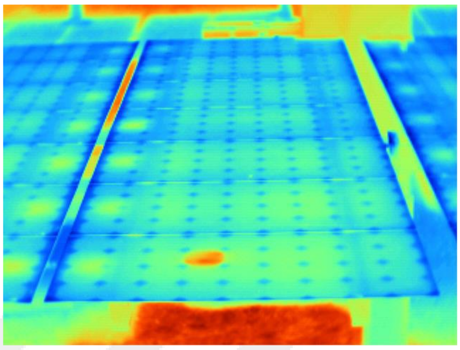

(b)

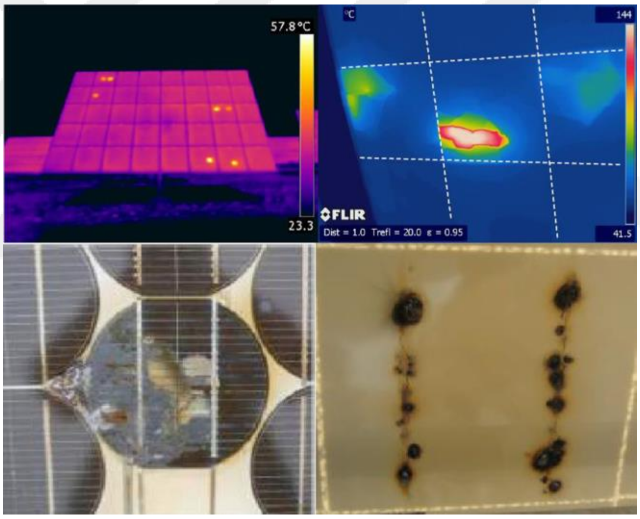

(c)

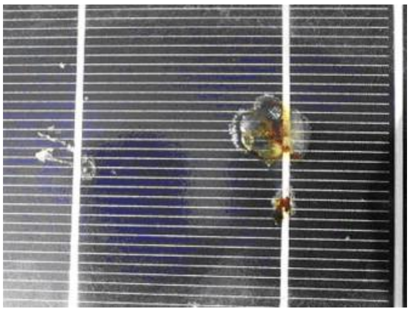

(d)

Figure 2.18 : (a), (b) Thermal imaging of Hot spot examples [117] ,(c) thermal imaging results and hot spot result in damages on front and back sheet of the PV module [118] and (d) Result of hot spot [114].

Hot spot is high temperature location on PV panel. It results from the generation of lesser current by solar cell than string current of the module which ultimately forms a hotspot on that cell, partial shadowing of cell in the PV panel and also electrically mismatched cells in the PV panel or interconnection failure [16]–[18]. The visual example of damage caused by hot spot is given in the figure above. Hot spot form local shunt, impurities, wafer resistance and deformation of p-n junction. Hot spot is detected by electrical characterization and IR imaging.

(a)

(b)

Figure 2.19 : Example of degradation mode; Delamination [118], [119].

Encapsulation is used for lamination in PV panels. However, use of cheap material and incorrect processing cause the adhesion loss at the interface between the encapsulating polymer and the front surface of a solar cell or between cells and front glass which is called as delamination and only detected by visual inspection [16]–[18]. The visual example of delamination is given in the figure above. This result in, increase in the light reflection and penetration of water into the module structure that accelerate the performance loss and increase the electrical risks for PV panel.

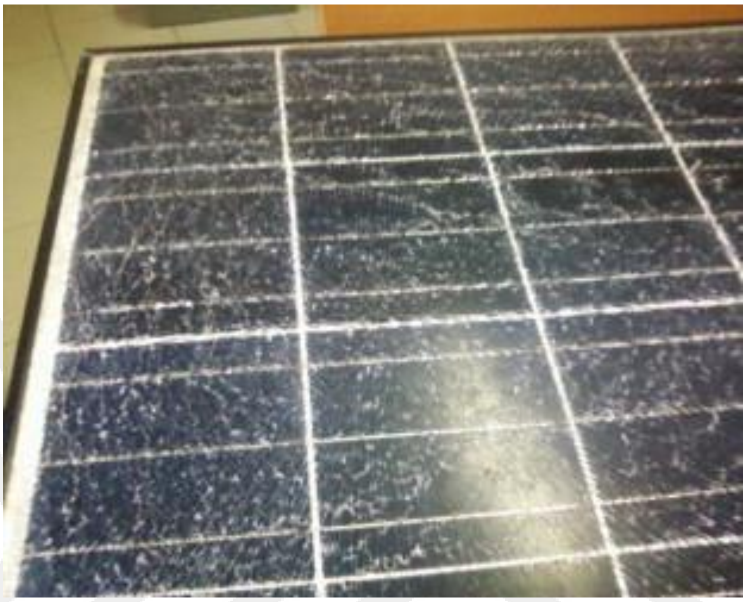

(a)

(b)

Figure 2.20 : Examples of breakages and cracks of **(a)** front surface [119] and **(b)** backsheet of the PV module [115].

Degredation mode that degrade the output power and also accelerate further degradation modes such as corrosion, delamination and discoloration is breakages and cracks such as micro-cracks that occur during the manufacturing process when mechanical and thermal stress is applied. The broken module may work properly; however, the risk of moisture infiltration and electrical shock will increase [16]–[18]. The visual examplse of breakages and cracks are given in the figure above. If breakages and cracks are large enough they can be visual inspected. Besides, electroluminesence imaging and electrical characterization (I-V Characteristics) can be used to detect degradation. The visual example of electroluminesence imaging of crack in the cell and crack seen via microscope are given in the figure below.

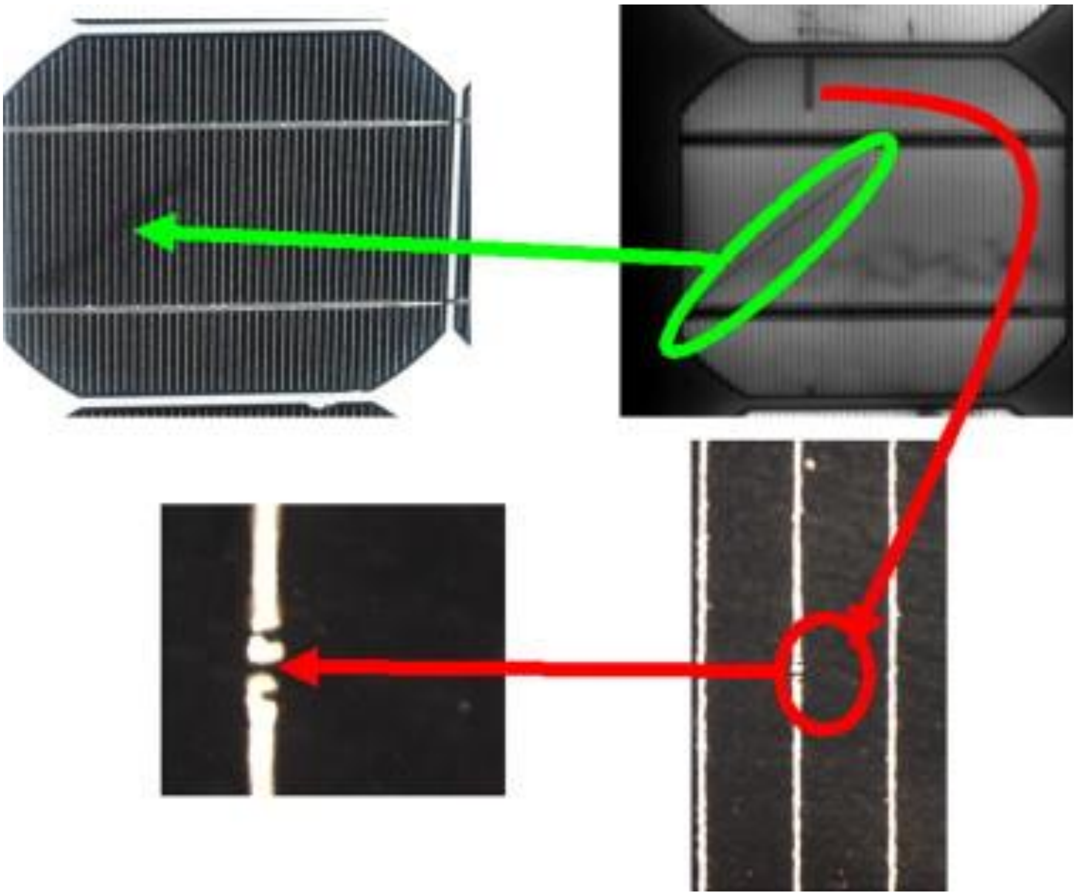

Figure 2.21 : Electroluminesence imaging of crack and crack seen via microscope [114].

Two defects detected with an EL image. The defect in the left upper image is visible by sight and consists of a crack in the cell. It can be detected using the EL method. The defect in the lower left image is only detectable using a microscope.

Soiling is another degradation mode that is seen on the surface of the PV caused by dirt, dust, bird dropping [16]–[18]. This result in reduction of the performance of the PV module with time. Soiling is detected via visual inspection.

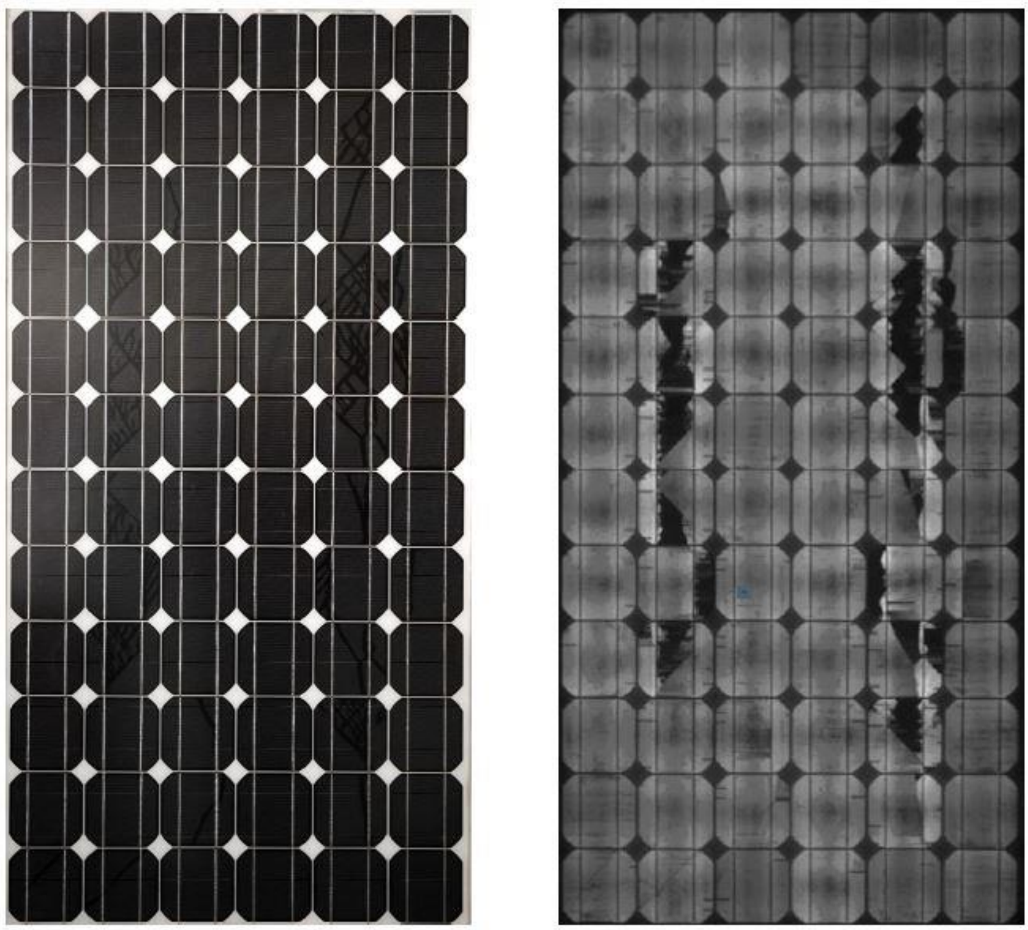

(a) (b)

Figure 2.22 : Example of snail trails; (a) front view and (b)Electroluminesence imaging [120].

The material and process related factors such as back sheet foil due to their water vapor permeability and EVA foil due to their chemical composition result in snail trails degradation. Snail trails reduces the sunlight approaching the PV panels. The visual example of snail trails is given in the figure above. The visual appearance of snail trails are irregular dark stripes and local discoloration of Ag contact fingers [16]–[18]. Close to micro-cracks across the solar cells and on the edges of solar cells. It can be detected via visual inspection, electrical characterization (I-V Characteristics).

The degradation mode; bubbles, is caused by similar to encapsulant delamination, but the difference in this case is that the area affected by the loss of EVA adhesion is comparatively small and combined with a swelling surface whose adhesion was already degraded [17]. The visual examples of bubbles is given in the figure above. It results in the overheating of modules and degrade the performance and therefore reduce the PV module lifetime and may seen in the encapsulant or module back side.

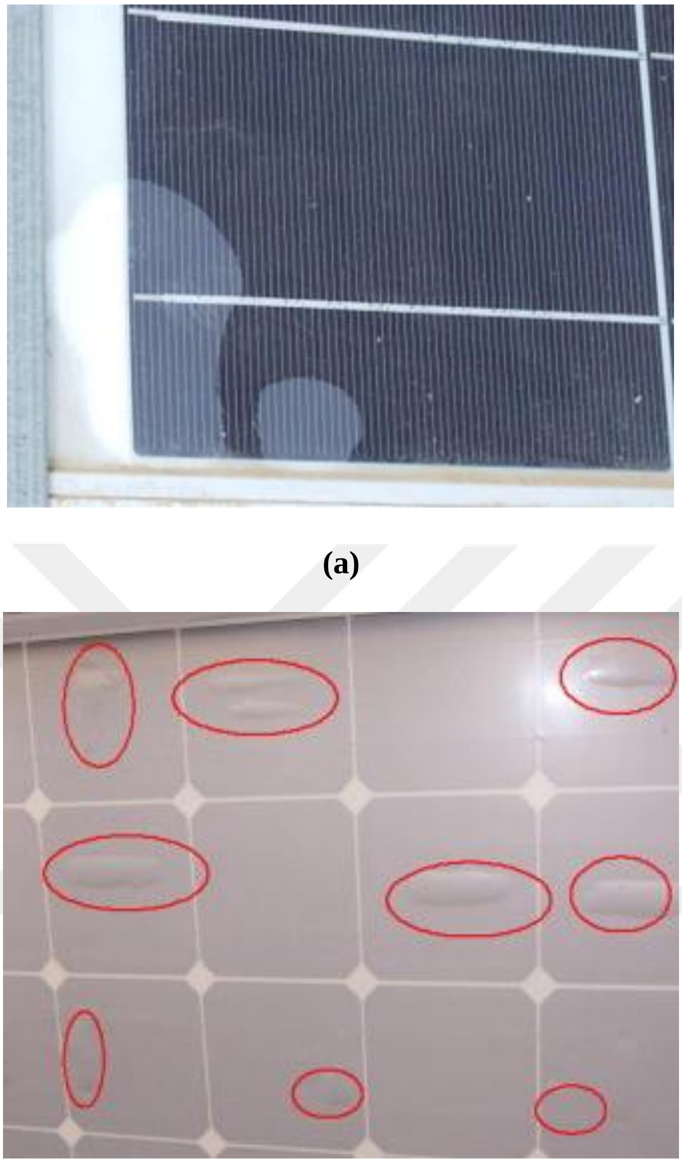

(a)

(b)

Figure 2.23 : Examples of bubbles on **(a)** front and **(b)** back surface of PV module [114].

Kumar and Kumar contributed a review to the literature at 2017 named ‘Performance assessment and degradation analysis of solar photovoltaic Technologies: A review’ [17] in which the causes and effects degradation modes via chart. According to review article; broken interconnect, broken cell, failure of solder bond, failure of junction box, arcing due to open circuits, corrosion, encapsulant delamination, loss of adhesion and elasticity, shunts at the scribe lines caused by high temperature, moisture or high voltage. Besides only high temperature cause; discoloration of encapsulant, hot spot as well.

Also the study bu Huang and Wang [121] states that increase in series resistance, decrease in parallel resistance and transmittance. The decrease in the transmittance cause in decrease in maximum power, short circuit current, open circuit voltage which is detected via I-V graph of PV module. On the other hand, it is mentioned that increase in series resistance effects short circuit current meanwhile does not change open circuit voltage. Decrease in parallel resistance make decrase in both short circuit current and open circuit voltage which decrease the fill factor so the quality of the PV.

Some of the degradation studies in the literature focuses on specificaly one or two degradation modes meanwhile others studies general performance losses by means of yearly degradation rate. Jordan and Kurtz, reviewed the litearature and summarize more than hundred paper at 2012. By the end of their study they gave degradation rates for each type of PV module. According to the review the degradation rate for monocrystalline and poly crystalline silicon PV module is 0,36%/years and 0,64%/years respectively [78].

Technology	Configuration	Number of. references		No. of Data Points		Median Exposure time (years)		R_d median (%/year)	
		Pre	Post	Pre	Post	Pre	Post	Pre	Post
a-Si	Module	10	12	45	31	7	2	0.96	0.87
	System	14	9	21	14	5	4	1.30	0.95
CdTe	Module	3	4	7	6	3	2	3.33	0.40
	System	3	2	3	6	10	3	0.69	0.30
CIGS	Module	2	6	20	10	8	3	1.44	0.96
	System	1	5	1	5	4	6	3.50	0.02
mono-Si	Module	31	11	1133	55	21	3	0.47	0.36
	System	19	13	42	37	7	5	0.90	0.23
multi-Si	Module	15	9	409	36	10	3	0.61	0.64
	System	6	8	5	21	9	5	0.60	0.59

Figure 2.24 : The screenshot of the degradation rates prior to (pre) and post (post) 2000 for different kind of PV modules from the study of Jordan and Kurtz [78].

On the other hand, the study by Dhoke and Mengede, gives the module degradation factor (MDF) correlation as eq.13. MDF is a result of decrease in the short circuit current which result in power loss [79].

$$\%MDF = \left(1 - \frac{\frac{I_{sc\_degrade}}{I_{sc\_ideal}} + \frac{V_{oc\_degrade}}{V_{oc\_ideal}}}{2}\right)100 \qquad (2.9)$$

For MDF, the ideal (the value at STC) and degraded value both for open circuit voltage and short circuit current need to be known. This correlation is used to define the degradation factor and afterwards has been compared with the degradation rate given in the figure above.

Besides the study by Er and et.al. [122] examines degradation modes and effects experimentally. They give degradation rate of electric key electric parameters such as short circuit current, open circuit voltage, maximum power, fill factor via eq.2.10 given below.

$$\mathrm{RD(X)\%} = \left(1 - \frac{\mathrm{X}}{\mathrm{X_0}}\right)\mathrm{x100} \qquad (2.10)$$

$$\mathrm{RDt(X)\%} = \left(\frac{\mathrm{RD(X)\%}}{\Delta \mathrm{t}}\right)\mathrm{x100} \qquad (2.11)$$

Key electric parameters represented as X for after degradation and X_0 for data at STC within this equation. Besides with the eq.11 above, the yearly degradation rate is given within perion of time Δt years. The experiments and analysis of the study as they stated open circuit voltage increased cause of hot spot which is result of partial shading.

2.4 Theoretical Performance Evaluation of Cell/Module/Panel

Dark IV measurements are made possible by comparing IV curves to a lot of information about the cell, as small fluctuations in light intensity bring a significant amount of noise to the system in lighting conditions, making it difficult to produce accurate readings. When a solar cell is dark, it can only be considered as a silicon diode with the knowledge we have. In the cell exposed to light, the silicon diode polarity is opposite to the current flow. For a string of solar cells, it is appropriate to consider a Schottky diode that can allow the cell to bypass and limit the reverse bias voltage to a safe level when a single cell in the dark interferes with current regardless of what other cells do. In the equivalent circuit design, the diode(s) are Schottky diodes. In the double diode model there are two Schottky diodes one represents diffusion of minority charge carriers into depletion region meanwhile other represents recombination in space charge region of the junction [42]. In the single diode model those diffusion and recombination mechanism is represented via single diode. The circuit equation can be obtained with regards to Kirchhoff's Laws as seen in the Eq.1. From the Current Law of Kirchhoff, the current passing through the circuit, and from the Voltage Law of Kirchhoff the potential difference between the edges of Schottky diode can be found in the Eq. 2.13, Eq. 2.14. Besides, by the help of Ohm's Law the current passing through the shunt resistor also found. The further explanation is given in the Photovoltaic (PV) cell/module/panel section above.

$$I = I_{ph} - I_D - I_{sh} \tag{2.12}$$

$$I_D = I_0(e^{qV_D/AkT} - 1) \tag{2.13}$$

$$V_D = V + IR_s \tag{2.14}$$

Where, Current through shunt resistor can calculate with the Eq. 2.15.

$$I_{sh} = \frac{V_D}{R_{sh}} = \frac{V + IR_s}{R_{sh}} \tag{2.15}$$

The current passing through diode is represented as I_D is illustrated in the equation above [104]. Ergo, for single diode model of ideal photovoltaic cell at standard test condition, the characteristic equation is given by the Eq. 2.16.

$$I = I_{ph} - I_0\left(e^{q(V+IR_s)/AkT} - 1\right) - \frac{V + IR_s}{R_{sh}} \tag{2.16}$$

where Saturation Current, Reverse Saturation Current and Photocurrent are

$$I_0 = I_{rs}\left(\frac{T}{T_{STC}}\right)^3 exp\left[\frac{qE_g\left(\frac{1}{T_{STC}} - \frac{1}{T}\right)}{nk}\right] \tag{2.17}$$

$$I_{rs} = \frac{I_{sc,STC}}{\exp\left[\frac{qV_{oc}}{nN_skT}\right] - 1} \tag{2.18}$$

$$I_{ph} = \left[I_{SC,STC} + \mu_{\mathrm{Isc,STC}}(T - T_{STC})\right]\frac{G}{G_{STC}} \tag{2.19}$$

With this set of equations, the output current of a photovoltaic module can be calculated by assuming the temperature of the PV module for single diode model (T) is equal to ambient temperature (T_{amb}).

Similar, inference can be done for double diode equivalent circuit design with regard to Kirchhoff' Laws and Ohm's Law. The important point is that first and second diode are parallel so the electric potential difference between the edges of the diodes are equal however as diodes are corresponds to different physical phenomena for ideal photovoltaic cell, the saturation current and diode ideality factors are different, so the current passing through diodes by the Eq. 2.21 and 2.22.

$$I = I_{ph} - I_{D1} - I_{D2} - I_{sh} \tag{2.20}$$

$$I_{D1} = I_{01}\left(e^{qV_{D1}/A_1kT} - 1\right) \tag{2.21}$$

$$I_{D2} = I_{02}(e^{qV_{D2}/A_2kT} - 1) \tag{2.22}$$

$$V_{D1} = V_{D2} = V + IR_s \tag{2.23}$$

$$I_{sh} = \frac{V_{D1}}{R_{sh}} = \frac{V_{D2}}{R_{sh}} = \frac{V + IR_s}{R_{sh}} \tag{2.24}$$

The current passing through the first and second diodes are represented as I_{D1} and I_{D2},respectively, are given in the equation above. For double diode model of ideal photovoltaic cell at standard test condition, the characteristic equation is obtained as below eq. 2.25.

$$I = I_{ph} - I_{01}\left(e^{qV_{D1}/A_1kT} - 1\right) - I_{02}\left(e^{qV_{D2}/A_2kT} - 1\right) - \frac{V + IR_s}{R_{sh}} \tag{2.25}$$

For both models, it is clearly seen from the equivalent circuit and the equations, the decrease shunt resistor will decrease the output current (I) so the output power (P) of the PV cell which will decrease the efficiency of the cell. Also, the increase series resistor will decrease the output current (I) so the output power (P) of the PV cell which will decrease the efficiency of the cell. Therefore, decrease in the shunt resistor points out the degradation of the cell. The shunt resistance might be accepted as it goes to infinity and the series resistor might be accepted as it goes to zero.

The electric equivalent circuit design of PV cell is explained above. The single diode model and double diode model for ideal PV cell is evaluated at standard test conditions. However, at the outdoor conditions module temperature varies with the solar radiation and ambient temperature as illustrated in the Eq. 2.26. By considering the change in the module temperature which is given in the equations 2.27 and 2.28 below, short circuit current and open circuit voltage will be affected as.

$$T_m = T_{amb} + \frac{G}{800}(NOCT - 20℃) \tag{2.26}$$

$$I_{SC}(G, T_m) = \frac{G}{G_{STC}}\left[I_{SC,STC} + \mu_{I_{sc}}(T_m - T_{STC})\right] \tag{2.27}$$

$$V_{oc}(G, T_m) = V_{OC,STC} + \frac{kN_s T_m A}{q}\ln(G) + \mu_{V_{oc}}(T_m - T_{STC}) \tag{2.28}$$

Temperature correlation with ambient temperature and solar irradiance dependence is considered from the study by Segado and et.al as seen in the Eq. 2.29 [76].The other correlations are considered from the study by Ibrahim and Anani where they listed modified correlations due to module temperature and solar irradiance as seen in the Eq. 2.30 [72].

$$I_0(G, T_m) = \frac{\left(\frac{G}{G_{STC}}\right)\left(I_{SC,STC} + \mu_{I_{sc}}(T_m - T_{STC})\right)\exp\left(\frac{q}{kN_s T_m n}\left|\mu_{V_{oc}}\right|(T_m - T_{STC})\right)}{\left(\frac{GI_{SC,STC}}{I_{0_{STC}}} + 1\right)^{T_{STC}/T_m} - \exp\left(\frac{q}{kN_s T_m n}\left|\mu_{V_{oc}}\right|(T_m - T_{STC})\right)} \tag{2.29}$$

where saturation current at STC is given with

$$I_{0\_STC} = \frac{I_{sc,STC}}{\exp\left[\frac{qV_{OC}}{nN_s kT}\right] - 1}\ . \tag{2.30}$$

When the PV module is not illuminated, it generates saturation current Io at the forward bias and reverse saturation current at reverse biased which is also called leakage current as reverse saturation current is extremely small. When the PV module is illuminated, it generates photocurrent Iph as seen in the Eq. 2.31 [104].

$$I_{ph}(G,T_m) = \left(\frac{G}{G_{STC}}\right) I_{ph}(T_m) \tag{2.31}$$

Where the temperature dependence of the photocurrent is given by the Eq. 2.32.

$$\begin{aligned} I_{ph}&(T_m) \\ &= \frac{I_{sc,STC}}{\exp\left[\frac{qV_{oc}}{nN_s kT_m}\right] - 1} \left(\frac{T_m}{T_{STC}}\right)^3 exp\left[\frac{qE_g\left(\frac{1}{T_{STC}} - \frac{1}{T_m}\right)}{nk}\right] \exp\left[\left(V_{OC,STC}\right.\right. \\ &\left.\left. + \mu_{V_{oc}}(T_m - T_{STC})\right)\frac{q}{kN_s\,T_m n}\right] + \frac{V_{OC,STC} + \mu_{V_{oc}}(T_m - T_{STC})}{R_{sh}} \end{aligned} \tag{2.32}$$

PV cell allows current in one direction while blocks in the opposite direction as it is considered as pn junction [103]. The correlation that is given by the Eq. 2.33 represents the single diode model output current of PV module that varies with the solar radiation and module temperature which is considered with this study.

$$I(V,G,T_m) = I_{ph}(G,T_m) - I_0(G,T_m)\left[\exp\left(\frac{q(V + IR_s)}{nkN_sT_m}\right) - 1\right] - \left(\frac{V + IR_s}{R_{sh}}\right) \tag{2.33}$$

The theoretical explanation of extraction methods is explained in the next section. Also the current voltage and power voltage graphs which indicate the performance, are generated theoretically with the characteristic equations and also experimentally as will be explained in the following sections.

2.4.1 Parameter identification for photovoltaic models

The PV cell/module/panel performance can have evaluated by diode methods with regards to the given parameters by manufacturer. However, to be more precise, the unknown paremeters such as series resistance, saturation current, ideality factor and photocurrent, should be extracting from known parameters such as open circuit voltage, short circuit current, voltage at maximum power point, currrent at maximum power point.

In the literature, there are several studies for extraction of unknown parameters and classifications of methods [22], [23], [25]–[30], [35]–[38], [64], [104]. For example, in the book written by Di Piazza and Vitale, the parameter extraction methods are classified under Analytic Solution, Numerical Solution, Heuristic Method-Based

Solution. Analytic Solution is based on the experimental results, meanwhile Numerical Solution can be conducted either with experimental results or manufacturer datasheet values. Heuristic Method-Based Solution is based on both the experimental results and the manufacturer datasheet [104]. On the other hand, in the study conducted by Toprak and et.al., they extracted parameters by Simplified Explicit Method which uses manufacturer datasheet values and by Slope Method which uses experimental results [37]. In the both study by Di Piazza and Vitale [104], Toprak and et. al. [37] had explained similar method with different classification as Analytic Solution and Simplified Explicit Method, respectively.

The PV cell/module/panel has characteristic key points such as open circuit voltage, short circuit current. Some key evaluations can be obtained by the experiments done in the STC (Standard Test Conditions) and NOCT (Normal Operating Cell Temperature) conditions with regard to the international standards which are given in the manufacturer datasheet of the device. The mentioned key evaluations are open circuit voltage, short circuit current, current and voltage at maximum power point which hereinafter expressed as known parameters. Besides, the saturation current, photocurrent, series resistance, shunt resistance and ideality factor are not commonly found in the manufacturer datasheet. Those values are obtained to be extracted considering known parameters and/or experiment results which hereinafter expressed as unknown parameters.

Table 2.1 : Model details in this thesis.

Model Number	Data Sets	Unknown Parameters	Extraction of Unknown Parameter	Diode	Condition
1	Manufacturer Datasheet	Five	Not extracted	Single diode	STC
2	Manufacturer Datasheet	Five	Not extracted	Single diode	Outdoor
3	Manufacturer Datasheet	Four	Extracted	Single diode	STC
4	Manufacturer Datasheet and Experimental Data	Seven	Extracted	Double diode	STC or Outdoor

Extraction can be data sheet data-based or experimental / operational data-based. There are many options available to suit the purpose of any analytical problem. PV cell properties of target compounds, parameter matrix and available instrumentation are decisive for choosing the best extraction technique and finding optimum extraction conditions. There are many different models for this purpose.

The PV cell current correlations for both single diode and double diode models, are analytic functions that do not satisfy polynomial equation and can be called as transcendental equations which makes the models implicit [28]. So, analytic solution of the PV cell current correlation cannot be obtained by only known parameter, because of the complexity of the single diode or double diode models. In this paper, to identify the unknown parameters, simplified explicit method, slope method and combination of simplified explicit method and slope method have evaluated. Extraction techniques can be classifying as Simplified Explicit Method and Slope Method, and Mixed.

2.4.2 Simplified explicit method

In the simplified explicit method, for single diode model of PV cell, the known parameters are manufacturer datasheet values which are current and voltage at maximum power point, voltage of open circuit, current of short circuit, where the unknown parameters are saturation current, photocurrent, series resistance and ideality factor. In the simplified explicit method explained in this section there are two acceptances. One of them is that the shunt resistance is large enough that there current through the resistance is equal to zero. The other acceptance is that photocurrent is equal to the short circuit current. With regard to acceptances, the current correlation of single diode model become as below.

$$I = I_{ph} - I_0 \left[\exp\left(q \frac{V + IR_s}{AkT} \right) - 1 \right] \tag{2.34}$$

There are two important points that is considered in this evaluation which are open circuit, where the current passes through the equivalent circuit design is zero and voltage is Voc, and maximum power point where the current passes through the equivalent circuit design is IM and voltage is VM that are illustrated with the equations below.

$$0 = I_{ph} - I_0 \left[\exp\left(q \frac{V_{oc}}{AkT} \right) \right] \tag{2.35}$$

$$I_M = I_{ph} - I_0 \left[\exp\left(q\frac{V_M + I_M R_s}{AkT}\right)\right] \tag{2.36}$$

As it is stated above that one of the acceptances is that photo generated current of PV cell is equal to short circuit current, the current equation at open circuit and maximum power point can be rewritten as below.

$$I_0 = I_{sc}\left[\exp\left(-q\frac{V_{oc}}{AkT}\right)\right] \tag{2.37}$$

$$I_M = I_{sc}\left[1 - \exp\left(q\frac{V_M - V_{oc} + I_M R_s}{AkT}\right)\right] \tag{2.38}$$

$$R_s = \frac{\left(\frac{AkT}{q}\ln\left(1 - \frac{I_M}{I_{sc}}\right) + V_{oc} - V_M\right)}{I_M} \tag{2.39}$$

$$A = \frac{[q(2V_M - V_{oc})]}{\left[kT\left(\frac{I_M}{I_{sc} - I_M} + \ln\left(1 - \frac{I_M}{I_{sc}}\right)\right)\right]} \tag{2.40}$$

So, saturation current is found by rearranging the current equation at open circuit point. Also, from the current equation at maximum power point, the series resistance is deduced. Besides, the ideality factor is also found by the use of both current equations at open circuit and maximum power point.

2.4.3 Slope method

As explained previously, there are characteristic points in the I-V curve of a PV cell such as open circuit voltage, short circuit current, voltage and current at maximum power point which are also called as known parameters. Apart from current and voltage values, the series and shunt resistances can be obtained from the I-V curve.

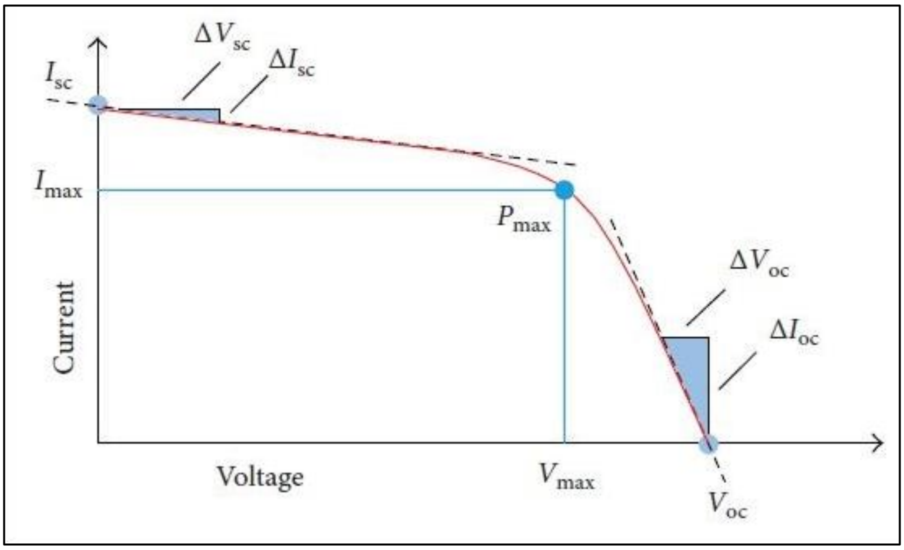

Figure 2.25 : Resistance extraction from I-V curve [55].

The figure above illustrates both known parameters and slopes at open and short circuit points.

$$R_{sh} = -\frac{\Delta V_{sc}}{\Delta I_{sc}} \tag{2.41}$$

$$R_s = -\frac{\Delta V_{oc}}{\Delta I_{oc}} \tag{2.42}$$

$$\frac{dI}{dV} = -I_0\left(\frac{q}{AkT}\right)e^{q(V+IR_s)/AkT}\left(1 + R_s\frac{dI}{dV}\right) - \frac{1}{R_{sh}} - \frac{R_s}{R_{sh}}\frac{dI}{dV} \tag{2.43}$$

$$\frac{dV}{dI} = -\frac{1 + \frac{R_s}{R_{sh}} + R_s\left[I_0\left(\frac{q}{AkT}\right)e^{q(V+IR_s)/AkT}\right]}{\frac{1}{R_{sh}} + I_0\left(\frac{q}{AkT}\right)e^{q(V+IR_s)/AkT}} \tag{2.44}$$

At open circuit voltage, shunt resistance goes to zero. Similarly, at short circuit current, series resistance goes to zero.

$$R_s = -\frac{dV}{dI}\bigg|_{oc} \tag{2.45}$$

$$R_{sh} = -\frac{dV}{dI}\bigg|_{sc} \tag{2.46}$$

2.4.4 Combination of simplified explicit method and slope method

In the literature, there are studies that use both simplified explicit and slope methods to identify the parameters so the performance and degradation of the PV cell/module/array with regard to the manufacturer datasheet values. However, in the case of unavailable information about the key points, there occurs a need to identify the performance and degradation of the PV cell/module/array with regard to experimental data. In the study of Wei and et al. [75] four known points are considered to identify the five unknown points of PV cell as listed in the table below.

Table 2.2 : Known and unknown parameters of the model.

Known Parameters	Unknown Parameters
$(I_{sc},0)$	A
(I_a, V_a)	R_s
(I_b, V_b)	R_{sh}
(I_c, V_c)	I_o
	I_{ph}

The known and unknown parameters are also illustrated in the figure below. As it is clearly seen the manufacturer datasheet values such as voltage at open circuit, voltage and current at maximum power point are not considered except current at short circuit. In this study, the PV cells used in the experimental study do not have manufacturer datasheet values. In order to, to identify the parameters so the performance and degradation of the PV cells, it is necessary to evaluate the device with only the experimental results.

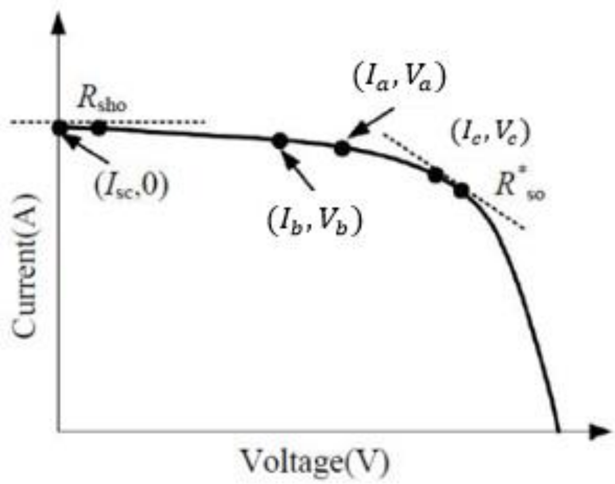

Figure 2.26 : Known parameters according to the model [75].

The current correlation for single diode five parameter model is evaluated to identify the unknown parameters. The derivative of current by voltage allow to find the shunt resistance at short circuit point.

$$I = I_{ph} - I_0\left(e^{q(V+IR_s)/AkT} - 1\right) - \frac{V + IR_s}{R_{sh}} \qquad (2.47)$$

$$\frac{dV}{dI} = -\frac{\frac{AkT}{q}}{I_{ph} - I_o - I - \left[\frac{V + IR_s - \frac{AkT}{q}}{R_{sh}}\right]} + R_s \qquad (2.48)$$

$$R_{sh} = \left[\frac{1}{R_{sho} - R_s} - q\frac{I_o}{AkT}exp\left(q\frac{I_{sc}R_s}{AkT}\right)\right]^{-1} \qquad (2.49)$$

Further, at short circuit point, from the current correlation for single diode five parameter model, photo generated current is found as;

$$I_{ph} = I_o\left[\exp\left(q\frac{I_{sc}R_s}{AkT}\right) - 1\right] + \left(1 + \frac{R_s}{R_{sh}}\right)I_{sc} \qquad (2.50)$$

Three different current equations can be obtained from the current correlation for single diode five parameter model for known selected points; I_a, I_b, $I_c$as listed below.

$$I_a = I_{ph} - I_0\left(e^{q(V_a+I_aR_s)/AkT} - 1\right) - \frac{V_a + I_aR_s}{R_{sh}} \qquad (2.51)$$

$$I_b = I_{ph} - I_0\left(e^{q(V_b+I_bR_s)/AkT} - 1\right) - \frac{V_b + I_bR_s}{R_{sh}} \qquad (2.52)$$

$$I_c = I_{ph} - I_0\left(e^{q(V_c+I_cR_s)/AkT} - 1\right) - \frac{V_c + I_cR_s}{R_{sh}} \qquad (2.53)$$

In this model there are assumptions that are considered as listed;

i. $R_{sh} \approx R_{sho} \gg R_s$
ii. $V_{oc} \gg I_{sc}R_s$
iii. $\exp\left[\frac{qV_{oc}}{AkT}\right] \gg \exp\left[\frac{qI_{sc}R_s)}{AkT}\right]$

The resistance values at point (I_{sc},0) and (I_c, V_c) are obtained by slope method which are $R_{sho}$and R_{so}^*, respectively. Considering, assumptions and current equations the following unknown parameters are obtained. To begin with, the ideality factor is;

$$A = \frac{q\left(-C_2 - \sqrt{{C_2}^2 - 4C_1C_3}\right)}{2C_1kT} \tag{2.54}$$

where C_1, C_2 and C_3 are constants.

$$C_1 = -\frac{ln\left[\frac{I_{sc} - I_a - \frac{V_a}{R_{sho}}}{I_{sc} - I_b - \frac{V_b}{R_{sho}}}\right]}{R_{sho}} \tag{2.55}$$

$$\begin{aligned} C_2 = -ln\left[\frac{I_{sc} - I_a - \frac{V_a}{R_{sho}}}{I_{sc} - I_b - \frac{V_b}{R_{sho}}}\right].\left[I_{sc} - I_c - \frac{V_c}{R_{sho}}\right] - [I_a - I_b] \\ + \frac{V_a - V_b + (I_a - I_b)R_{so}^*}{R_{sho}} \end{aligned} \tag{2.56}$$

$$C_3 = [V_a - V_b + (I_a - I_b)R_{so}^*].\left[I_{sc} - I_c - \frac{V_c}{R_{sho}}\right] \tag{2.57}$$

After finding ideality factor, series resistance and saturation current is found as;

$$R_s = R_{so}^* - \frac{\frac{AkT}{q}}{I_{sc} - I_c - \frac{V_c}{R_{sho}} + \frac{AkT}{qR_{sho}}} \tag{2.58}$$

$$I_o = \left(I_{sc} - I_a - \frac{V_a}{R_{sho}}\right) \exp\left[\frac{q(V_a + I_aR_s)}{AkT}\right] \tag{2.59}$$

According to the model, while implementing, the shunt resistance at short circuit point and series resistance at selected known parameter point should be obtained by slope method. Then, ideality factor, series resistance and saturation current are solved respectively, according to the explicit method. By calculating $R_s, I_o$and A, shunt resistance and photo generated current are found with the equations given above.

In the following section within this thesis, it is aimed to adapt this idea of selecting four known parameters rather than key points given in the manufacturer data sheet, to double diode seven parameter model which depends on the solar irradiance and temperature. It is foreseen that by improving single diode five parameter model to double diode seven parameter model will give more appropriate performance and degradation results compared with the experimental results.

2.4.5 Seven parameter double diode model

The PV cell current correlations according to the equivalent circuit design both single diode and double diode models, are analytic functions that do not satisfy polynomial equation and can be called as transcendental equations which makes the models implicit [28]. Because of the complexity of the problem, the solution to the PV cell current equation can be obtained by extracting unknown parameters such as first and second diode saturation current, ideality factor of first and second diode, series resistance, shunt resistance. The single diode model was evaluated with the equation 1 below. However, in the double diode model the equation is given as eq. 2.61 below. For the seven parameter double diode model the study by Orioli and Di Gangi [74] is considered.

$$I = I_{ph} - I_0\left[\exp\left(q\frac{V+IR_s}{AkT}\right) - 1\right] \tag{2.60}$$

$$I = I_{ph} - I_{01}\left(e^{\frac{V+IR_S}{n_1 T}} - 1\right) - I_{02}\left(e^{\frac{V+IR_S}{n_2 T}} - 1\right) - \frac{V+IR_S}{R_{sh}} \tag{2.61}$$

Where $n_1 = \frac{a_1 N_s k}{q}$ and $n_2 = \frac{a_2 N_s k}{q}$. The extracted parameters' correlations for STC are given as below. In this model, the photovoltaic device is evaluated at standard test condition by considering the datasheet values and experimental data. The simplified explicit method and slope method are used together to extract the seven unknown parameters of the model. Later, the performance results are evaluated by current correlation of photovoltaic device.

$$I_{ph,STC} = I_{01,STC}\left(e^{\frac{V_{oc,STC}}{n_1 T_{STC}}} - 1\right) + I_{02,ref}\left(e^{\frac{V_{oc,STC}}{n_2 T_{STC}}} - 1\right) + \frac{V_{oc,STC}}{R_{sh,STC}} \tag{2.62}$$

$$R_{sh,STC} = \frac{R_{sho} - R_{s,STC}}{1 + \left(R_{s,STC} - R_{sho}\right)\left[\frac{I_{01}}{n_1 T_{STC}} e^{\frac{I_{sc,STC} R_{s,STC}}{n_1 T_{STC}}} + \frac{I_{02}}{n_2 T_{STC}} e^{\frac{I_{sc,STC} R_{s,STC}}{n_2 T_{STC}}}\right]} \quad (2.63)$$

$$I_{01,STC} = \frac{m_{22}A - m_{12}B}{m_{11}m_{22} - m_{12}m_{21}} \quad (2.64)$$

$$I_{02,STC} = \frac{m_{11}B - m_{21}A}{m_{11}m_{22} - m_{12}m_{21}} \quad (2.65)$$

Where $m_{11}, m_{12}, m_{21}, m_{22}, A\ and\ B$ are given as below;

$$m_{11} = e^{\frac{V_{oc,STC}}{n_1 T_{STC}}} - \left(1 + \frac{V_{oc,STC} - I_{sc,ref} R_{s,STC}}{n_1 T_{STC}}\right) e^{\frac{I_{sc,STC}}{n_1 T_{STC}}} \quad (2.66)$$

$$m_{12} = e^{\frac{V_{oc,STC}}{n_2 T_{STC}}} - \left(1 + \frac{V_{oc,STC} - I_{sc,STC} R_{s,STC}}{n_2 T_{STC}}\right) e^{\frac{I_{sc,STC}}{n_2 T_{STC}}} \quad (2.67)$$

$$m_{21} = e^{\frac{V_{oc,STC}}{n_1 T_{STC}}} - e^{\frac{V_{mp,STC} - I_{mp,STC} R_{s,STC}}{n_1 T_{STC}}} - \left(\frac{V_{mp,STC} - I_{mp,STC} R_{s,STC}}{n_1 T_{STC}}\right) e^{\frac{I_{sc,STC}}{n_1 T_{STC}}} \quad (2.68)$$

$$m_{22} = e^{\frac{V_{oc,STC}}{n_2 T_{STC}}} - e^{\frac{V_{mp,STC} - I_{mp,STC} R_{s,STC}}{n_2 T_{STC}}} - \left(\frac{V_{mp,STC} - I_{mp,STC} R_{s,STC}}{n_2 T_{STC}}\right) e^{\frac{I_{sc,STC}}{n_2 T_{STC}}} \quad (2.69)$$

$$A = I_{sc,STC} - \left(\frac{I_{sc,STC} R_{s,STC} - V_{oc,STC}}{R_{sho} - R_{s,STC}}\right) \quad (2.70)$$

$$B = I_{mp,STC} - \left(\frac{I_{mp,STC} R_{s,STC} + V_{mp,STC} - V_{oc,STC}}{R_{sho} - R_{s,STC}}\right) \quad (2.71)$$

In the equations above, the R_{sho} is the shunt resistance that is received from the I-V graph of the considered PV cell/module. In the study by Orioli and Di Gangi [74] they consider STC as references conditions and further in that study they use reference extracted parameters to identify the unknown parameters at conditions different than STC. In this thesis report, the performance evaluated with the study by Orioli and Di Gangi [74] for STC conditions.

2.4.6 Computational studies with regard to theoretical evaluations

MATLAB is a matrix-based language and a platform that can be used not only for to solve wide range of scientific problems but also design the problem. The high quality graphics allow user to visualize data and evaluate problem results easily. MATLAB can be integrated with SQL, Excel etc. and so enable user to receive data from other sources [12]. Also it has an environment within itself which is called Simulink. Simulink is a simulation and model-based design environment integrated with MATLAB. The integration between MATLAB and Simulink allows user to export simulation results to MATLAB and import algorithms into Simulink, which makes easier to design a system and simulate the dynamic behavior of the designed system [123], [124].

Simulink is a platform within its own library. These libraries have blocks with specific functions. System setup can be done by means of blocks. By using the blocks containing the mathematical functions of the Simulink platform, the investigation of the considered system can be examined through the equations of the system for instance current correlation of solar module depending on the environmental conditions. On the other hand, the Simulink platform also has its own unique systems for instance with solar cell block the current characteristics can also have evaluated without defining correlations as it is embedded in the block [124].

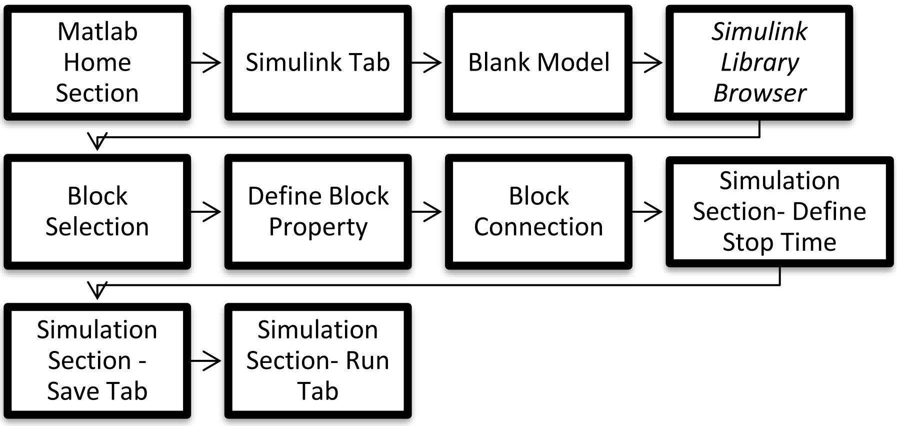

Figure 2.27 : Flowchart diagram of creating Simulink System.

In order to create a system via Simulink, the flowchart of steps is given above. First it is necessary to open a Simple Simulink Model from the Simulink button at Home tab of Matlab. When Simulink Start Page opened, the Blank Model should be selected to create new model different from sample projects. To built and edit a model in the

Simulink Editor, the Blocks that the code is embedded within themselves, should be selected via ‘Simulink Library Browser’ and drag to model untitled on Simulink Editor. The blocks, used within this PhD thesis, that is listed in the table below added. If necessary, the block properties should be defined such as the maximum and minimum values of X axis and Y axis of XY Scope Block which creates plot with its input data. To find the definition and further information about the block, right-click the block and select the help section.

Most of blocks has both input ports which the input data of the block fuction is given to process and output ports which the processed data via the block is optained. The blocks connected between input and output ports by creating lines which is simply dragging output port arrow to the input port arrow of other block. The block connecting is conducted regarding to the considered current correlations. Stop Time should be defined Simulation Section which is the time simulation will stop after runtime. Besides, the system generated should be saved, therefore Save tab from Simulation Section selected. Afterwards, the simulation run to process and receive the output of the model.

Table 2.3 : Block List and Libraries.

Block	**Block Function**	**Library**
Constant	Generates constant value signal	Simulink/Sources
XY Scope	Generates X-Y Graph with the input data assigned.	Simulink/Sinks
Add	The block is used to sum or subract the input data that is given to the block.	Simulink / Math Operations
Product	The block is used to product or divide the input data that is given to the block.	Simulink / Math Operations
Pow	The block is used take the power of the input data that is given to the block.	Simulink / Math Operations
Exponential	The block is used take the exponential of the input data that is given to the block.	Simulink / Math Operations
Ramp	Block generates signal with Start Time, Initial Output and change rate defined by the user.	Simulink / Sources
Input	Used as input port for subsystem which the input data is shared via model.	Simulink/Sinks
Outport	Used as output port to shows the output data.	Simulink/Sinks
To Workspace	Send data to the Matlab Workspace to save data.	Simulink/Sinks
From Workspace	Receive saved data from Matlab Workspace.	Simulink/Sinks

The library that consist the considered block is also given in the table. The libraries are Sources, Sink and Math Operations. The Sources Library consist of blocks with signal data to simulate model. The Sink Library consist of blocks that store and share data. The Math Operation Library consist of blocks that performs mathematical function. If further detail information about any consept or item is necessary, the Documentation Service of MATLAB/Simulink can be at the ‘help textbox button’ on the upper part of the programme. Also there are examples that might be found related with blocks, libraries or any other consepts, function, definition etc.

There are two blocks given in the table above related to workspace. The stated ‘Workspace’ is the Matlab base workspace which allows to save data to workspace and used saved data in furher evaluations or to receive data from workspace to Simulink to process it within the Simulink model.

After creating system either with series of correlation or a single block and run the simulation, to analyze the output data, the simulink platform can be used or data can be sent to Matlab's workspace.

In this PhD study, Simulink platform is used to evaluate single diode model for crystalline silicon solar modules within the Zuhal ER’s Laboratory at ITU Faculty of Arts and Sciences. The existing solar cell or PV array blocks are not used, instead the performance correlations are evaluated by generating block system and a unique PV module system of this PhD. Each current correlation (which are explained in the previous section in detail and also given in each subgroup explanation below) is generated within subgroups to form performance evaluation system of a crystalline module under varying ambient temperature and solar radiation single diode model.

The illustration of PV module via MATLAB-Simulink is given in the fig.2.8(a) below. The temperature in °C and solar irradiance in W/m^2 values are input data submitted by the user via constant block. The input data process within the PV MODULE model which the model detailed in the following. By the end of the simulation, the electrical characteristics, current-voltage data seperaretly are obtained via arrays as output data.

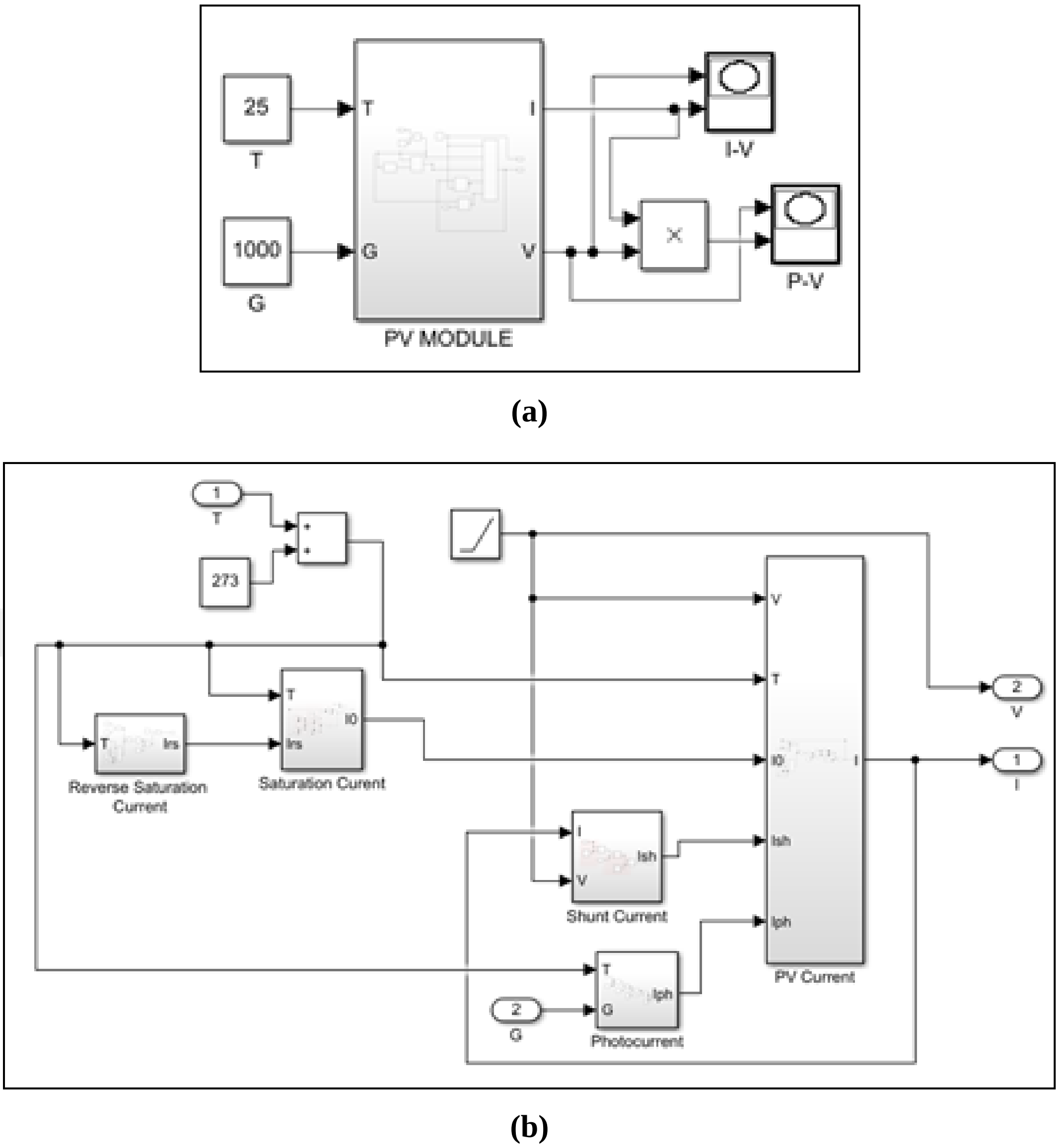

Figure 2.28 : (a) The simulation outline of PV module via MATLAB-Simulink **(b)** Inside of the PV module.

At first step of modelling, the values of PV module such as short circuit current, open circuit voltage, ideality factor, are previously assigned to constants as they can not be changed during the modelling and to avoid repeating the values in each step. Within the PV MODULE model consists of subgroups such as reverse saturation current, saturation current, current through shunt resistance, photocurrent, PV output current as shown in the fig.2.8(b). The currents generated via PV module at forward bias and riverse bias are saturation and reverse saturation currents, that detailed in the previous sections, are calculated via subgroups with the same name by using the input data of temperature in Kelvin. Besides the output data of reverse saturation current subgroup system is the input data of saturation current subgroup system of the model as the reason can be seen in the saturation current correlation. The other current calculated theoretically via different subgroup is photocurrent definedpreviosuly as generated current via solar radiated PV module. The input data to calculate photocurrent are solar radiation in W/m^2 and temperature in Kelvin. After solar radiation and temperature processed in the photocurrent subgroup of the system which will detailed in the following, the result of photocurrent data used as input of PV Current subgroup of the system. For the single diode model there ara two resistance series and shunt resistance. The current passing through shunt resistance is also an input data of PV Current subgroup of the system. It is also calculated via shunt current subgroup which uses voltage and current data as input and result in data of current through shuntresistance. The voltage data is the result of ramp block of Simulink Library. The current data start with the current of short circuited module and continue by the rise of voltage data which will explain in detail in the shunt current subgroup explanation part in the following. In short the output data of Saturation Current, Shunt Current, Photocurrent Submodels and voltage, temperature data used as input for PV Current subgroup of the system which result in the current data of radiated PV module. To understand each subgroup and relation between each group they should be evaluated separately.

Firstly, the input constant data of the model depending on the PV module should be defined. The temperature data and solar radiation data are submitted via user before beginning of the simulation. Further, in this model the extraction of unknown parameters such as series resistanceRs, shunt resistanceRsh, ideality factor A, is not considered and some characteristic parameters specific to PV module such as bandgap energy E_{go}, short circuit current I_{sc}, open circuit voltage Voc, number of series connected cells N_s, are assigned as constant values via user before beginning of the simulation so does not change unless the module changes. The constant values are assigned at the Matlab's editor so while settling the model the developer does not have to write the value of the constant data for instance Boltzmann constant. The only thing developer should do is to name the constant block of Simulink as 'K' for Boltzmann constant, the data of K will directly assign to that constant block.

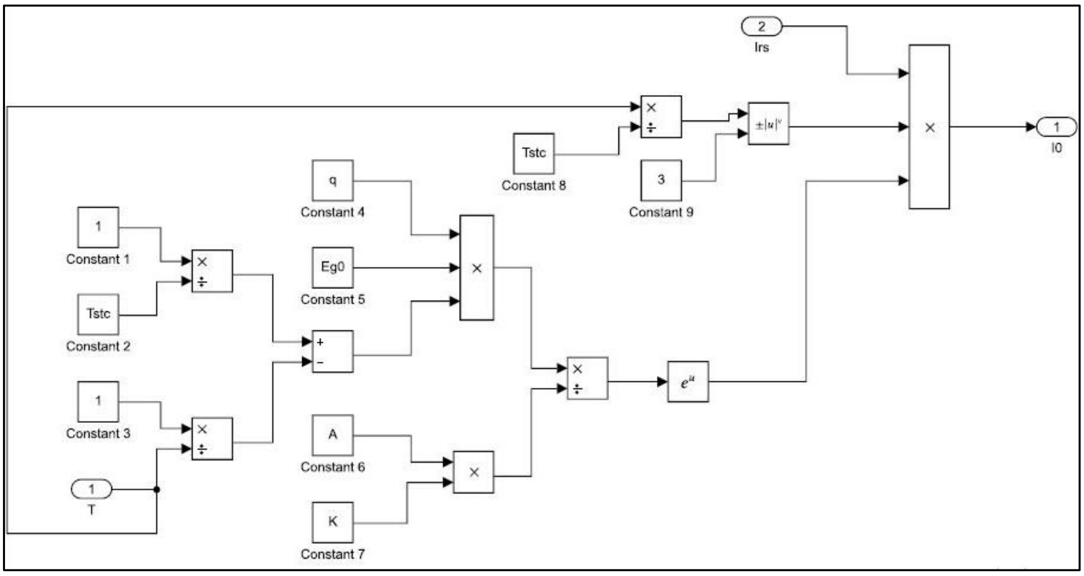

(a)

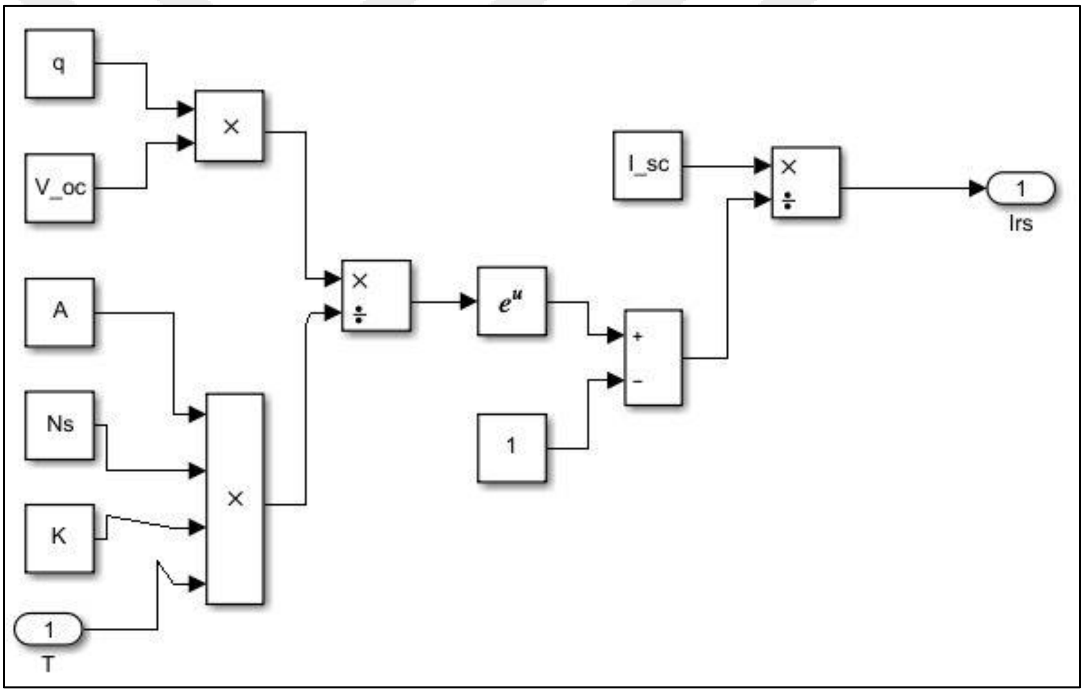

(b)

Figure 2.29 : (a) Saturation Current Submodel **(b)** Reverse Saturation Current Submodel.

The Fig 2.29(a) illustrates the inside block relation of Saturation Current Submodel which depend on the saturation current correlation I_0 as given below. To set the correlation via connecting constant blockswith block names are ideality factor 'A', Boltzmann constant 'K', temperature at STC 'Tstc', bangap energy 'Eg_0', electric charge 'q' and input blockswith block names are reverse saturation current 'Irs' and ambient temperature 'T', mathematical functions which are also illustrated as blocks used are sum function for both summation and subtraction, pow function for power in which both the exponent and the number itself can be adjusted, exp function for to take the exponential of input data.

$$I_0 = I_{rs}\left(\frac{T}{T_{STC}}\right)^3 \exp\left(\frac{qE_g(\frac{1}{T_{STC}}-\frac{1}{T})}{AK}\right) \tag{2.72}$$

Where reverse saturation I_{rs} correlation is;

$$I_{rs} = \frac{I_{sc}}{\exp\left(\frac{qV_{oc}}{N_s AKT}\right)-1} \tag{2.73}$$

The input datareverse saturation current 'Irs' received from the output data of Reverse Saturation Submodel that is formed according the correlation above. The only input block is the ambien temperature and constant blocks are electric charge, key electric characteristics points, number of series connected cells, ideality factor. The Reverse Saturation Current Submodel is modelled before Saturation Current Submodel. To return the reverse saturation current as an output data, the temperature value is inserted into submodel illustrated in fig.2.29(b) above. Afterwards, the output of Reverse Saturation Submodel is used for the input of Saturation Current Submodel.

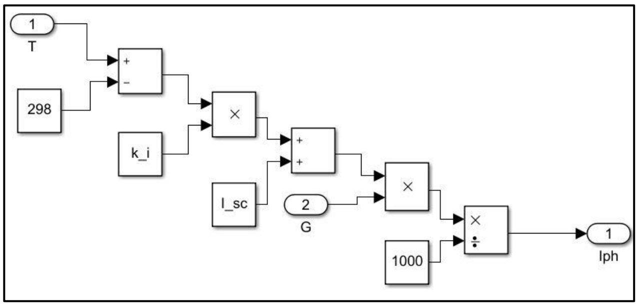

(a)

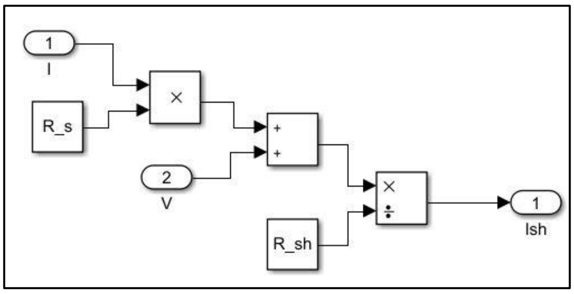

(b)

Figure 2.30 : (a) Photo-Currrent Submodel **(b)** Current Through Shunt Resistor Submodel.

The photocurrent is generated under radiation and is modelled as a subgroup of PV model as well. The constant blocks are short circuit current and temperature coefficient, while the input blocks; temperature and solar irradiance. The only mathematical functions used to connect constant blocks and input and output block are sum function and product function. The theoretical correlationI_{ph} used to form block connections as below. The value 298 and 1000 in the correlation are temperature and radiation at STC. Besides k_i constant is the temperature coefficient.

$$I_{ph} = [I_{sc} + k_i(T - 298)]\frac{G}{1000} \tag{2.74}$$

$$I_{sh} = \left(\frac{V + IR_s}{R_{sh}}\right) \tag{2.75}$$

Current passing through shunt resistance is I_{sh} is also the input data of the PV Current Submodel. The correlation that is used to form Shunt Current Submodel is given above. The constant blocks are the ones contains series and shunt resistance values. The input voltage data is generated via ramp signal block that starts at the beginning of the runtime of the simulation to create voltage value from zero to open circuit voltage by 0,01 volt steps [14]. At the runtime of the simulation the voltage is zero and current is the short circuit current value.

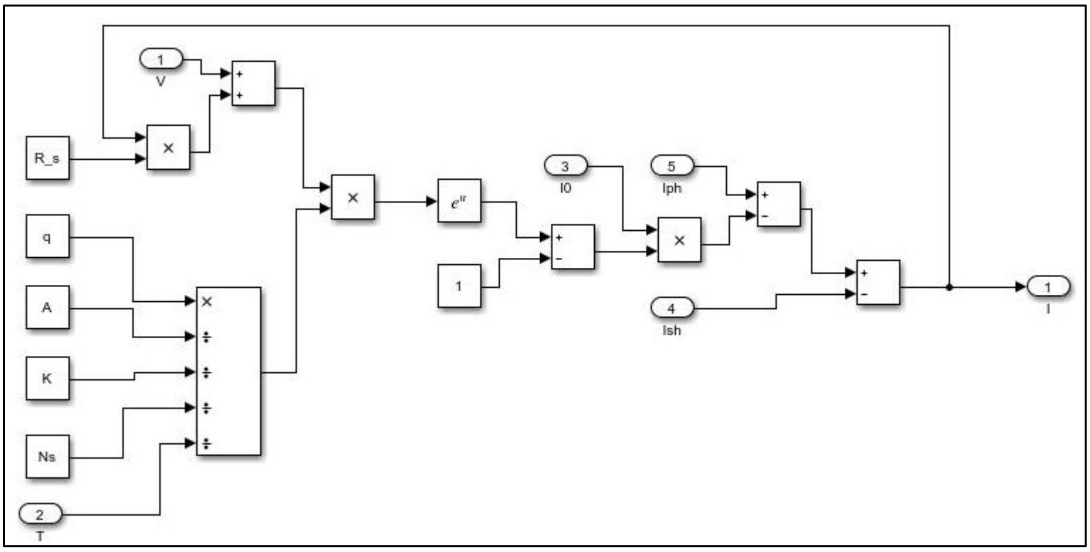

Figure 2.31 : PV Module Output Current Submodel.

At last by using the output data of Saturation Current Submodel, Current Through Shunt Resistor Submodel and Photocurrent Submodel, the PV Current

Submodelformed which consist of input values of saturation current, current through shunt resistance and photocurrent.

$$I = I_{ph} - I_o \left[\exp\left(\frac{q(V + IR_s)}{AKTN_s}\right) - 1\right] - I_{sh} \tag{2.76}$$

The output current correlation I, is given with the correlation above. Besides, there are also two other input value as temperature and voltage. The temperatureand radiation values are inserted at the before the simulation begins and the voltage value is generated by the ramp block.

As at the end, the submodels are connected as shown in the fig. 2.28(b) and form a PV model illustrated in the fig. 2.28(a). The temperature and solar irradiance values are input values of the model that are inserted before the beging of the simulation. Afterwards each set of current and voltage value are kept within an array for the next step to evaluate the solar irradiance and temperature dependence of the model via I-V and P-V graphs as output figures. The graphs are formed by using XY scope from the Sinks Library with the blocks that show or export simulation results. The maximum and minimum data for each XY scope should be defined. The minimum X and Y value of I-V graph are zero which the maximum X and Y value are open circuit voltage value and short circuit current of the module respectively. The minimum X and Y value of P-V graph are zero which the maximum X and Y value are open circuit voltage value and maximum power point of the module respectively. Besides, the output current, voltage and power data sent to the workspace of the Matlab by ‘to Workspace’ block of Sinks Library, in order to process the output data for further studies.

The model explained upto this point is single diode model without extracting unknown parameters that areseries resistance Rs, shunt resistance Rsh, ideality factor A. In the following study, the single diode four parameter model with extracting unknown parameters in which the Simulink model is given in the figure below. The known parameters of the model are the manufacturer datasheet key parameters that are with the block names are short circuit current as ‘I_sc’, open circuit voltage ‘V_oc’, voltage at maximum power ‘V_mpp’, current at maximum power ‘I_mpp’, number of cells connected in series ‘N_s’. The unknown parameters extracted by simplified explicit method detailed previously that are with the block names are areseries resistance ‘R_s’, ideality factor ‘A’, photocurrent ‘I_ph’, saturation current ‘I_o’. The known parameters are taken from the user as input values and model extracts unknown parameters. The model uses the extracted parameters to calculate the output current of the module under defined temperature and radiation. Afterwards, the unknown parameters, current, voltage and power data of the Simulink model exported to Matlab' s workspace incase of further evaluation again with the 'to Workspace' block. Besides, I-V and P-V graphs as output figures that are formed by using XY scope block. The minimum X and Y value of I-V graph are zero which the maximum X and Y value are open circuit voltage value and short circuit current that user defined before runtime, respectively. The minimum X and Y value of P-V graph are zero which the maximum X and Y value are open circuit voltage value and maximum power point that user defined before runtime, respectively.

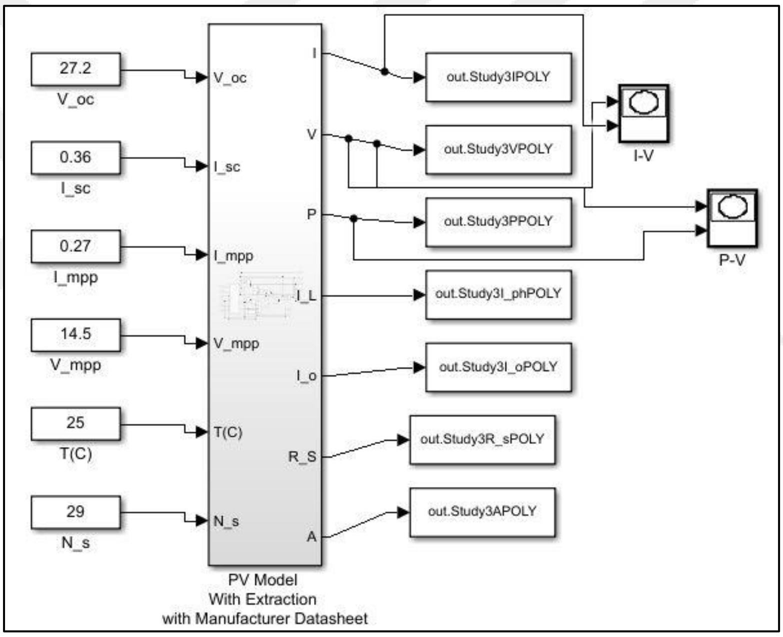

Figure 2.32 : PV Model.

The PV Model has two stages. At the first stage model uses the input values to extract the unknown parameters. Afterwards, by the generation of the voltage value by the ramp block, the current output is found with regard to the current equation of Pv module given below. The extraction of unknown parameters is detailed previously by the simplified explicit method.

$$I = I_{ph} - I_0 \left[\exp\left(q \frac{V + IR_s}{AkT} \right) - 1 \right] \tag{2.77}$$

The figure below illustrates the submodel of simplified explicit method and the performance simulation.The Fig 2.33(a) illustrated the block and submodel relation for the current calculation corresponding the equation above. Apart from using the extracted unkown parameters to obtain current data, they sent as output data after extraction via output blocks. After extraction of unknown parameters, obtainin current via Simulink is almost the same with the previous model.

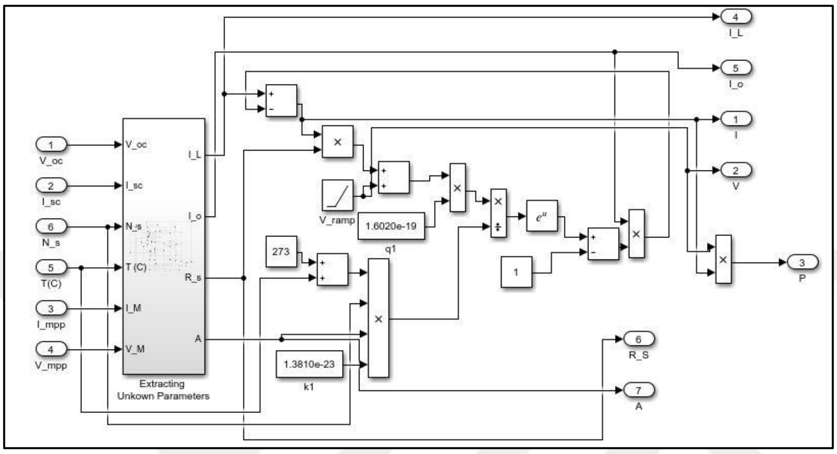

(a)

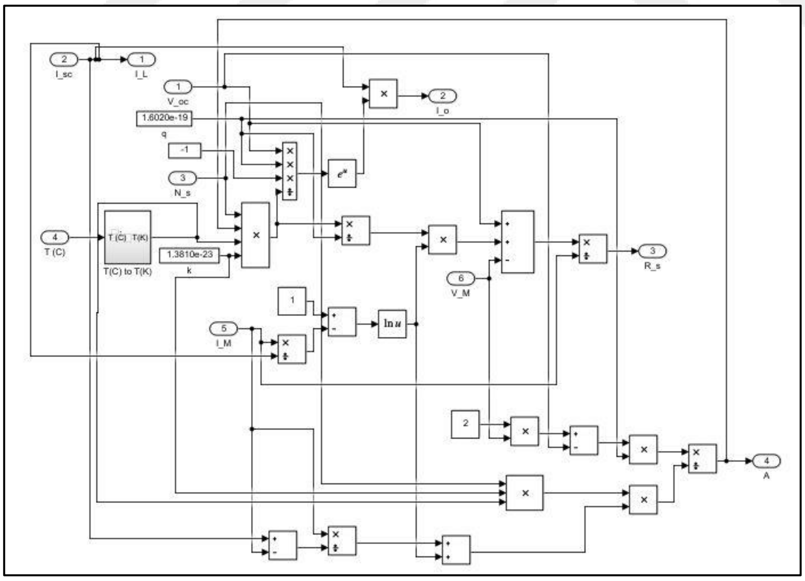

(b)

Figure 2.33 : (**a)** Current and Power Calculation After Extraction **(b)** Extraction of Unknown Parameters.

Fig.2.33.(b) illustrates the extraction of unknown parameters by using the correlations below. In this model, no further submodels are generated for extraction process as to obtain series resistance, ideality factor and saturation current the data used are data that user inserted as input such as open circuit voltage, short circuit current, current

and voltage at maximum power point, Boltzmann constant, electric charge, temperature as seen by the correlations given in the simplified explicit method section of this thesis. Therefore, not to use same blocks again and again for each calculation, those values are used ones and connected via mathematical functions to find series resistance, ideality factor and saturation current. Besides as it is seen, there is acceptance about the photocurrent that is equal to the short circuit current data. In short, the manufacturer datasheet and environmental data are used for four parameters single diode model with etraction method is done within Simulink model and PV performance received as output via I-V and P-V data and exported.

Apart from Simulink models for single diode model, a programme is generated for seven parameter double diode model at Matlab. The theory behind the model is detailed in the combined method section previously. According to the combined method there should be experimental I-V data should be available.

The code of Matlab study of combined method is given in the appendixes. The existing I-V data imported from Excel file via xlsread function of Matlab. The voltage value is received from the first coloumn and current value from second coloumn of Excel file via data(:,1) and data(:,2) functions, respectively. The I-V data ploted to define the three slope points that are open circuit voltage point to define the series resistance, short circuit current point to define the shunt resistance and one selecte point to use in the simplified explicit method part of the combined method.

```
[filename, path] = uigetfile('*.*','Select
data.','MultiSelect', 'off');
 data = xlsread(fullfile(path, filename));
 V = data(:,1);
 I = data(:,2);
 plot(V,I)
 hold on
 %%Slope At (0,V_oc) for R_so

ft=fittype('a1*x1+b1','coefficients',{'a1'
,'b1'},'indep','x1');
 [f,gof,output] =
fit(V(20:22),I(20:22),ft);
 c = coeffvalues(f);
 fv = V(14:22);
 fy = c(1)*fv+c(2);
 %%Slope At (I_sc,0) for R_sho
 ft1=fittype('a2*x2+b2','coefficients',
{'a2', 'b2'}, 'indep', 'x2');
 [f1,gof1,output1]=fit(V(1:3),I(1:3),ft1);
 c1=coeffvalues(f1);
 fv1=V(1:20);
 fy1=c1(1)*fv1+c1(2);
 %%Slope At (I_c,V_c)=(I(15),V(15)) for
R_Co
 ft2=fittype('a3*x3+b3','coefficients',
{'a3', 'b3'}, 'indep', 'x3');

[f2,gof2,output2]=fit(V(15:17),I(15:17),ft
2);
 c2=coeffvalues(f2);
 fv2=V(13:17);
 fy2=c2(1)*fv2+c2(2);
 plot(fv,fy)
 plot(fv1, fy1)
 plot(fv2, fy2)
% Determination of R_sho, R_soslope and
R_Cso
% Slope at (0,Voc);
slope_Voc=c(1);
% Slope at (Isc,0);
slope_Isc=c1(1);
% Slope at (Ic,Vc);
slope_Ic=c2(1);
R_soslope=-1*slope_Voc;
R_sho=-1/slope_Isc;
R_Cso=-1/slope_Ic;
```

Figure 2.34 : Import of experimental data and Slope Method.

The constant parameters for the model that are electric charge, Boltzmann constant, temperature, number of series and parallel connected cells, open circuit voltage, short circuit current, are defined for extractions. Besides, the I-V points that is used to define slope are also assigned to current voltage constants instead of exporting them everytime from the excel. The remaining part of the code is calculation of unknown parameters; ideality factor, shunt and series resistance, saturation current, photocurrent by the correlations defined in the combined method section of this thesis.

As a result, these computational studies are Simulink Models and Matlab programme that is used in this thesis to evaluate the electric charactetistics of PV modules. The results of those studies are given in the result and discussion secton of this PhD thesis.

2.5 Experimental Performance Evaluation of Cell/Module/Panel

2.5.1 Arduino studies

In the outdoor experiment, 10 solar modules are used where four of them is monocrystalline solar module 5,2x2,7cm with 1,5V 100mA, the other four is polycrystalline solar module 5,2x2,7cm with 1,5V 100mA, the other two are 15,7x15,7cm monocrystalline and polycrystalline solar modules. The names of the modules are given in the table below.

Table 2.4 : PV modules used in the experiments.

Modules Name	Modules Type	Modules Size	V_{mpp} (V)	I_{mpp} (mA)
A1.1.	Polycrystalline Silicon	5,2x2,7cm	1,5	100
A1.2.	Polycrystalline Silicon	5,2x2,7cm	1,5	100
A1.3.	Polycrystalline Silicon	5,2x2,7cm	1,5	100
A1.4.	Polycrystalline Silicon	5,2x2,7cm	1,5	100
M1.1.	Monocrystalline Silicon	5,2x2,7cm	1,5	100
M1.2.	Monocrystalline Silicon	5,2x2,7cm	1,5	100
M1.3.	Monocrystalline Silicon	5,2x2,7cm	1,5	100
M1.4.	Monocrystalline Silicon	5,2x2,7cm	1,5	100
BA	Polycrystalline Silicon	15,7x15,7cm	0,536	$8{,}3.10^3$
BM	Monocrystalline Silicon	15,7x15,7cm	Not available	Not available

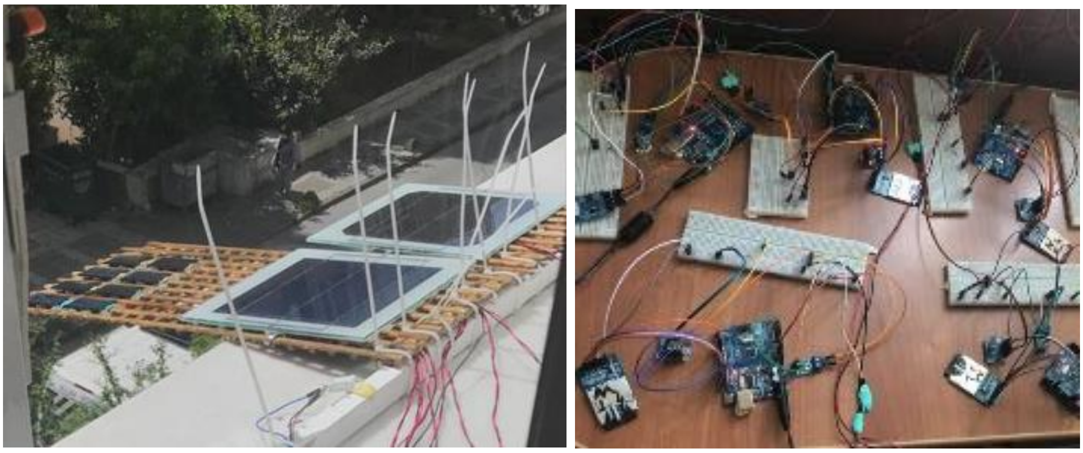

(a) **(b)**

Figure 2.35 : Experimental setup; **(a)** PV modules and **(b)** performance measurement devices.

The experiments are conducted in the Bostanci district of Istanbul/Turkey. The experiment setup and performance measurement devices which collects current, voltage, humidity and temperature, are given in the above figure in which detailed explanation is given below however apart from collecting electric data, receiving the solar radiation data is important as the importance of solar radiation is detailed in the previous section of this thesis.

The experiments are conducted in the Bostanci district of Istanbul/Turkey. The PV modules receive solar radiation between 12:20 to 18:00 for May of 2020. To make sure the data is collecting within this period, the measurement devices collect and save data for every five minutes from 11:30 to 20:00 every day. As if the performance measurement devices collect current, voltage, humidity and temperature values, there is a need of collecting solar radiation is occurred. Therefore, the Copernicus Atmosphere Monitoring Service (CAMS) [125], [126] is considered to receive data for solar radiation. CAMS provides direct solar radiation, diffuse solar radiation and sum of diffuse and solar radiation which is global solar radiation within time step of 1 minute, 15 minutes, hour, day or month for actual weather condition which uses Meteostat satellite, for the time period of first of February of 2004 up to two days ago [127]. The provided solar radiation data is for clear sky and also for on horizontal plane at ground level.

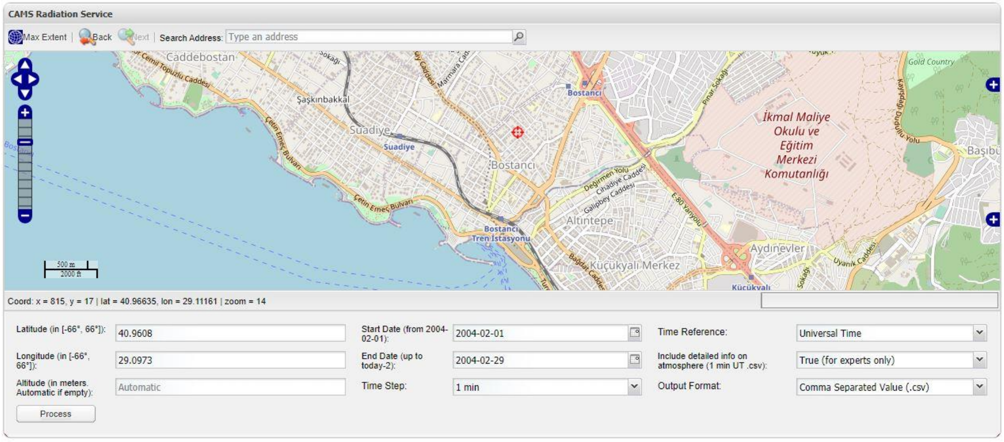

Figure 2.36 : CAMS Radiation Service [127].

After entering the online site of Copernicus Atmosphere Monitoring Service [127], a map and under the map input text labels can be found as illustrated above. Besides the flowchart of obtainin Solar Radiation Data from CAMS is given below. The first step is the coordinate enterence of considered region; the latitude and longitude of the considered experimental region should either be entered manually or selected via map. The altitude of the considered experimental region is given by the CAMS automaticly. The start date and end date for the time period of experiment should be selected. After defining each of these inputs, the data can be reached by process button.

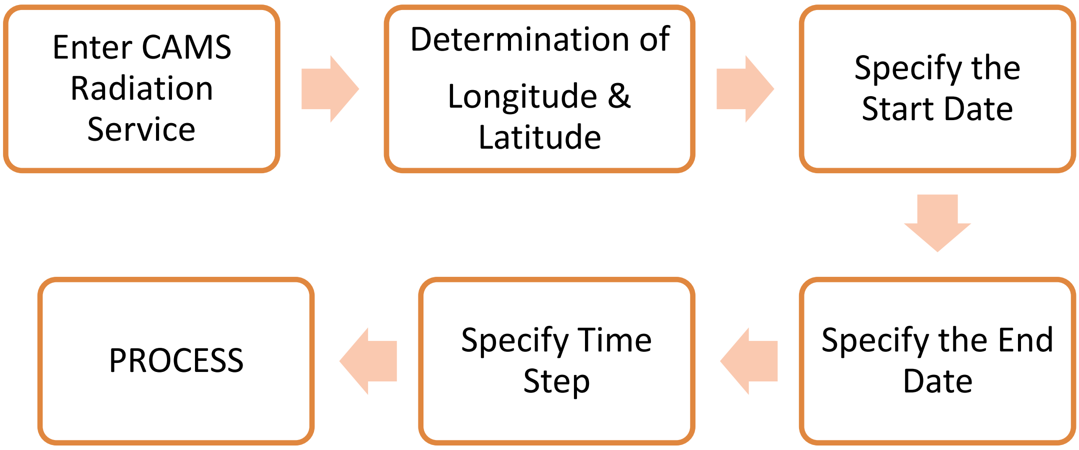

Figure 2.37 : Flowchart of obtainin Solar Radiation Data from CAMS.

Apart from solar radiation data received via CAMS, in the outdoor experiments of this PhD thesis Arduino sets are created and electric data is collected and stored. Arduino is an open source software and hardware platform. Arduino is a microcontroller platform which is basically a brain that receive input data and process due to system rules. This microcontroller platform was improved at Ivrea Interaction Design Institute at 2005 for the students to develop new applications who do not have electronic background [128].

The current and voltage measurements are done with low cost power monitoring system which the simple circuit design and scheme is given in the figure below consists of Arduino platform and several sensors such as F031-06 Voltage Sensor, INA219 current sensor and DHT22 humidty sensor.The measurement system conducted within this thesis is given in the figure below. The measurements are done for each five minutes during the daylight and stored via SD card module.

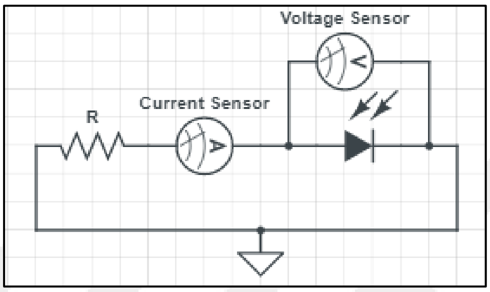

Figure 2.38 : Circuit diagram of the system.

The simple circuit diagram is illustrated in the figure above. The photodiode in the circuit represents solar module. The voltage sensor connected to circuit like voltmeter negative interval of the sensor is connected to the negative interval of PV module and positive interval of the sensor is connected to the positive interval of PV module. The current sensor connected to circuit like ammeter in series.

The schematic design of Arduino project is given in the figure. There are ten PV modules so there are ten Arduino sets to receive voltage and current data. All of the Arduino sets contain voltage sensor module, current sensor module and SD card module. One of them also contains DHT22 temperature and humidity sensor module apart from the other sets. Before expalanation of the device creation steps, each sensor is detailed in the following.

In this thesis, Arduino Uno with ATmega328 microcontroller, which has 5V operating voltage, is used and supplied with 20V external supply. It has 6 analog pins where F031-06 and INA219 sensors are connected and 14 digital pins where DHT22 sensor and SD card module are connected.

In this PhD thesis, the voltage of the solar module is measured by a voltage sensor F031-06 which is basically a voltage divider. The passive circuit element, voltage divider, consist of two resistors as illustrated in the figure below. The voltage divider is used to reduce the input voltage. The input voltage, Vin, is applied between two resistors where the output voltage, Vout, is the potential difference between the terminals of on the second resistor which cause voltage drop.

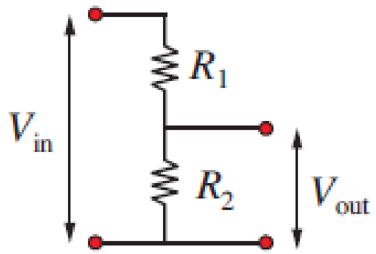

Figure 2.39 : Voltage divider electric circuit design [129].

The electric circuit design of F031-06 Voltage Sensor is given in the figure below. Sensor has 30kΩ and 7,5 kΩ resistance values of R1 and R2 resistors, respectively. The input voltage range is 0 V to 25 V for direct current and the analog voltage resolution is 0,00489 V. As analog input of the Arduino can only be supplied up to 5 V and analog voltage resolution is 0,00489 V, the minimum input voltage is multiplication of supplied voltage (5V) and analog voltage resolution (0,00489 V) which is equal to minimum voltage detection value 0,02445V. So the voltage detection range is between 0,02445 V to 25 V for direct current [130].

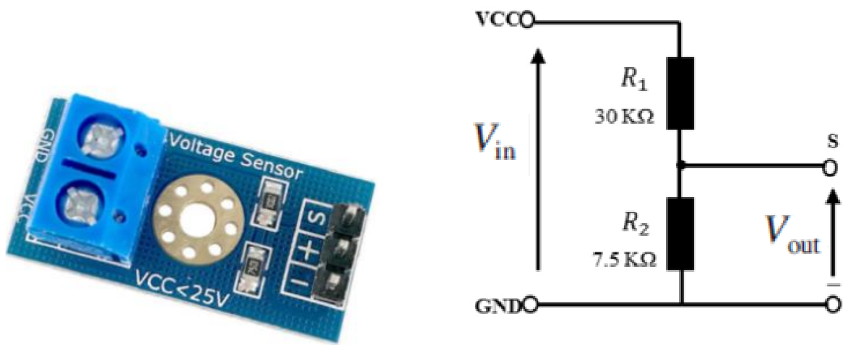

(a) **(b)**

Figure 2.40 : (a) The device illustration and **(b)** the electric circuit design of F031-06 Voltage Sensor Module. [130]

The input voltage V is supplied with the solar module to the sensor where the output voltage is supplied to the Arduino from the sensor. The positive leg of the resistor R2, which is connected to the point S, connects to the A0 analog pin of the Arduino board.

As the analog input of the Arduino can only be supplied up to 5 V, the voltage divider is used which is F031-06 Voltage Sensor. This sensor is able to reduce the voltage up to 5 times of the input value, as it is basically a voltage divider.

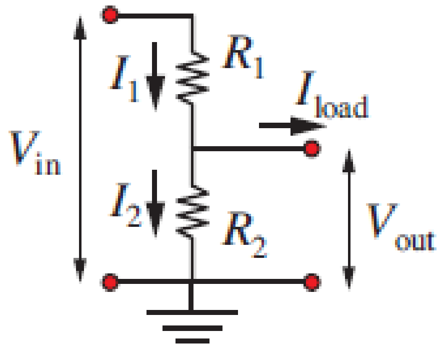

Figure 2.41 : Current illustration of voltage divider [129].

According to the voltage divider circuit design and the Kirchhoff's Current Law, the summation of current passing through the second resistor I_2 and the load Iload is equal to the of current passing through the first resistor I_1. However, in the case of infinite load resistance the Iload is equal to zero, the current passing through first and second resistor is equal. In this case, the voltage equation is as given below according to the Ohm's Law which is used to calculate the voltage drop in the sensor.

$$V_{out} = \frac{R_2}{R_1 + R_2} V_{in} \tag{2.78}$$

However, this equation does not give the output voltage of a solar module. The sensor is connected to the circuit in parallel where the output voltage value is sent to the A0 analog pin of the Arduino. The microcontroller of the Arduino converts this analog value to digital value. Each analog pin of the Arduino has 10 bits of resolution which means the digital value has a range between 0 and 1023[128].

$$V_{in} = \left(\frac{R_2}{R_1 + R_2}\right)^{-1} V_{out} \frac{5}{1023} \tag{2.79}$$

As analog input of the Arduino can only be supplied up to 5 V and an analog pin has 10 bits of resolution, the analog voltage resolution of the voltage sensor is 5 V divided by 1023 which is equal to the value mentioned above 0,00489 V [130]. So, for the output voltage of solar module, the equation is rewritten as above.

Current sensor, INA219, is used to measure the current generated by the solar module. This sensor is basically a digital current sense amplifier and can measure both current passing through shunt and power. INA219 Current Sensor's pins (connection intervals) and definitions are given in the table below.

Table 2.5 : Pins and description of the pins – INA219 Current Sensor [131].

PIN	Description	Connected to
V_{in+}	Positive analog input	Positive interval of the PV module
V_{in-}	Negative analog input	Positive interval of the resistor
V_{cc}	Power Supply INA219 can oparete between 3 V to 5,5V	5V interval of Arduino which is supply voltage of INA219
GND	Ground	Ground of Arduino
SCL	Serial Bus Clock Line – Digital Input	SCL of Arduino
SDA	Serial Bus Data Line – Digital Input/Output	SDA of Arduino

The current sensor is connected to the circuit in series where one of the analog input V_{in-} interval of the sensor connects to the 10kΩ resistor and the other analog input V_{in+} of the sensor connects to the positive interval of the solar module. To calculate the current passing through the shunt resistor by the use of Ohm's Law, the sensor measures potential difference between the intervals of shunt resistor V_{shunt}. Also device measures bus voltage V_{bus}directly from negative differential shunt voltage V_{in-} and ground [131], [132].

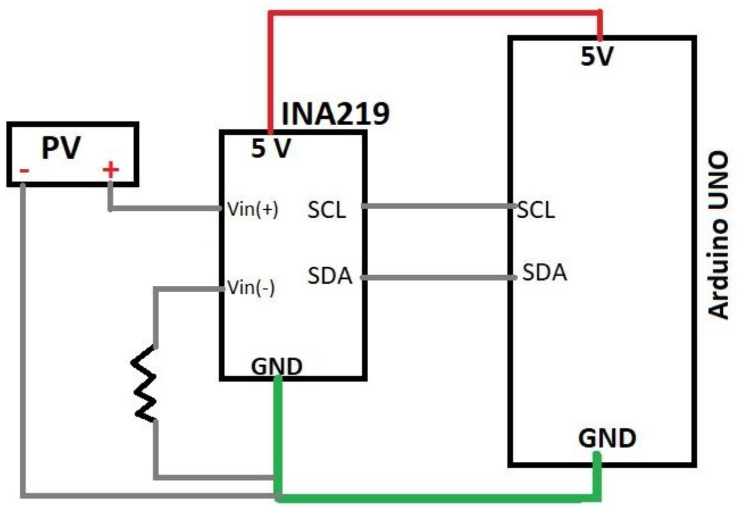

Figure 2.42 : INA 219 – Arduino connection.

For INA219 to operate is important which is executed by connecting to 5V interval of Arduino. However, other important point is communication between INA219 and Arduino which is provided by the SCL and SDA intervals according to SPI communication and protocols. Expansion of SPI is Serial Peripheral Interface and as name suggest it is a serial communication which is data transmission one bit per time where bit is deifned as 1 or 0 basic unit of information [133]. SPI is between slave (secondary device) which in this relation it is INA219 and master (primary device) which in this relation it is Arduino. This communication is controlled and initialized via master. After communication is started via SCL which is serial clock output from Master and defined as 'The clock pulses which synchronize data transmission generated by the master' via Arduino.cc [134], data transfer is contuniued in two dimention via SDA-Serial Bus Data Line intervals of INA219 and Arduino [133]–[135].

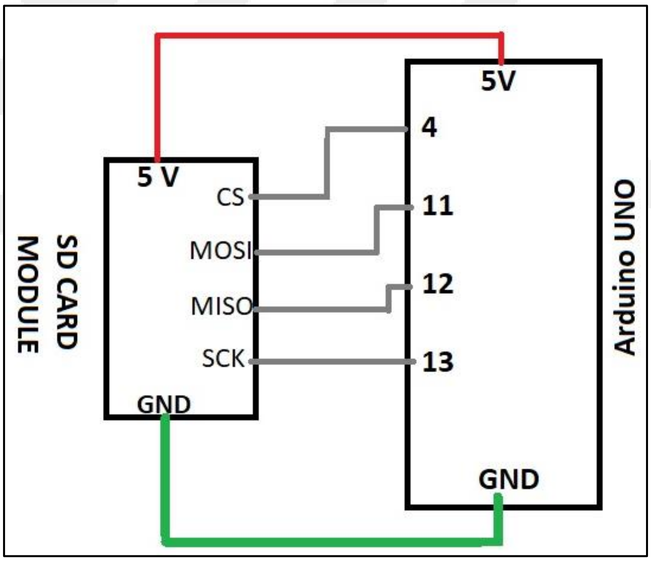

Figure 2.43 : SD Card Module – Arduino connection.

Similarly, the SD card module is also slave in this device system. The pins and connection of the pins are given in the table below. Communication between SD card module and Arduino is also conducted according to SPI protocols. Note that type of the microcontroller unit (MCU) Arduino is stated in the table as the pin connections differ for types of Arduino MCU devices. The data transmittion start with the serial clock output from Master – Arduino UNO. MISO-Master Input Slave Output is the connection that data transfers from slave (SD Card Module) to master (Arduino UNO). In contrary MOSI- Master Output Slave Input is the connection that data transfers from master to slave. Data transfer via MOSI and MISO is synchronized to SCK clock signals. Besides, CS – Chip select is also called Slave Select Pin is for master to choose slave to communicate.

Table 2.6 : Pins and description of the pins – SD Card Module.

PIN	Description	Connected to
MISO	Master Input Slave Output	Digital Pin 12 of Arduino UNO
SCK	Serial Clock	Digital Pin 13 of Arduino UNO
MOSI	Master Output Slave Input	Digital Pin 11 of Arduino UNO
CS	Chip Select	Digital Pin 4 of Arduino UNO
5V	Power Supply; can operate with 5V	5V interval of Arduino
GND	Ground	Ground of Arduino

The data transferred from Arduino to SD Card Module stored via SD (Secure Digital) Card. SD Cards are used for to write, read and store data. The SD card operates under range of 2,7V to 3,6V bu in average 3,3V [136]. The data transfer is aslos conducted via SPI protocol. There are 9 pins within a SD Card that are illustrated in the figure below.

Table 2.7 : Pins and description of the pins – SD Card [128].

PIN	Description
1	DAT3/CS - Chip Select
2	CMD/DI - Master Output Slave Input
3	VSS1 - Ground
4	VDD - Power Supply; can operate with 5V
5	CLK - Serial Clock
6	VSS2 - Ground
7	DAT0/D0 - Master Input Slave Output
8	DAT1 – Data Link
9	DAT2 - Data Link

Further, the temperature and humidity values are also measured with DHT22 sensor module. The sensor has four pins where the sensor is supplied with 3,3 V to 5V direct current via first pin and the data is transmitted to the microcontroller unit of Arduino via second pin. Sensor measures humidity with ±2%RH and temperature with ±0.5℃ accuracy [137].

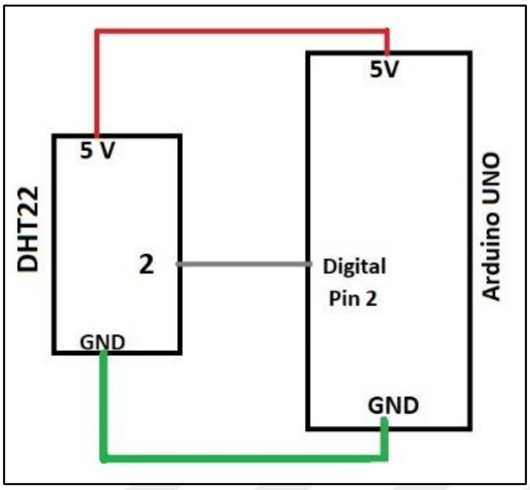

Figure 2.44 : Connection between DHT22 sensor and MCU [137].

In the experimental setup, the DHT22 sensor module is just near the PV modules. This means, both module and PV modules receives the same solar radiation which is quite different from ambience temperature that is obtained from Solcast datasets. So the data received from DHT22 module give information about the heat that PV modules faced.

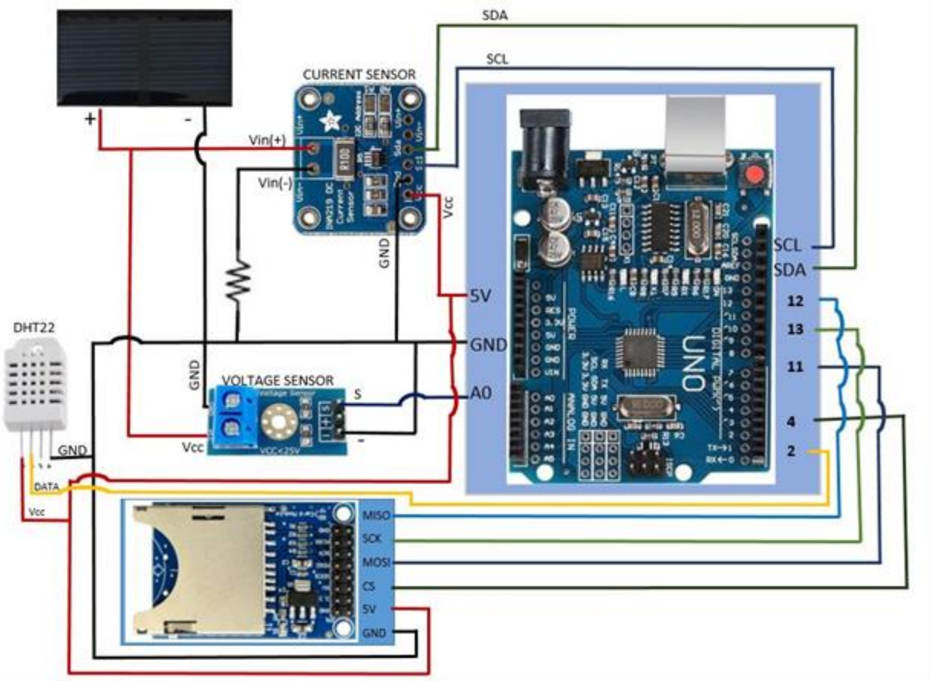

Figure 2.45 : Schematic design of measurement system.

Before settling the PV modules outside, the connection between modules and devices are done, the red colored cable is soldered to the positive interval and black colored cable is soldered to the negative interval of PV module so that black colored cable is connected to the negative interval (ground interval) of the voltage measurement sensor F031-06 and red colored cable is connected to the positive interval of voltage measurement sensor F031-06 and current measurement sensor INA219. Later S interval of the voltage sensor is connected to any analog interval of the Arduino Uno in this case A0 is selected and negative '- 'interval of the voltage sensor is connected to ground interval of the Arduino. The current sensor INA219 connected to the circuit series; Vin+ interval is connected to PV module's positive interval and Vin- interval is connected to resistance. In order current sensor to operate it is connected to 5 V of the Arduino and to transfer the data SDA interval of INA219 connected to SDA interval of Arduino and for clock SCL interval of INA219 connected to SCL interval of Arduino. Besides, the data received is stored via SD card module. The intervals of SD card module MISO, SCK, MOSI and CS is connected to digital intervals of 12, 13, 11 and 4 of the Arduino Uno, respectively. In order SD card module to operate it is connected to 5 V and the ground interval of SD card module connected to the ground of the Arduino. Besides DHT22 humidity sensor is also connected to 5 V to operate via 1st interval of sensor and 4th interval is connected to the ground of the Arduino. To transfer data 2nd interval of DHT22 is connected to the digital interval 2 of the Arduino. In order to operate the total system an Arduino programme is written. The Arduino code for the system is given in the appendix. The functions and libraries used in the code are given in the table below.

At the beginning of the code librarires are included, the sensor types and chip select pins on Arduino (if necessary) defines, and a file object is created. Later, in the 'void setup' function, DHT sensor and INA219 sensor activates. Besides file object is opened and SD card is checked if it is able to written. In the 'void loop' function the main programme is written which include receiving current, voltage, temperature and humidity values and writing the data to SD card. At the end of the 'void loop' function to receive data for every 5 minutes so 300000 milliseconds the delay (300000) function is used to give system the waiting time to collect data again.

Table 2.8 : Code functions– SD Card Module.

Function	Detail
#include <SPI.h>	Includes SPI(Serial Peripheral Interface) Library
#include <SD.h>	Includes SD Library
#include <Adafruit_INA219.h>	Includes INA219 Sensor Library
#include "DHT.h"	Includes DHT (Humidity and Temperature Sensor) Sensor Library
#include <Wire.h>	Includes Wire Library that allows communication SDA and SCL pins
#define DHTPIN 2	Defines DHT Data Pin of Arduino In this study, Arduino Digital Pin number is 2.
#define DHTTYPE DHT22	Defines the DHT sensor type DHT sensor can be either DHT11 and DHT22 In this stud, DHT sensor type is DHT22
DHT dht(DHTPIN, DHTTYPE)	Generates an object that represents DHT sensor used in the system.
Adafruit_INA219 ina219;	Generates an object that represents current sensor
const int chipSelect = 4;	Defines SD card module’s CS pin on Arduino
File myFile;	Creates a file object named myFile from the SD card library.
void setup(void)	Function that sensors are activated, a file object is opened and SD card is checked if it is able to written.
Serial.begin(9600)	Function starts serial communication. 9600 means bits sends and receives every second
Serial.print()	The serial port screen is screen used to instantly see the output of the code written with the arduino. Serial.print() is used to print the text written in parentheses on the serial port screen.
dht.begin()	Function make DHT object to start.
SD.begin()	Function activate SD card
SD.open()	Opens the specified file path in the sd card.
Void loop()	The function where the main programme is written.
dht.readHumidity()	Make DHT to read humidity
dht.readTemperature()	Make DHT to read temperature in celcius
dht.readTemperature(true)	Make DHT to read temperature in Fahrenayt
myFile.print()	Writes the text in parentheses to the myFile file object.
myFile.close()	Closes mFile object.
delay(3000000)	Stop system for 5 minutes before starting again measurement again

At the beginning of the code librarires are included, the sensor types and chip select pins on Arduino (if necessary) defines, and a file object is created. Later, in the 'void setup' function, DHT sensor and INA219 sensor activates. Besides file object is opened and SD card is checked if it is able to written. In the 'void loop' function the main programme is written which include receiving current, voltage, temperature and humidity values and writing the data to SD card. At the end of the 'void loop' function to receive data for every 5 minutes so 300000 milliseconds the delay (300000) function is used to give system the waiting time to collect data again.

The experimental data received from the Arduino sets that contain date, time, humidity, temperature, current, voltage, shunt voltage, bus voltage, load voltage and power evaluated under MATLAB. Besides, direct solar radiation, diffuse solar radiation and sum of diffuse and solar radiation which is global solar radiation, within time step of 5 minutes clear sky and also for on horizontal plane at ground level are received from CAMS. To evaluate current voltage data of modules, solar radiation and ambient temperature data sets with regard to one another a performance analysis code is generated within the MATLAB environment which is given in the appendix C. There are two main function in the code one of them import data from Excel to MATLAB and selects the columns related to the parameters that will be evaluated. The other main function creates previously customized graph which is I-V graph colored according to the solar radiation change. In the following section the experimental data is evaluated with regards to a parameter extraction method.

2.5.2 PV200 and Fluke Studies

The performance of two modules that are 10W monocrystalline and 7W polycrystalline photovoltaic modules within the Zuhal ER's Laboratory at ITU Faculty of Arts and Sciences, are conducted via Seaward PV200 Solar PV Test Equipment, Seaward Solar Survey 200R and Fluke Ti90_9Hz Thermal Imager. The electrical specifications of Seaward PV200 Solar PV TestEquipment and Seaward Solar Survey 200Rgiven in the below.

The Seaward PV200 Solar PV Test Equipment used to define current-voltage curve, open circuit voltage, short circuit current, current and voltage at maximum power point and fill factor of the module. The resolution and the measurement range of each parameter is given in the table above.

Table 2.9 : Electrical Specifications of **(a)** PV200 PV Test Equipment [138], [139] and **(b)** Solar Survey 200R. [140]

(a)

PV200	
Open Circuit Voltage Measurement	
Measuring Range	5.0VDC – 1000VDC
Resolution	0.1VDC maximum
Accuracy	± (0.5 % + 2digits)
Short Circuit Current Measurement	
Measuring Range	0.50ADC – 15.000 ADC
Resolution	0.01 ADC Maximum
Accuracy	± (1% + 2digits)
Operating Current	
Current Measuring Range	0.1A – 40.0 A DC 0.1A – 40.0 A AC 50-60Hz
Resolution	0.1A
Accuracy	± (5% + 2digits)
DC Operating Power	
Measuring Range	0.50 kW – 40.0 kW
Resolution	0.01 kW
Accuracy	± (5% + 5digits)
I-V Curve	
Voltage measurement range	5.0V-1000V
Voltage measurement accuracy	±(0.5%+2digits)
Current measurement range	0.5A-15.0A
Current measurement accuracy	1%
Power measurement range	5W-15kW
Power measurement accuracy	2%

(b)

Solar Survey 200R	
Irradiance	
Display Range	100 – 1500 W/m2
Measurement Range	100 – 1250 W/m2
Resolution	1 W/m2
Temperature	
Display Range	-30°C to +125°C
Measurement Range	-30°C to +125°C
Resolution	1°C
Compass Bearing	
Display Range	0° to 360°
Measurement Range	0° to 360°
Resolution	1°
Inclinometer	
Display Range	0° to 90°
Measurement Range	0° to 90°
Resolution	1°

Besides, Seaward Solar Survey 200Ris used define the solar radiation in which the measurement can be conduct with 1 W/m2 resolution and measurement range of 100 W/m2 to 1250w/m2, and the temperature of ambient and surface of PV modulein which the measurement can be conduct with 1° resolution and measurement range of -30°C to +125°C. Both devices connected via wireless connection so the temperature and solar radiation data is stored within the same storage which is PV200 SD card.

The experiments via PV200, Seaward Solar Survey 200R and Fluke Thermal Imager conducted Bostancı district in Istanbul, Turkey. The experimental setup, measurement devices and 26°inclined PV modules are given in the figure below.

(a) (b) (c)

Figure 2.46 : **(a)** Fluke Ti90_9Hz Thermal Imager **(b)** Seaward PV200 Solar PV Test Equipment Kit. **(c)** Experimental Setup.

In the experiments conducted via Solar Survey 200R device in this thesis consist of solar radiation value in W/m2, ambient temperature and PV module temperature in Celsius. The important point here is to put the Solar Survey 200R device just near the PV module and with the same angle between horizontal surface to detect the solar radiation on the PV surface by the help of inclinometer and compass within device [140]. Also there are two temperature probe on measure the ambient temperature and should not contact with any surface, the other probe is for to detect the PV temperature which should be to fixed to the back of the PV module to not to electric conversion of solar radiation.

In the experiments conducted via Seaward PV200 Solar PV Test Equipment, the connection of the device probes to the PV module is important as if the connection is incorrectly, the solar polarity indicator will give an error with an icon on the device and does not allow to make the measurement. After it is make sure that the probe connection is correct which means positive interval of the PV is connected to positive interval of the PV200 device and negative interval of the PV is connected to negative interval of the PV200 device, by the end of the I-V curve measurement theopen circuit voltage, short circuit current and fill factor data is displayed on the screen. Besides there is a tiny I-V curve figure appears on the screen which is either normal I-V curve if fill factor is greater than 60 or as a not corrent I-V curve if fill factor is smaller than 60. The low fill factor indicator indictes that there might be a problem related to PV device or system under test conditions. Therefore, if fill factor is smaller that 60 the experiment should be conducted again [141]. Besides, the polycrystalline module within laboratory is 7 W which is too low for the power requirements of this device.

Table 2.10 : Electrical Specifications of Fluke Ti90-9Hz Thermal Imager [142].

Fluke Ti90-9Hz Thermal Imager	
Temperature Measurment Accuracy	± 2 °C or 2 % (at 25 °C nominal, whichever is greater)
Temperature measurement range (not calibrated below -10 °C)	-20 °C to +250 °C (-4 °F to +482 °F)
Infrared spectral band	9 μm to 15 μm (long wave)
Operating temperature	-10 °C to +50 °C (14 °F to 122 °F)
Thermal sensitivity	≤ 0.15 °C at 30 °C target temp (150 mK)
Relative humidity	10 % to 95 %, non-condensing

In the experiments conducted via Ti90_9 Hz Thermal Imager device consist of the maximum, minimum and average surface temperatures in Kelvin and surface temperature alteration of the module. Non destructive test; thermal imaging of PV module under operation allow to detect anomalies degradation of the module such as hot spots, potential defects at cells [143]. Hotspots appear in the thermal image because of temporary shadowing such as pollution, humidity, bird dropings, manufacturing defects such as impurities and gas pockets. On the other hand, to make accurate measurement position of the camera is important as shadowing and reflections must be prevented, due to changes in the sky solar radiation might change during measurement [144]. The data collected via each device are examined via Microsoft Excel and Matlab programs.

2.5.3 TSE studies

International Electrotechnical Commission (IEC) is a non-profit organization who generates international standards that consist of qualified tests to ensures reliability and quality of products [145]. Another international organization is International Organization for Standardization (ISO) who creates global standards to support innovations whose central secretariat is in Switzerland [146]. In Turkey, Turkish Standards Institution (TSE)maintain its presence in this field. TSE is one of the member of both ISO and IEC [147]. TSE has services for PV performance and reliability inspection. According to and vary with the considered standard there are experimental procedures such as visual inspection, maximum power determination, insulation test, measurement of temperature coefficients, measurement of nominal operating cell temperature NOCT, performance at STC and NOCT, performance at low irradiance, outdoor exposure test, hot spot endurance test, UV preconditioning test, thermal cycling test, humidity freeze test, damp heat test, robustness of terminations test, wet leakage current test, mechanical load test, hail test, bypass diode thermal test.

The standards that are followed for tests mentioned above at the Energy Technologies Laboratory Ostim-Ankara are listed as below [20,22].

- TS EN 61215: Crystalline silicon terrestrial photovoltaic (PV) modules - Desing qualification and type approval
- TS EN 61646: Thin film terestial photovoltaic (PV) modules - Desing qualification and type approval
- TS EN 61730-1: Photovoltaic (PV) module safety qualification - Part 1: Requirements for construction
- TS EN 61730-2: Photovoltaic (PV) module safety qualification - Part 2 : Requirements for testing
- TS EN 61345: UV Test Photovoltaic (PV) modules
- TS EN 61701: Salt mist corrosion testing of photovoltaic (PV) modules

Maximum power determination experimentsfor two modules that are 10W monocrystalline and 7W polycrystalline photovoltaic modules within the Assoc.Prof.Dr.Zuhal ER’s Laboratory at ITU Faculty of Arts and Sciences, aredone by the contacts of Assoc.Prof.Dr. Zuhal ER in the TSE Laboratuary’s opportunities, under the standard IEC 61215: Crytalline silicon terrestrial photovoltaic (PV) modules-Design qualification and type approval [148],at the begining of 2019 at Ankara. According to the standard IEC 61215, there are several experimentssuch as visual inspection, maximum power determination, insulation test, measurement of temperature coefficients, measurement of nominal operating cell temperature NOCT, performance at STC and NOCT, performance at low irradiance, to certify the PV module however, the experiment conducted within this thesis is maximum power determination that covers the defining power under 1000 W/m^2 and 25 °C. The importance of maximum power determination experiment isto ensure the repeatability of the experiment. The current voltage characteristics of modules are defined under specific cell temperature between 25°C to 50°C and radiation between 700 W/m^2 and 1100W/m^2. The module has to placed perpendicular to radiation source so the module receives the direct simulated radiation and result in reaching the maximum power.After module is exposed to adjusted radiation, the surface temperature is measured as well.

2.5.4 Neutron and gamma studies

In the literature, there are studies that evaluate the effects of irradiations such as electron, proton, neutron, gamma etc[81], [83], [85], [86], [88]–[90], [92]–[96], [98], [100], [102], [149]–[153]. Some of these literature studies detailed in the table below.

In this thesis, it is planned to carry out studies on the exposure of modules to neutron and gamma rays and the behavior of module materials under radioactivity, in line with the idea and direction presented by the thesis advisor. With regards to aims and plans of this thesis, the interaction between ${}_{0}n^{1}$, γ and the solar cell is evaluated. For neutron source with the activity of 12 Bq and for gamma source Co-60 with the activity of 0,27 μCi and Cs-137 with the activity of 0,8 μCi is used.

In solar cells, ionization and/or displacement effects can be seen as a result of damage caused by radiation. The solar modules irradiated via gamma rays both effects can be seen such as, ionization effect which result in pair production, photoelectric effect and Compton scattering, and displacement effect which result in cluster of defects by high energy photons and single point defects by low energy photons in the atomic lattice. As a result of displacement an intermediate energy state between conducting and valance band so bandgap defects which result in two effects. Bandgap defects result in either generation and recombination of hole and electron pairs cause degradation of minority carrier lifetime, or trapping and compensation effects causes majority carrier density and carrier mobility changes. These results as decrease in photogenerated current.

Table 2.11 : Neutron and Gamma Irradiation studies.

Ref.	Considered Parameters	Detail
[99]	I-V characteristics	Irradaited Optoelectronic devices: monocrystalline silicon solar panel (maximumpower voltage 4.0V, maximum power current 100.0 mA, dimension: 70 ∗ 65 ∗ 3.2 mm),four types of silicon PIN photodiodes, two types of silicon NPN phototransistors. The Amprobe 33XR digital multimeter used for I-V measurement. Measurements of I-V characteristics have been performed for radiation levels of 10W/m2 for phototransistors , 4.32W/m2 for solar panels and 0.45W/m2 for phototransistors and all photodiodes.
[90]	Isc, Voc, Impp, Vmpp, FF, Efficiency	All 15 samples are irradiated with 60Co gamma source with energy of 1.23MeV. The batches samples are irradiated with dose 50, 100, 500, 1000, 2000 krad respectively. Solar cells are illuminated by reflective lamp with Light intensity equal to 100mw/cm^2, at room temperature. 15 aged solar cells that are irradiated by gama rays under 5 sets by 50, 100, 500, 1000, 2000 krad of dose. Voltage-current (I-V) characteristics and output parameters of all samples before and after irradiation were measured.
[94]	Rs, Rsh, Isc, Voc, Impp, Vmpp, FF, Efficiency	Measurements done; 1) Before the irradiation, 2) Immediately after irradiation, 3) One month after the irradiation.
[85]	I-V characteristics	Irradiated neutron source of 252Cf source with average energy of 2.14 MeV.
[86]	I-V characteristics	The cells were characterized by solar simulator with 1000 W/m2. (I-V) data recorded every 15 min up to 435 min, under 80W/m2 radaition or under radaitiona and neutron irradiation. The I-V data of cells are measured before and after radaitiona and neutron irradiation.

Table 2.11 (continued) : Neutron and Gamma Irradiation studies.

Ref.	Considered Parameters	Detail
[92]	Jm, Pm, efficiency	60Co gamma source & Pu-Be point neutron source.Before and after each irradiation, I-V measurements done. One group of solar cells were irradiated with a 60Co gamma source. The irradiation was performed through glass, in a controlled environment. An other group of solar cells were irradiated with a Pu-Be point neutron source. This point source is a mixture of 238Pu, with beryllium source of neutrons. A direct contact of the samples and the source was established.
[150]	I-V characteristics	Both p on n cells and n on p cells were irradiated with neutrons and 96 Mev, 69 Mev, 48 Mev protons.
[98]	I-V characteristics	Neutron irradiation experiments conducted on 68 number of silicon solar cell Neutrons energy more than 10keV. Current-voltage characteristics, spectral response, and diffusion length considered parameters. The three separate irradiations at different power levels and placing cells at different distances from the reactor core. Besides eigth cells did not irradiated as control samples. Changes caused by irradiation derived from change of of minority carrier diffusion length of the solar cell.
[82]	I-V characteristics	Neutron irradiated photodiodes.
[96]	I-V data Power output	Irradiation by gamma and neutron. Solar cell, are n-p junction form. A 60Co source was used and temperature of the solar cell during irradiation was controlled over the range from 25C to 100C. The induced I-V data and power data calculated. Annealing of the cell following neutron or gamma irradiation was performed in heat box to control the heat of the cell and power data of cell was measured. During irradiation by increase of temperature decreases power. Damage caused by gamma irradiation improved by annealing. Damage caused by thermal neutrons more compared to damage by fast neutrons. Annealing after neutron not improved by annealing.

Neutron irradiation cause atomic displacement which result in destruction and distortion of local lattice structure and formation of defects. Besides, neutron irradiation form complex defects acting as recombination sites or traps that make increase in the minority carrier lifetime which degrades the electrical parameters; increase in the series resistance and decrease in photocurrent and efficiency

Apart from, performance experiments of solar radiated modules, four monocrystalline and polycrystalline PV modules are irradiated with neutron and the other four are irradiated gamma rays. Besides, there are also monocrystalline and polycrystalline PV modules that are neither irradiated with neutron and gamma or radiated with solar rays. The considered solar modules are listed as below.

Table 2.12 : PV modules used in the experiments within this six months' period.

#	Name	Irradiation	Module Type	Size (cm)	V_{mpp} (V)	I_{mpp} (mA)
1	A2.2.	Gamma Irradiated	Polycrystalline Silicon	5,2x2,7	1,5	100
1	A2.3.	Gamma Irradiated	Polycrystalline Silicon	5,2x2,7	1,5	100
1	M2.2.	Gamma Irradiated	Monocrystalline Silicon	5,2x2,7	1,5	100
1	M2.3.	Gamma Irradiated	Monocrystalline Silicon	5,2x2,7	1,5	100
2	A2.4.	Neutron Irradiated	Polycrystalline Silicon	5,2x2,7	1,5	100
2	A2.5.	Neutron Irradiated	Polycrystalline Silicon	5,2x2,7	1,5	100
2	M2.4.	Neutron Irradiated	Monocrystalline Silicon	5,2x2,7	1,5	100
2	M2.5.	Neutron Irradiated	Monocrystalline Silicon	5,2x2,7	1,5	100
3	T.P.	Not irradiated	Polycrystalline Silicon	5,2x2,7	1,5	100
3	T.M	Not irradiated	Monocrystalline Silicon	5,2x2,7	1,5	100

The first set of modules left under gamma rays for 30 days. Later, the second set of modules left under neutron irradiation for 15 days at the research laboratory of Science and Letter Faculty of SuleymanDemirel University, Isparta, specials thanks to Prof. Dr. Iskender Akkurt. Both sets of modules are set under the solar radiation just after they are received. The modules are connected to Arduino sets as same as explained in the previous section to receive the current voltage data under outdoor conditions. The data collected between 12:00 to 18:00 at Bostanci district of Istanbul, Turkey. In the next section of this PhD thesis, the data received from devices and evaluation of results via Matlab are mentioned.

3. RESULT AND DISCUSSION

3.1 Performance and Degradation Studies

In the previous section, there are several PV performance models are explained. In order to, examine those models there are several datasets are used from literature and manufacturer companies, and there are several datasets are received from the experiments conducted. The list of models considered within this PhD thesis are listed in the table below.

Table 3.1 : PV performance models considered within this PhD thesis.

#	Data Sets	Unknown Parameters	Extraction of Unknown Parameter	Diode	Condition
1	Manufacturer Datasheet	Five	Not extracted	Single diode	STC
2	Manufacturer Datasheet	Five	Not extracted	Single diode	Outdoor
3	Manufacturer Datasheet	Four	Extracted	Single diode	STC
4	Manufacturer Datasheet and Experimental Data	Seven	Extracted	Double diode	STC or Outdoor

At the first part of this section the performance results are evaluated by using single diode models without extracting unknown parameters that the Model number 1 is single diode model where PV module temperature does not change by the change of ambient temperature and the Model number 2 is single diode model where PV module temperature vary with the change of ambient temperature. In order to achive this aim, two different commercial PV modules' datasheets from a solar panel company are used. The panel specifications are given in the table below. Those two panels are certified with both IEC and ISO. The results for both performance models are given with the graphs below.

By the first set of graphs, the temperature response under 1000 W/m^2 solar radiationand solar irradiance response under 25 °C ambient temperature are evaluated for two models. Afterwards, to compare models more specifically, two model calculated under STC conditions and I-V & P-V graphs are illustrated under one figure. Later, the two model are evaluated via real temperature and solar irradiance data taken from Turkey Meteorology Station in order to see the yearly and seasonly responses.

Table 3.2 : Polycrystalline Silicon & Monocrystalline PV Module Characteristics.

Polycrystalline 325W		Monocrystalline 355W	
k_i	0.05 (%/°C)	k_i	0.05 (%/°C)
E_g	1.1 eV	E_g	1.1 eV
N_s	60	N_s	60
N_p	1	N_p	1
R_s	0.221 Ω	R_s	0.221 Ω
R_{sh}	415.405 Ω	R_{sh}	415.405 Ω
Length	1.965m	Length	1.965m
Width	0.992m	Width	0.992m
P_{mp}	325 W	P_{mp}	325 W
V_{mp}	37.19 V	V_{mp}	38.69 V
I_{mp}	8.74 A	I_{mp}	9.18 A
$V_{oc,STC}$	45.72 V	$V_{oc,STC}$	47.52 V
$I_{sc,STC}$	9.31 A	$I_{sc,STC}$	9.66 A

As to define the suitable model between those two for the future studies is aimed the evaluations are done only for monocrystalline PV. However, at last the efficiency of both monocrystalline and polycrystalline is also examine

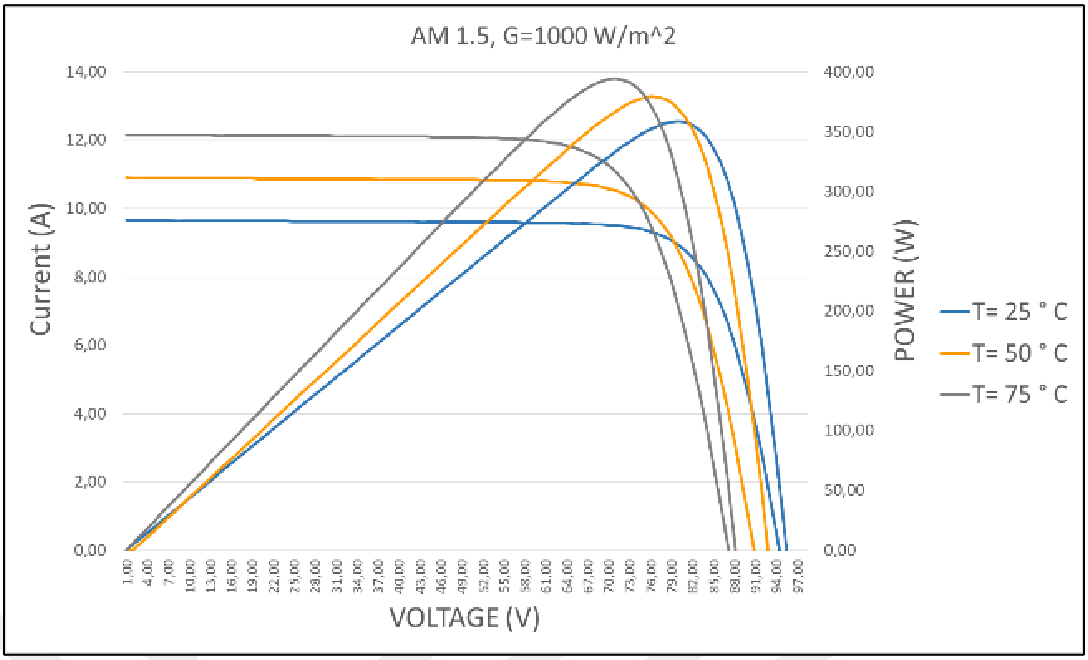

(a)

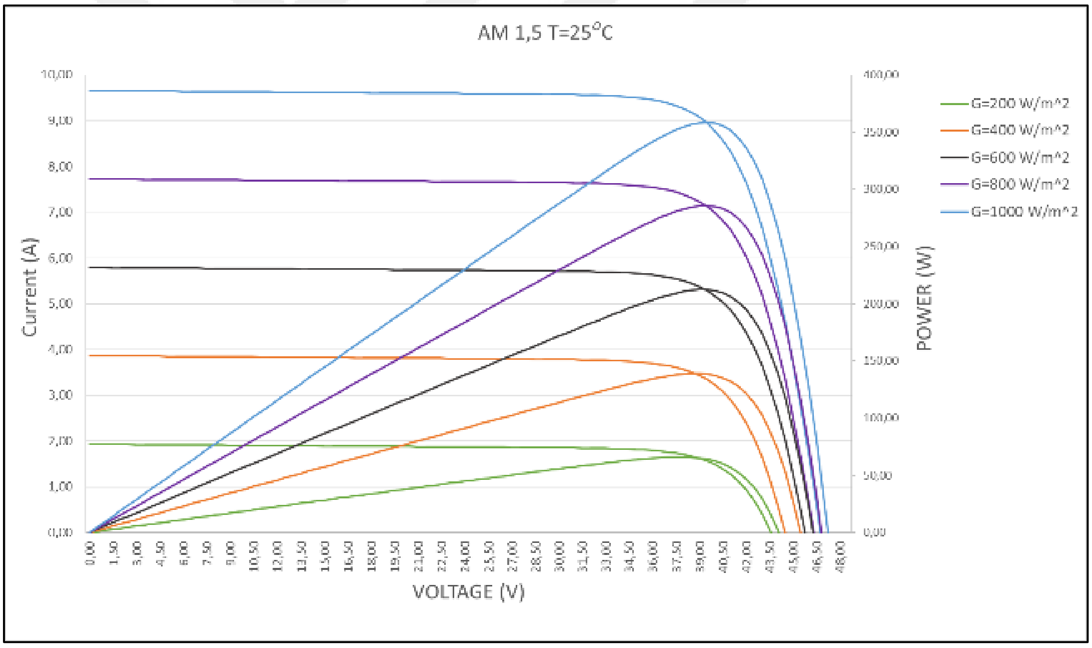

(b)

Figure 3.1 : (a) Temperature dependence and **(b)** Solar Radiation dependence of PV Module evaluated with Model 1.

By the increase of temperature Voc decreases and Isc increases under stable solar irradiance with 1000 W/m^2 according to the results of Model 1 as illusted above. However, for Model 2, by the increase of temperature both Voc and Isc decreases under stable solar irradiance with 1000 W/m^2 as illustrated below.

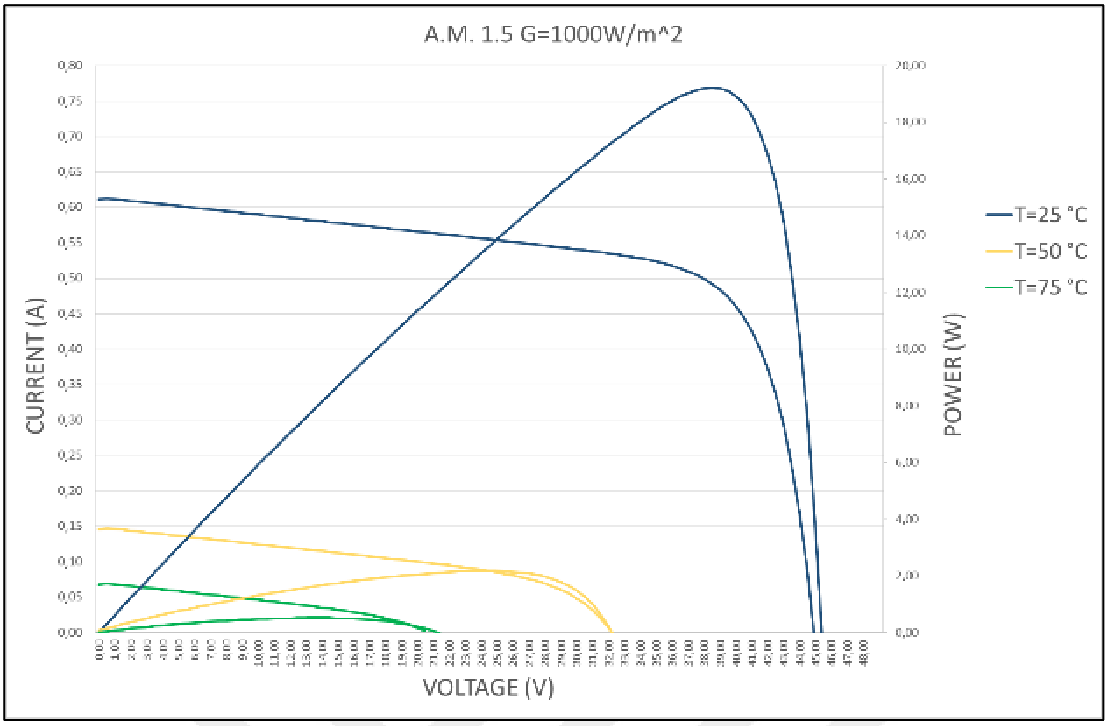

(a)

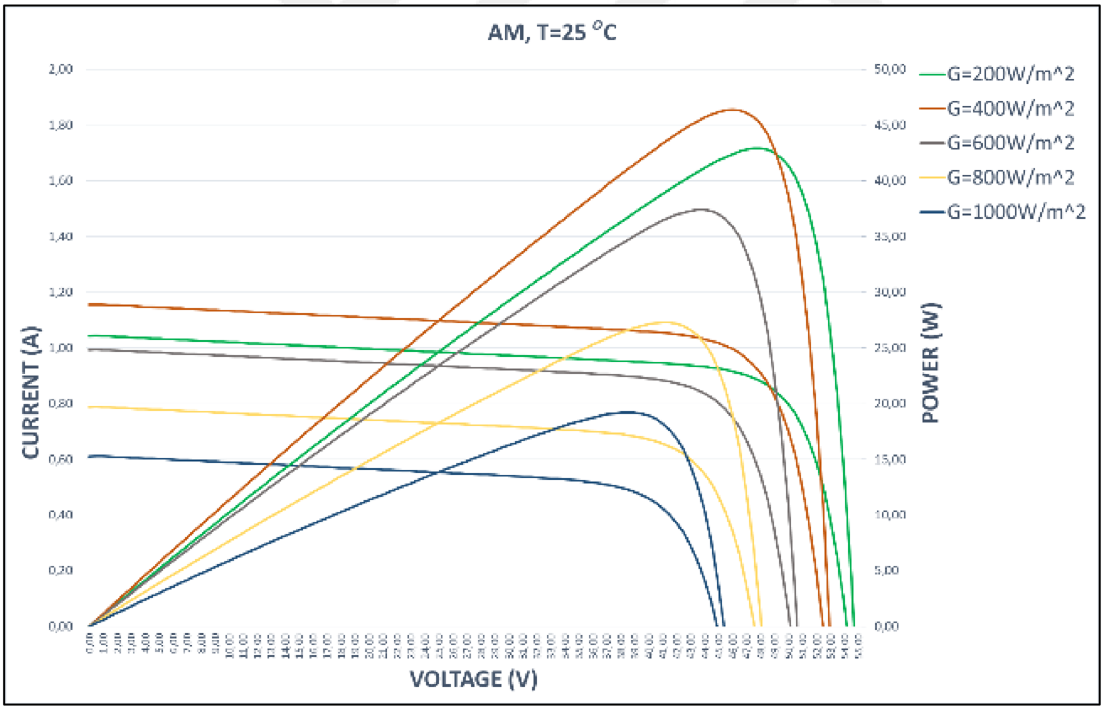

(b)

Figure 3.2 : (a) Temperature dependence and **(b)** Solar Radiation dependence of PV Module evaluated with Model 2.

By the increase of solar irradiance both Voc and Isc increase, according to the results of Model 1 under stable temperature 25 C. However, for Model 2, by the the increase of solar irradiance generally both Voc and Isc decrease. Isc there is slight increase while irradiance increases from 200 W/m^2 to 400 W/m^2.

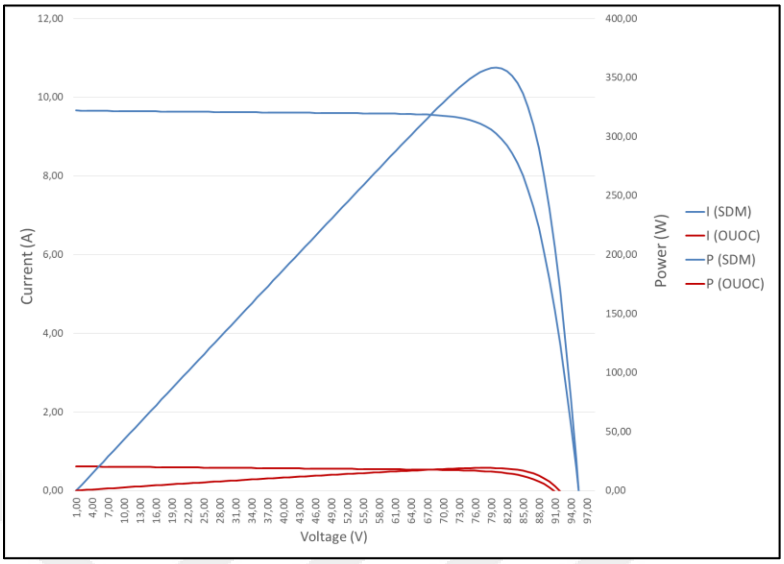

Figure 3.3 : The comparison between Model 1 and Model 2 at 1000W/m^2 and 25 °C.

Graph above shows that there is difference between two model under same solar irradiance and temperature. The reasons is that the consideration of the ambient temperature. In Model 2 the ambient temperature affects the module temperature where at Model 1 ambient temperature is directly equal to module temperature.

Besides, the temperature affect on maximum power point is also seen clearly at Model 2. If tests are done under laboratuary conditions, it is expected to be close to the results of Model 1. If tests are done under outdoor conditions where ambient temperature affects both module temeperature and the current values, it is expected to be close to the results of Model 2.

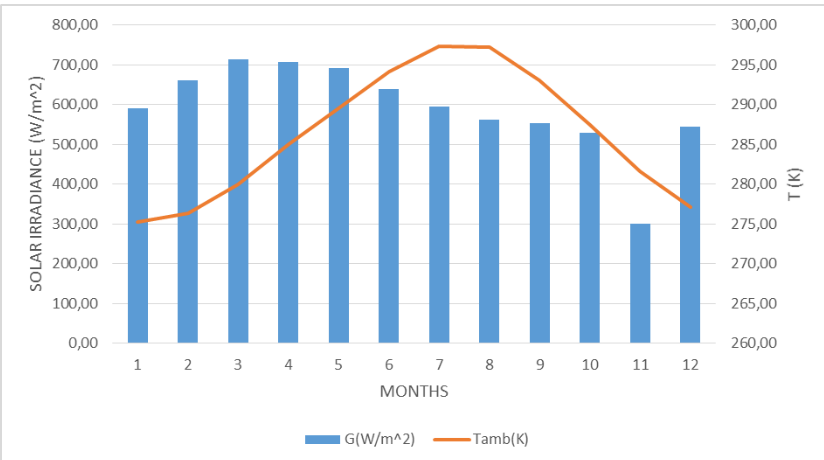

Figure 3.4 : Solar irradiance and temperature values [154]–[156].

The temperature and solar irradiance dependence of both Model 1 and Model 2 are compared above with the selected data. In order to be make more precise comparison, the monthly average data received from Turkey Meteorology State [154]–[156] Monocrystalline Silicon PV module operating under both Model 1 and Model 2 are evaluated.

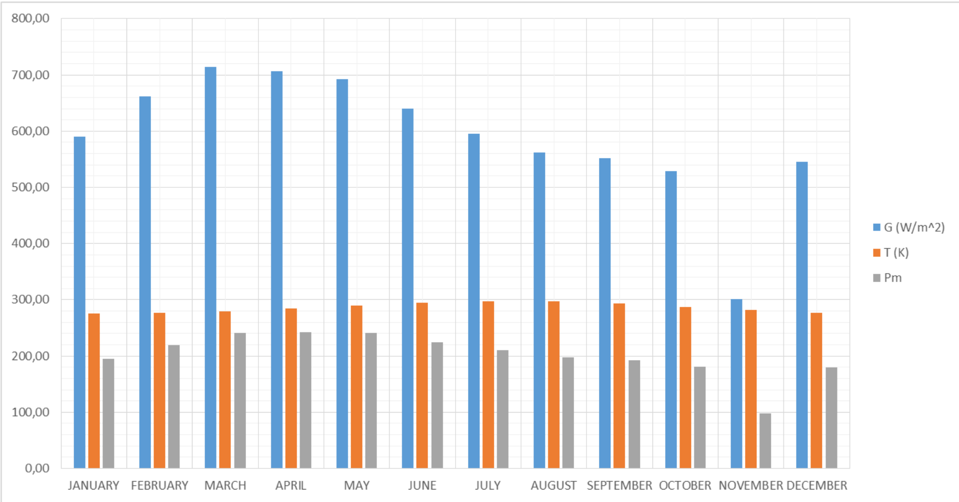

(a)

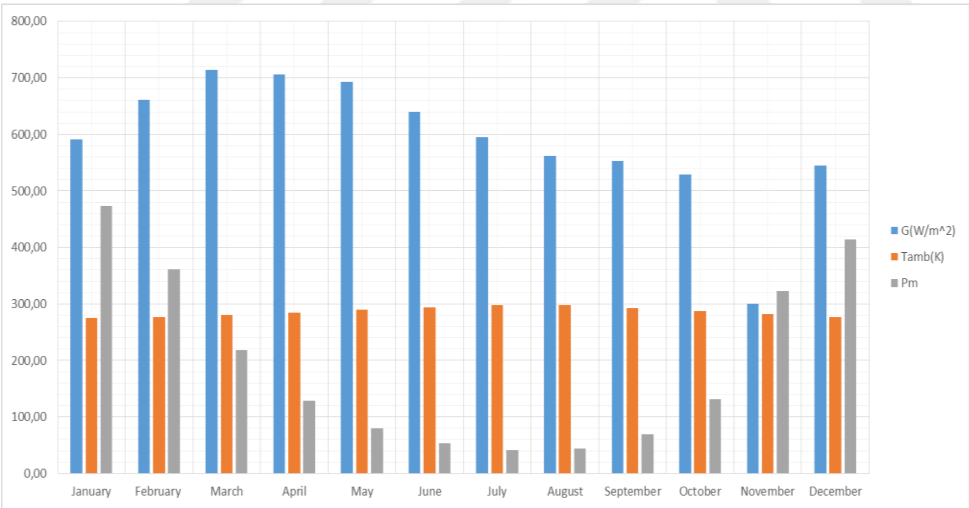

(b)

Figure 3.5 : PV module maximum power results according to **(a)** Model 1 and **(a)** Model 2.

As Model 1 does not consider the temperature change in the module due to the ambient temperature and irradiance change, the P_m value changes mostly according to the irradiance values. When the results of January and August are compared, it is seen that with small amount of rise in temperature cause huge decrease in P_m value according to Model 2. To be more clear, slightly differences in T, cause sharp changes in P_m value.

It is clearly seen from the difference between Fig.3.51. (a) and (b) that considering the change in the module temperature has high impact on the module maximum power output. The results illustrated that to examine PV module operating under the outdoor conditions, single diode model where PV module temperature vary with the change of ambient temperatureis more reliable for preliminary studies of PV systems. So, efficiency comparison of both monocrystalline and polycrystalline is done under the correlation sets for Model 2.

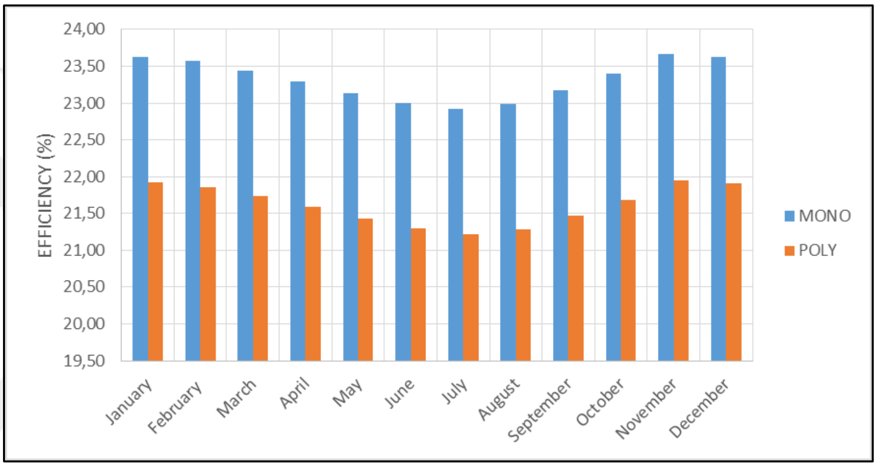

Figure 3.6 : Efficiency comparison of Monocrystalline and Polycrystalline Silicon PV modules according to the results of Model 2.

The yearly general trend is similar for both type of PV modules. Eventhough the size and the parasitic resistances taken same for both panels, the monocrystalline silicon PV module has higher efficiency. It is observed that this is because of multiplication of open circuit voltage and short circuit current is greater than polycrystalline silicon PV module. In more realistic systems, the efficiency of monocrystalline is expecting to be higher, as polycrystalline silicon PV module has more layers and so more losses compared to monocrystalline silicon PV module.

Upto this point, the difference between monocrystalline and polycrystalline silicon PV modules are compared without extracting the unknown parameters which are series resisttance, saturation current, ideality factor and photocurrent. Those unknown values are reached from the literature and examined. Now, Model 1 which is single diode model where PV module temperature does not change by the change of ambient temperature,and Model 3 which uses simplified explicit method for single diode model are compared by using two MATLAB/Simulink simulations. For Model 1, unknown parameters are assigned. Meanwhile for Model 3 unknown parameters are extracted by simplified explicit method.

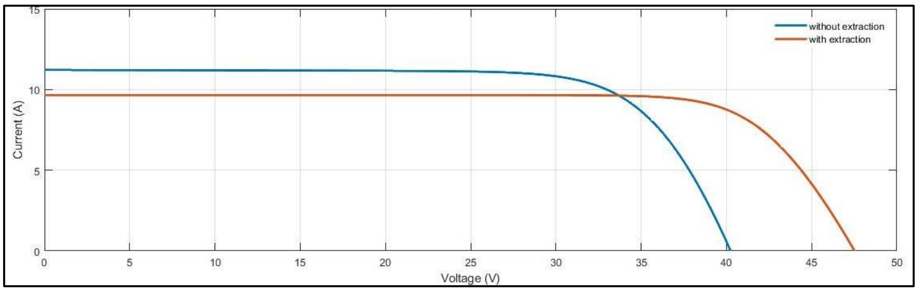

(a)

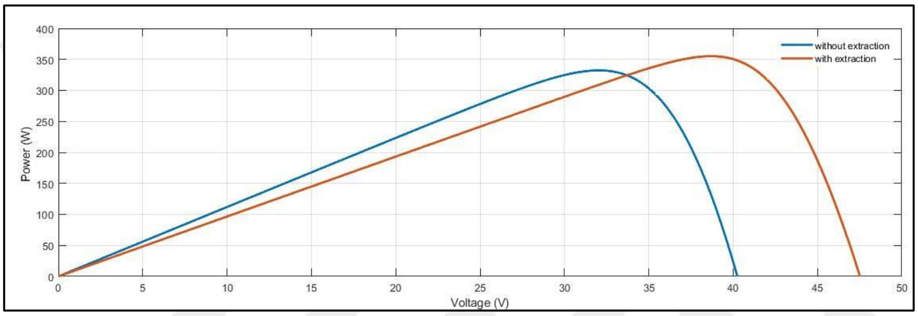

(b)

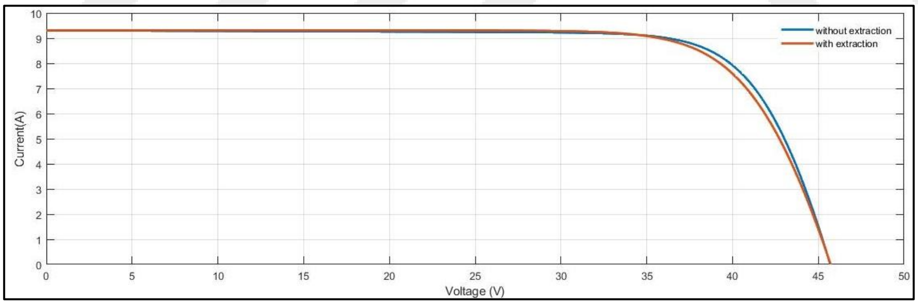

(c)

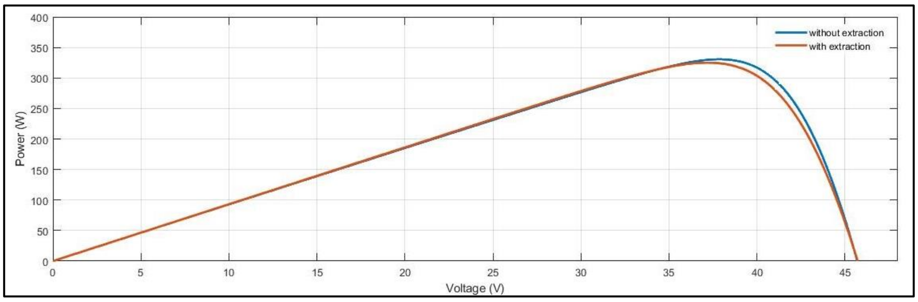

(d)

Figure 3.7 : (a) Current Voltage and **(b)** Power Voltage Graph for Monocrystalline PV Module with and without extraction. **(c)** Current Voltage and **(d)** Power Voltage Graph for Polycrystalline PV Module with and without extraction.

The figure above represents the simulation difference when the exraction method is considered and ignored. The results for graph (a) and (b) for the simulation that considers the simplified extraction method has more close to the manufacturer datasheet values. Meanwhile, the simulation without considering extraction of unknown values result in even different open circuit voltage and short ciruit current values. However, the graphs for polycrystalline PV module there is not a significant difference. This is because of the simulation is conducted for ideal single diode which may differ for the polycrystalline silicon PV module.

Table 3.3 : Known and Extracte Parameters of Devices.

	mc-Si	CdTe/Cds	CIS
V_{mpp} (V)	29,9	46,7	33,9
I_{mpp} (A)	8,37	1,68	2,21
V_{oc} (V)	37,1	62,5	43,1
I_{sc} (A)	8,76	1,98	2,4
μ_{Isc} (%/K)	0,0043	0,02	0,05
Ns	5	5	8
Np	1	2	2
Size(m^2)	8	7,2	11,7
Eg (eV)	1,12	1,45	1
q (C)	1,602E-19	1,602E-19	1,602E-19
k (J/K)	1,381E-23	1,381E-23	1,381E-23
T (K)	298	298	298
G (W/m^2)	1000	1000	1000
A	9,63	64,79	13,21
R_s	0,40	0,06	1,05
I_0	8,27888E-13	0,00108424	3,07308E-07
I_{ph}	8,76	1,98	2,40

On the other hand, rather than only monocrystalline and polycrystalline modules, for different types of PV modules/panels are compared. The datas are taken from both manufacturer datasheets and literature. The table below represents the known and extracted values with regard to Model 3 for the mentioned PV modules/panels

The bandgap value for CIS is smaller than CdTe/Cds so the open circuit voltage is proportional to the relation of the bandgap between thode technologies. This result is expected according to the theory about the open circuit voltage-bandgap relation and short circuit current- bandgap relation. So the theory and the simulation results are compatible with eachother.

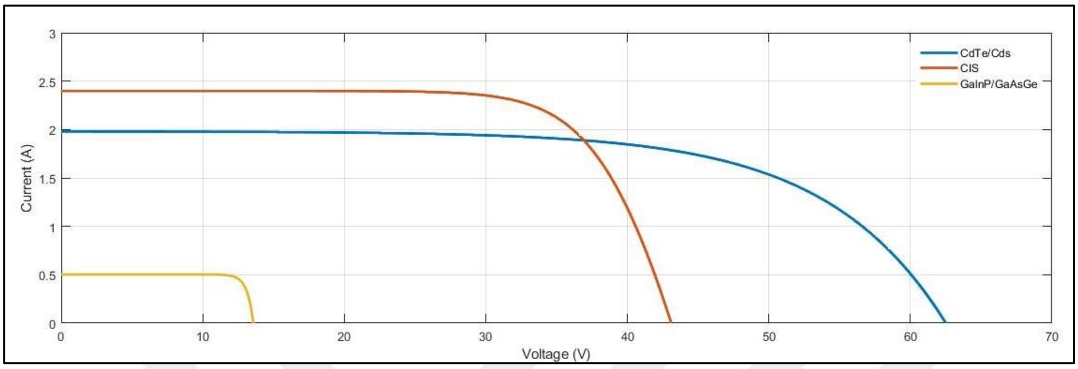

(a)

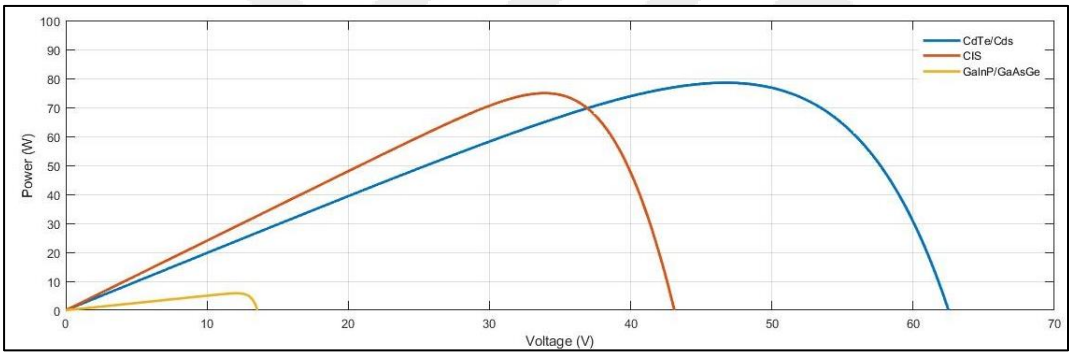

(b)

Figure 3.8 : Simulation results illustrated as **(a)** current-voltage graph and **(b)** power-voltage graph.

On the other hand, extraction of unknown parameters for the existing PV module within Zuhal Er’s Laboratory at ITU Faculty of Arts and Sciences is also conducted by using Model 3 and the results are given in the table below.

The data for 10 W Monocrystalline Photovoltaic Module and 7 W Polycrystalline Photovoltaic Module within the Zuhal ER’s Laboratory at ITU Faculty of Arts and Sciences are received from manufacturer datasheet and PV200 device. The manufacturer datasheet values and PV200 data also are given in the Table 2.16.

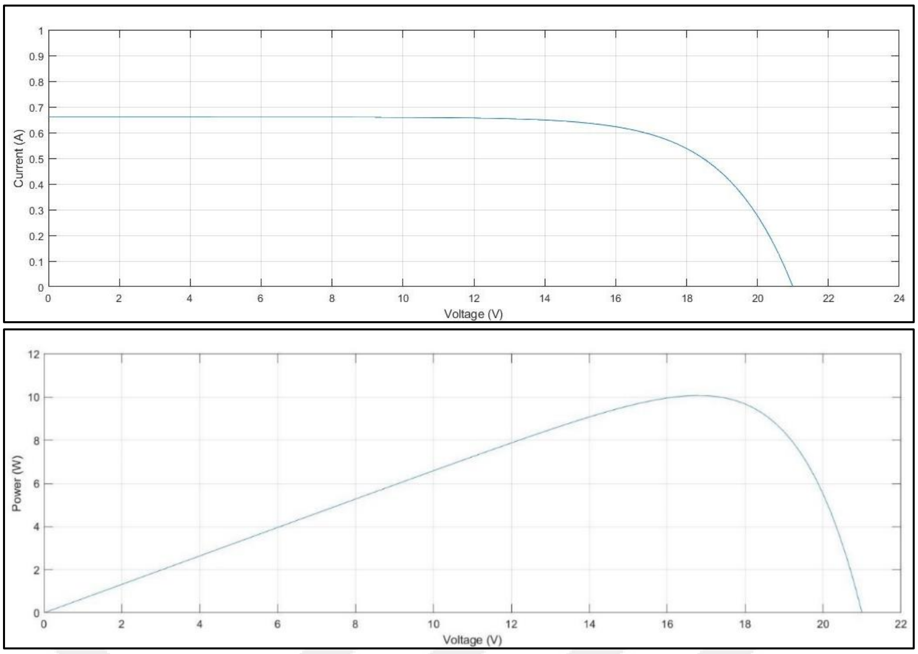

Figure 3.9 : Extraction result for the existing PV modules within Zuhal Er's Laboratory at ITU Faculty of Arts and Sciences.

To begin with, the performance of a photovoltaic module has evaluated at standard test conditions without extracting unknown parameters of the single diode model, but considering the manufacturer datasheet values. Later, the unknown parameters of a photovoltaic module have extracted by simplified explicit method, at standard test conditions and again the manufacturer datasheet values are considered. Afterwards, performance results of those two models have compared.

Table 3.4 : PV Modules.

Standard Test Conditions				**Outdoor Conditions**			
Monocrystalline PV Module		Polycrystalline PV Module		Monocrystalline PV Module		Polycrystalline PV Module	
I_{sc}	0.49 A	I_{sc}	0.36 A	I_{sc}	0.398 A	I_{sc}	0.187A
V_{oc}	25 V	Voc	27.2 V	V_{oc}	19.5 V	V_{oc}	22.2 V
I_{mpp}	0.43 A	I_{mpp}	0.27 A	I_{mpp}	0.3 A	I_{mpp}	0.1 A
V_{mpp}	19.6 V	V_{mpp}	14.5 V	V_{mpp}	15.89 V	V_{mpp}	14.51 V
T	25℃	T	25℃	T	32℃	T	32℃
G	1000 W/m^2	G	1000 W/m^2	G	781.1 W/m^2	G	773.4 W/m^2
Ns	36			N_s	36		

In the examination of Model 1, the performance of a photovoltaic module has evaluated at standard test conditions by only considering the manufacturer datasheet values. Meanwhile, the ideality factor and resistance values have assigned according to the ideal single diode model where shunt resistance goes to infinity and series resistance is equal to zero. In Model 3, only manufacturer datasheet values have considered at standard test conditions.

Various considerations in photovoltaic energy conversion by single connected solar modules are shown in Figure 7 with graphs generated. There are two curves in these graphs for each evaluation. One of them is the I-V characteristic in Figure 7a which represents that the short circuit current Isc is equal to the photogenerated current Iph in the ideal case. The other graph curve is for P-V characteristic which the power P = IV produced by the module is shown in Figure 7a. The module generates the maximum power Pmax at a voltage Vm and current Im.

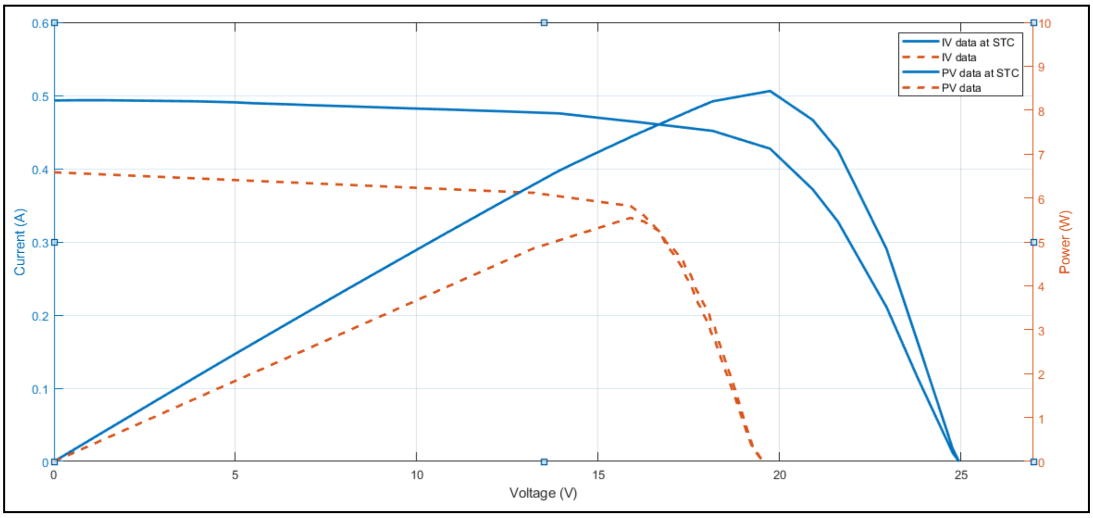

(a)

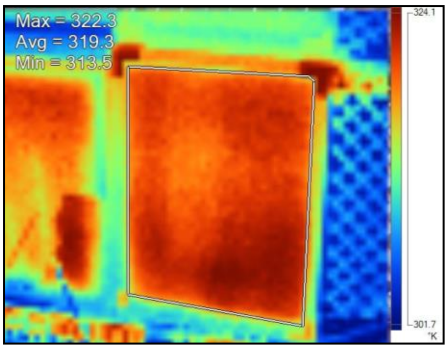

(b)

Figure 3.10 : (a) The I-V and PV graph of Monocrystalline PV Module at STC and at Outdoor Condition. **(b)** The IR image of Monocrystalline PV Module at Outdoor Condition.

The experimental study consists of electric and thermal evaluation via the Seaward PV200 Solar PV Test Equipment and Fluke Ti90_9Hz Thermal Imager for

Monocrystalline and Polycrystalline PV Modules. The Figure 3.55 illustrates results for Monocrystalline PV Module, meanwhile Figure 8 shows the electrical and thermal characteristics of Polycrystalline PV Module.The experiment conducted for Monocrystalline PV module at the outdoor condition such as solar radiation is 781.1 W/m2 and ambient temperature is 305K where the current-voltage and power-voltage results illustrated via dashed orange lines in the fig.3.55.a. and related key points of the experiment are given in the table 5. While the ambient temperature is 305K, the average surface temperature is 319.3 K as shown in the Fig.3.55. b.

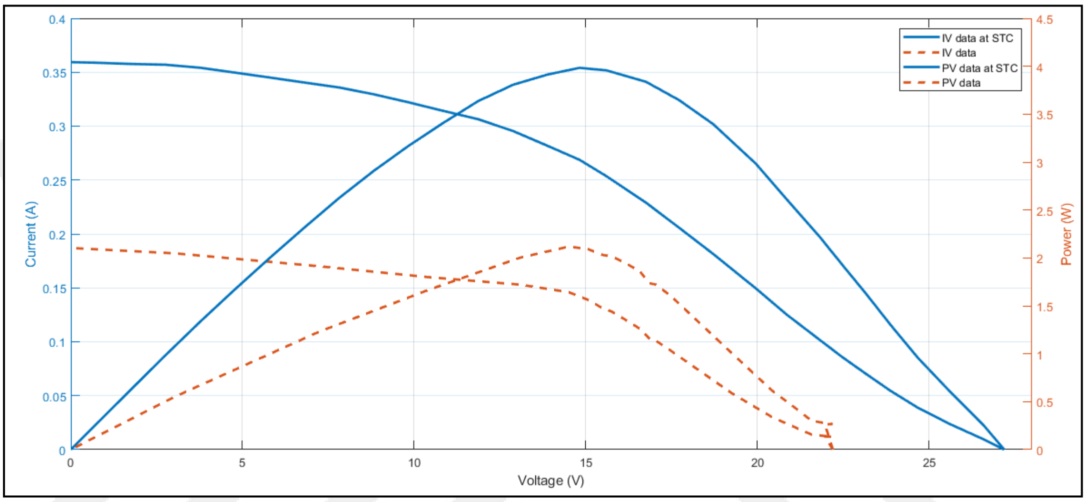

(a)

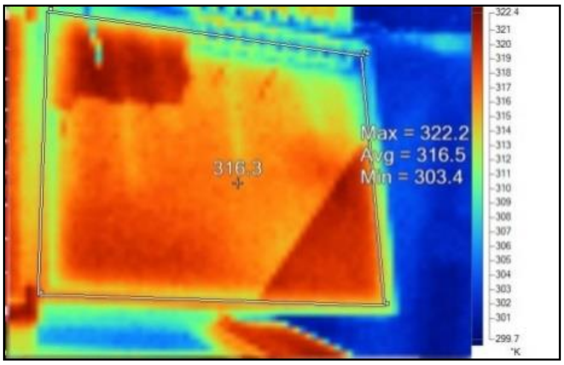

(b)

Figure 3.11 : (a) The I-V and PV graph of Polycrystalline PV Module at STC and at Outdoor Condition**. (b)** The IR image of Polycrystalline PV Module at Outdoor Condition.

Similarly, the results for 7 W Polycrystalline PV Module is given in the figure below. The experiment conducted at the outdoor condition as solar radiation is 773.4 W/m2 and ambient temperature is 305K in which the electric performance results are illustrated via dashed orange lines in the fig. 3.56.a. The data received from the thermal imager shows that, while the ambient temperature is 305K, the surface temperature has values between 322.2 K and 303.4 K with an average value of 316.5K.

It is clearly seen from both Figure 3.55 and Figure 3.56 that the key points such as short circuit current, open circuit voltage and maximum power point is decrease by the decrease of the solar radiation and increase of ambient temperature. For further evaluations of the performance of PV cell/module/panel, there exists equivalent circuit models as explained in the previous sections. The manufacturer datasheet values as given in the Table 3.16 and experimental results as illustrated in the figures above are considered for the performance models.

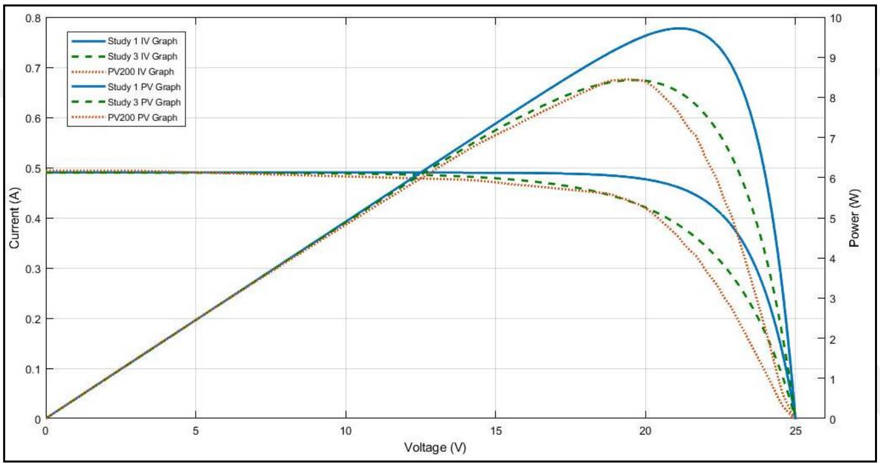

(a)

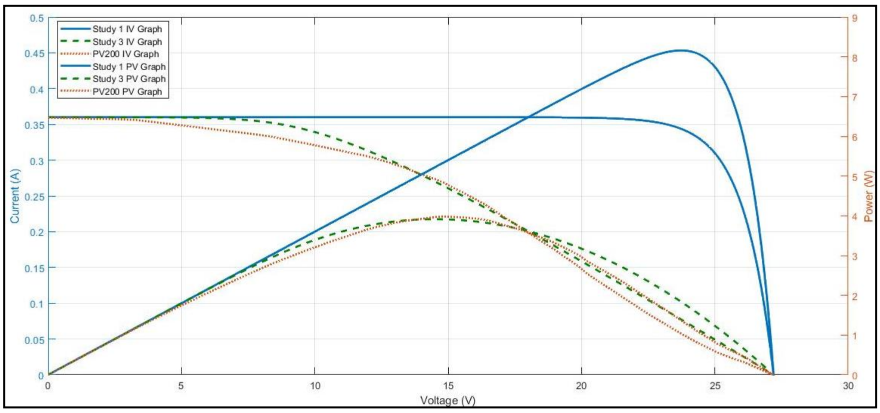

(b)

Figure 3.12 : (a) The I-V and PV graph of Monocrystalline PV Module. **(b)** The I-V graph and PV graph of Polycrystalline PV Module.

In the study conducted with regard to Model 1, SDM without extracting unknown parameters at STC with manufacturer datasheet is evaluated, meanwhile in the studyconducted with regard to Model 3, SDM considering extracting unknown parameters at STC with manufacturer datasheet is examined. The comparison results between the study conducted with regard to Model 1, studyconducted with regard to Model 3 and the experimental data received from PV200 device for both monocrystalline and polycrystalline PV module at STC are shown with the figure below. The short circuit and open circuit values of both studies and the experimental results are corresponding. The maximum power value for monocrystalline PV module is 8.428 W as stated in the manufacturer datasheet and measured by PV200 device. At the studyconducted with regard to Model 3, that considers extracting unknown parameters, the maximum power values are close to theoretical and experimental values compared to the results received from the studyconducted with regard to Model 2 which enables to evaluate the performance of PV module by assigning the resistance and ideality factor values for ideal PV module and ignores the extraction of unknown parameters. Similarly, for the polycrystalline PV modules are the maximum power value is 3.915 W according to the manufacturer datasheet and PV200 device. Again, as expected the study that considers extracting the unknown parameters has shown more reasonable results.

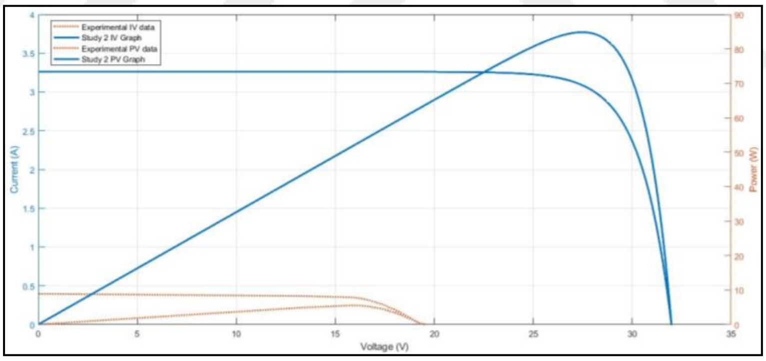

(a)

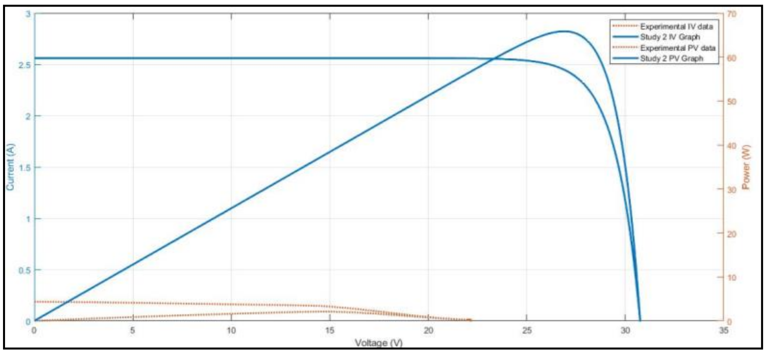

(b)

Figure 3.13 : The I-V graph and PV graph of **(a)** Monocrystalline PV Module and **(b)** Polycrystalline PV Module at outdoor condition without extraction.

The performance of a monocrystalline and polycrystalline PV module is examined at outdoor conditions without extracting unknown parameters of SDM at studyconducted with regard to Model 2. The results are compared with the experimental data receive from PV200 Solar PV Test Equipment as illustrated in the Figure 3.58.a and in the figure 3.58.b.

The results between the studyconducted with regard to Model 2 and the experimental data for both monocrystalline and polycrystalline PV module are shown with the Figure 3.58. As in the studyconducted with regard to Model 2 the unknown parameters are not extracted before performance evaluation, the results are not compatible with the experimental data. Besides the relation between temperature, solar radiation and key points such as open circuit voltage and short circuit current is linear which result in dramatic increase in the current and voltage values.

Apart from the methods mentioned above, the seven parameter double diode model is evaluated at standard test condition by considering the datasheet values and experimental data. At this model again the simplified explicit method and slope method are used together to extract the seven unknown parameters of the model. Later, the performance results are evaluated.

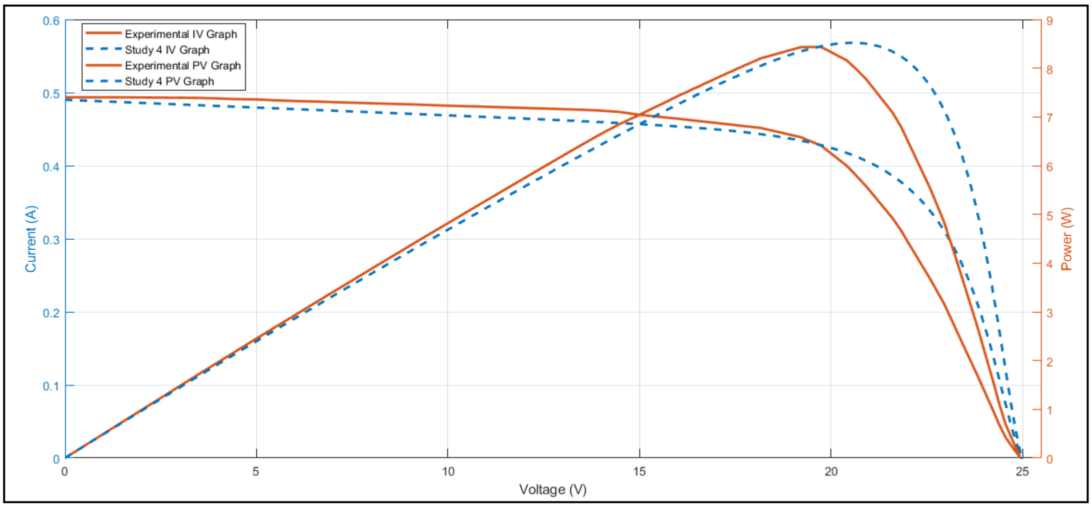

Figure 3.14 : The I-V graph and PV graph of Monocrystalline PV Module at STC.

The results between the studyconducted with regard to Model 4 and experimental data for monocrystalline PV module at STC is shown in the Fig.3.14 above. Apart from extracting unknown parameters of the model, two Schottky diodes and so their ideality factors and currents are considered. Ergo, that is the reason that the model results and experimental results that received from PV200 device are compatible for 10 W

Monocrystalline Photovoltaic Modules at standard test conditions as it is clearly seen from the Figure 3.14.

Table 3.5 : The calculated-measured data comparison and percentage error.

	Calculated Data	Measured Data	Statistical Analysis for Current		Calculated Data	Measured Data	Statistical Analysis for Power
	7 Parameter DDM Results	PV200 Results	Percentage Error		7 Parameter DDM Results	PV200 Results	Percentage Error
V	I	I	I	V	P	P	P
0,001	0,490	0,494	0,816	0,24	0,007	0,007	0,000
0,38	0,489	0,494	0,952	0,55	0,018	0,018	0,000
0,64	0,489	0,494	1,088	0,89	0,029	0,029	0,000
0,91	0,489	0,494	1,088	1,21	0,040	0,040	0,000
1,17	0,488	0,494	1,225	1,52	0,050	0,050	0,000
1,44	0,487	0,494	1,361	1,82	0,060	0,060	0,000
1,70	0,487	0,494	1,362	2,08	0,068	0,069	1,952
1,97	0,485	0,493	1,635	2,33	0,075	0,077	2,624
2,23	0,485	0,493	1,635	2,59	0,084	0,086	2,352
2,50	0,485	0,493	1,771	2,86	0,092	0,094	2,138
2,76	0,484	0,493	1,907	3,13	0,100	0,103	3,260
3,03	0,483	0,493	2,044	3,39	0,109	0,112	3,003
3,29	0,483	0,493	2,180	3,66	0,117	0,120	2,790
3,56	0,483	0,493	2,046	3,93	0,125	0,129	3,127
3,82	0,482	0,492	2,184	4,19	0,133	0,137	2,936
4,09	0,481	0,492	2,185	4,46	0,142	0,146	2,762
4,35	0,481	0,491	2,188	4,72	0,151	0,155	2,175
4,62	0,480	0,491	2,189	4,98	0,160	0,163	2,060
4,88	0,481	0,491	2,054	5,25	0,167	0,171	2,352
5,15	0,479	0,490	2,329	5,51	0,175	0,180	2,613
5,42	0,478	0,490	2,333	5,78	0,184	0,188	2,140
5,68	0,479	0,489	2,197	6,04	0,192	0,197	2,390
5,95	0,477	0,489	2,337	6,31	0,200	0,205	2,618
6,21	0,477	0,488	2,340	6,57	0,209	0,214	2,199
6,48	0,476	0,488	2,478	6,84	0,217	0,222	2,419
6,74	0,475	0,488	2,481	7,10	0,225	0,231	2,330
7,01	0,475	0,487	2,484	7,37	0,233	0,239	2,529
7,27	0,475	0,487	2,347	7,63	0,241	0,247	2,715
7,54	0,475	0,486	2,349	7,90	0,249	0,256	2,626
7,80	0,474	0,486	2,491	8,16	0,258	0,264	2,543
8,07	0,473	0,486	2,630	8,43	0,267	0,273	2,219
8,33	0,472	0,485	2,632	8,69	0,274	0,281	2,391
8,60	0,472	0,485	2,497	8,96	0,282	0,289	2,555
8,86	0,471	0,484	2,775	9,22	0,289	0,298	2,934
9,13	0,470	0,484	2,778	9,49	0,298	0,306	2,637
9,39	0,470	0,483	2,642	9,75	0,306	0,314	2,567
9,66	0,469	0,483	2,923	10,02	0,314	0,322	2,710
9,92	0,468	0,482	2,926	10,29	0,322	0,331	2,642
10,13	0,468	0,482	2,929	10,55	0,329	0,339	2,975
10,45	0,468	0,482	2,791	10,82	0,337	0,347	2,903
10,72	0,468	0,481	2,793	11,08	0,346	0,355	2,648
10,98	0,467	0,481	2,936	11,35	0,353	0,364	2,958
11,25	0,466	0,480	3,078	11,61	0,360	0,372	3,074
11,51	0,466	0,480	2,941	11,86	0,368	0,380	3,008
11,78	0,466	0,479	2,804	12,14	0,376	0,388	3,117
12,04	0,464	0,479	3,226	12,41	0,384	0,396	3,054
12,31	0,463	0,479	3,229	12,67	0,391	0,404	3,159
12,58	0,463	0,478	3,093	12,94	0,399	0,412	3,260
12,84	0,462	0,478	3,235	13,20	0,406	0,420	3,357
13,11	0,461	0,477	3,379	13,47	0,414	0,428	3,294
13,37	0,461	0,477	3,383	13,73	0,421	0,436	3,543
13,64	0,460	0,476	3,386	14,00	0,429	0,444	3,329

Table 3.5 (continued) : The calculated-measured data comparison and percentage error.

	Calculated Data	Measured Data	Statistical Analysis for Current		Calculated Data	Measured Data	Statistical Analysis for Power
	7 Parameter DDM Results	PV200 Results	Percentage Error		7 Parameter DDM Results	PV200 Results	Percentage Error
V	I	I	I	V	P	P	P
13,90	0,460	0,476	3,391	14,26	0,436	0,452	3,423
14,17	0,460	0,475	3,114	14,53	0,444	0,459	3,364
14,43	0,458	0,474	3,263	14,96	0,456	0,470	2,862
14,7	0,457	0,472	3,131	15,49	0,471	0,482	2,233
15,01	0,457	0,471	2,857	15,76	0,478	0,490	2,334
15,29	0,456	0,468	2,443	16,0	0,485	0,496	2,301
15,55	0,455	0,467	2,449	16,29	0,492	0,503	2,138
15,81	0,454	0,465	2,455	16,55	0,499	0,509	2,111
16,07	0,454	0,464	2,173	16,82	0,506	0,516	1,954
16,3	0,452	0,462	2,180	17,08	0,512	0,522	1,930
16,6	0,451	0,461	2,042	17,35	0,519	0,529	1,780
16,87	0,450	0,459	2,049	17,61	0,525	0,535	1,759
17,13	0,448	0,458	2,056	17,88	0,531	0,541	1,863
17,40	0,447	0,456	1,916	18,14	0,537	0,547	1,844
17,66	0,447	0,455	1,774	18,41	0,542	0,551	1,586
17,9	0,444	0,453	1,928	18,67	0,547	0,555	1,453
18,19	0,443	0,451	1,788	18,94	0,552	0,559	1,203
18,46	0,441	0,448	1,650	19,20	0,557	0,562	0,956
18,72	0,439	0,445	1,360	19,46	0,560	0,562	0,478
18,99	0,436	0,442	1,218	19,86	0,564	0,559	0,962
19,25	0,434	0,438	0,921	20,12	0,567	0,552	2,801
19,49	0,431	0,433	0,466	20,39	0,569	0,544	4,571
19,86	0,428	0,422	1,434	20,65	0,568	0,532	6,824
20,12	0,423	0,411	2,943	20,90	0,569	0,518	9,727
20,39	0,417	0,400	4,371	21,13	0,566	0,503	12,423
20,64	0,413	0,386	6,782	21,3	0,562	0,489	14,989
20,8	0,408	0,373	9,177	21,54	0,558	0,476	17,376
21,08	0,402	0,360	11,761	21,7	0,553	0,462	19,640
21,30	0,396	0,346	14,366	21,87	0,548	0,447	22,703
21,52	0,389	0,332	16,988	22,00	0,542	0,432	25,497
21,72	0,382	0,318	20,089	22,12	0,537	0,419	28,064
21,90	0,374	0,303	23,520	22,24	0,531	0,405	31,012
22,07	0,365	0,288	26,834	22,36	0,524	0,392	33,588
22,24	0,357	0,273	30,724	22,50	0,515	0,377	36,524
22,41	0,348	0,259	34,569	22,63	0,506	0,362	39,760
22,58	0,337	0,244	38,346	22,75	0,496	0,346	43,074
22,74	0,325	0,229	41,936	22,87	0,482	0,331	45,681
22,88	0,316	0,216	46,461	22,98	0,470	0,316	48,968
23,01	0,304	0,202	50,609	23,07	0,459	0,300	52,791
23,13	0,292	0,188	55,367	23,17	0,446	0,285	56,584
23,25	0,281	0,174	60,873	23,27	0,433	0,269	60,952
23,37	0,267	0,161	66,062	23,36	0,420	0,253	65,833
23,50	0,255	0,147	73,071	23,46	0,403	0,237	70,043
23,62	0,236	0,134	76,473	23,56	0,387	0,221	75,175
23,74	0,218	0,120	81,851	23,65	0,367	0,205	79,148
23,86	0,202	0,106	90,517	23,75	0,346	0,188	83,446
23,98	0,182	0,092	96,930	23,83	0,328	0,174	88,570
24,10	0,161	0,078	106,147	23,92	0,307	0,158	93,811
24,22	0,140	0,064	119,285	24,01	0,285	0,141	102,205
24,34	0,113	0,049	130,104	24,28	0,208	0,091	128,851
24,47	0,088	0,035	152,946	24,10	0,258	0,126	105,280
24,64	0,052	0,020	156,162	24,18	0,232	0,110	111,088
24,97	0,000	0,000	0,000	24,91	0,001	0,001	0,000

The comparison between theoretical seven parameter double diode model results and experimental PV200 device results is conducted. The theoretical data seven parameter double diode model results for current and power are corresponds to calculated data. The experimental data received from PV200 device of current and power are corresponds to measured data. The difference between measured and calculated data divided with the measured data in other word deviation of data is percentage error[9]. The deviation between current data recevied from seven parameter double diode model and current data recevied from PV200 device for same voltage values and also the deviation between power data recevied from seven parameter double diode model and power data recevied from PV200 device for same voltage values are given in the Table 3.5 below. For both percentage results it is seen that up to maximum power point the percentage is close to zero. Further for both percentage results it is seen that after maximum power point the percentage values increases by the increase of voltage value. This an expected results as it is also seen from the Figure 3.14 above, as the values up to maximum power point almost seen the same, and differs by the decrease of current.

The further statistical analysis between theoretical seven parameter double diode model results and experimental PV200 device results is conducted as well. The MPE is mean percentage error as it can be understood from the definition of abbreviation MPE is the average value of percentage error [9]. The MPE result of current dataset is more close to zero compared to the MPE result of power dataset. Besides, information of the accuracy and performance the seven parameter double diode model given by mean bias error (MBE) which result in values of under and over estimated and the ideal value is where the MBE is equal to zero [9]. For this comparison the result illustrates over estimation but very close to the ideal data as shown in the Table 3.6. The root mean square error (RMSE), gives accuracy data for short term period, is the square root of the MBE so gives always positive values where the ideal value is also equalt to zero. Besides the t statistical analysis method consist RMSE and MBE. The greater the t-stat result, unaccurate the result of the model[9]. The results of all statistical analysis for current data is more close to zero compared to power data which shows the current-voltage calculation via seven parameter double diode model is more accurate.

Table 3.6 : Statistical analysis results.

For Current Data		For Power Data	
MPE	17,465	MPE	26,862
MBE	0,028	MBE	0,043
RMSE	0,238	RMSE	0,293
t-stat	1,218	t-stat	1,551

Besides, the Power – Radiation and Current – Radiation relation for Monocrystalline and Polycrystalline PV Module with regard to the data received from PV200 Solar PV Test Equipment and Solar Survey 200R.

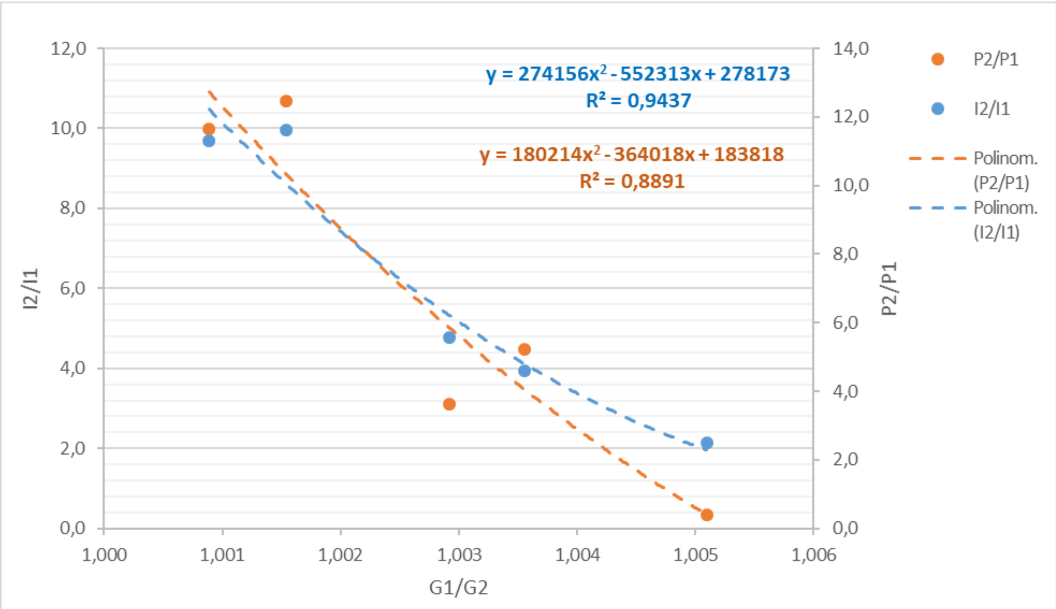

Figure 3.15 : The Power – Radiation and Current – Radiation relation for Monocrystalline PV Module.

The Figure 3.15 illustrates the results for 10W Monocrystalline PV module. The subcripts 1 and 2 represents the sequential datasets. The P_2/P_1 data set represents the power ratio data corresponding to the solar radaition ratio. The relation between P_2/P_1 and G_2/G_1 is result in second order polinomial relation with R_2 data,which is expected to be as close as to 1, is 0,9437 in the result of the power-solar radiation relation. Similarly, the I_2/I_1 sata set represents the current ratio data corresponding to the solar radiation ratio. The relation between I_2/I_1 and G_2/G_1 is result in second order polinomial relation with R_2 data is 0,8891 in the result of the current-solar radiation relation.

The Figure 3.16 illustrates the results for 7W Polycrystalline PV module. The relation between P_2/P_1 and G_2/G_1 is result in exponential relation with R_2 data,which is expected to be as close as to 1, is 0,8869 in the result of the power-solar radiation relation. The relation between I_2/I_1 and G_2/G_1 is result in exponential relation with R_2 data is 0,8789 in the result of the current-solar radiation relation.

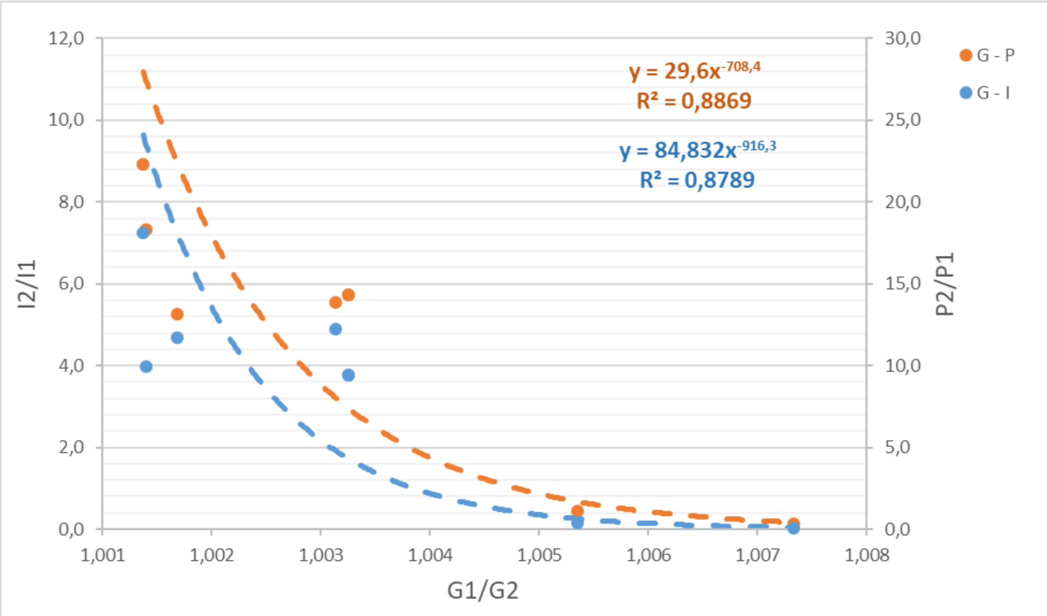

Figure 3.16 : The Power-Radiation and Current-Radiation relation for Polycrystalline PV Module.

Apart from performance, degradation modelling has been studying recently. The efficiencies for both previously mentioned commercial 355 W monocrystalline and 325 W polycrystalline silicon PV module is exposed degradation for 25 years theoritically illustrated in the table below. The efficiencies are considered from the datasheet that the manufacturer provide us for both new productions of monocrystalline and polycrystalline PV module which are 18,20 and 16,68 respectively.

By the end of 25 years which is the period manufacturer guarantees, and with the degradation rates taken from the review results that Jordan and Kurtz has done [78], the degradation is evaluated.

The efficiency for monocrystalline silicon PV module is decreased from 18,20 to 9,20 and the efficiency for polycrystalline silicon PV module is decreased from 16,68 to 0,68 within 25 years. As, degradation rate of polycrystalline silicon PV’s is higher, the efficiency loss over 25 years is more compared to monocrystalline silicon PV.

Table 3.7 : Efficiency change within 25 years due to degradation rate.

Year	$\eta_{monocrystalline}$	$\eta_{polycrystalline}$	Year	$\eta_{monocrystalline}$	$\eta_{polycrystalline}$
New production	18,20	16,68	13	13,52	8,36
1	17,84	16,04	14	13,16	7,72
2	17,48	15,40	15	12,80	7,08
3	17,12	14,76	16	12,44	6,44
4	16,76	14,12	17	12,08	5,80
5	16,40	13,48	18	11,72	5,16
6	16,04	12,84	19	11,36	4,52
7	15,68	12,20	20	11,00	3,88
8	15,32	11,56	21	10,64	3,24
9	14,96	10,92	22	10,28	2,60
10	14,60	10,28	23	9,92	1,96
11	14,24	9,64	24	9,56	1,32
12	13,88	9,00	25	9,20	0,68

Rd_mono=0.36%/year Rd_poly=0.64%/year

Upto this point, degration of commertial PV modules is evaluated. However, there are PV modules within Zuhal Er's Laboratory at ITU Faculty of Arts and Sciences and maximum power determination experiment is done in the TSE Energy Technologies Laboratory Ostim-Ankara. The two PV modules within the Zuhal Er's Laboratuary which are polycrystalline PV and monocrystalline silicon PV's specifications are listed the table below.

Table 3.8 : Monocrystalline Silicon &Polycrystalline PV Module Characteristics.

Constant Values for PV Modules			
Monocrystalline 10W		Polycrystalline 7W	
P_{mp}	10 W	P_{mp}	7 W
V_{mp}	16.8 V	V_{mp}	15.6 V
I_{mp}	0.60 A	I_{mp}	0.46 A
$V_{oc,STC}$	21 V	$V_{oc,STC}$	-
$I_{sc,STC}$	0.66 A	$I_{sc,STC}$	-
Width	-	Width	0.315m
Length	-	Length	0.40m

The results of maximum power determination experiment are illustrated in the fig. 3.17 below. The maximum power output of PV modules under different temperature and radiation shows that the radiation and temperature alteration effects slightly the power output of PV modules as the exposure time is too short though the temperature of the modules does not change sufficiently.

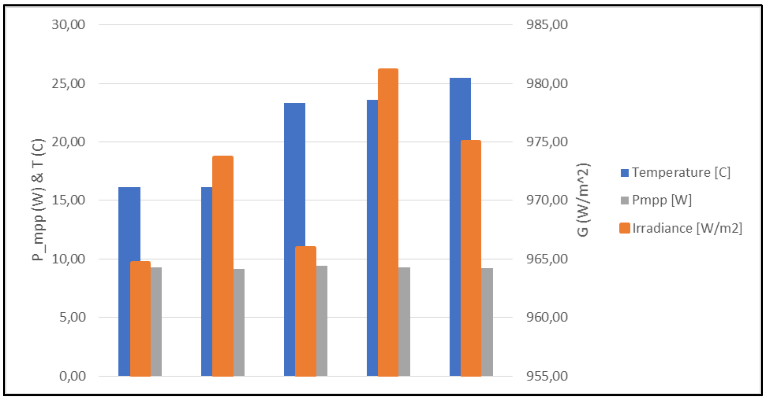

(a)

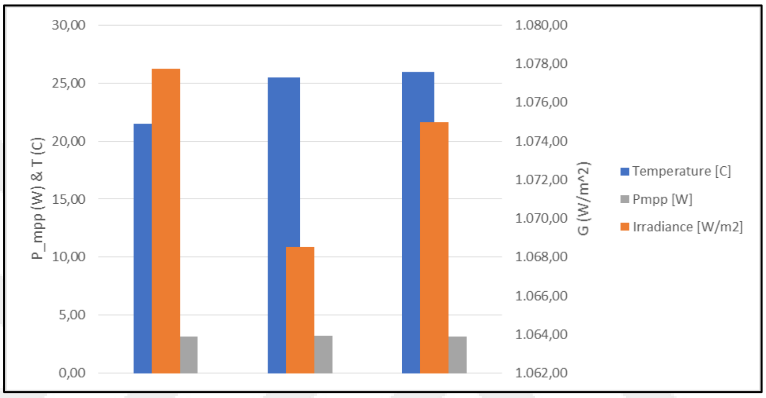

(b)

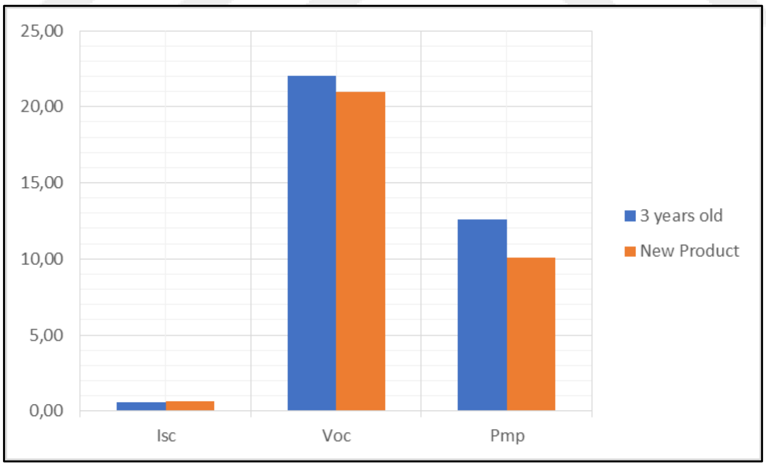

(c)

Figure 3.17 : TSE experimental results of **(a)** 3 years old Monocrystalline Silicon Solar PV module Performance **(b)** 3 years old Polycrystalline Silicon Solar PV module Performance **(c)** 3 years old Monocrystalline Silicon Solar PV module Degradation**.**

On the other hand, the comparison between the datasheet values as they illustrate the new production values and 3 years old values is shown in the fig 3.17.(c) and fig 3.18. 3 years old Monocrystalline Silicon Solar PV module electrical characteristics shows that the short circuit current increased meanwhile the open circuit voltage and output power are decreased. As the short circuit current and open circuit voltage values for Polycrystalline Silicon PV Module has not reachable from the datasheet, the only comparison is done for power output which shows maximum power output is decreased during 3 years.

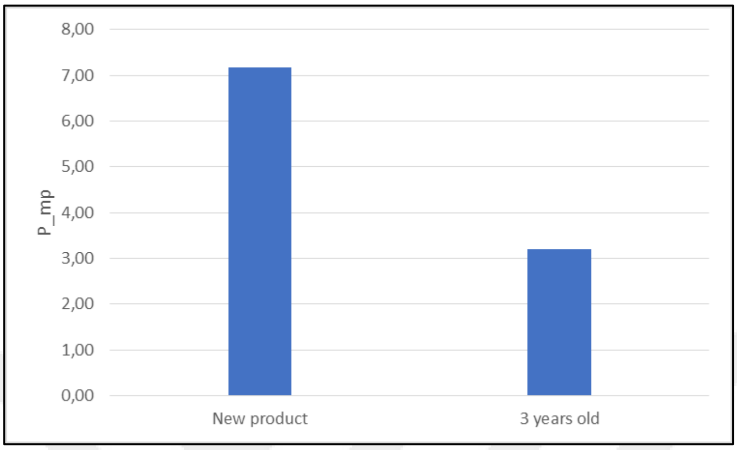

Figure 3.18 : 3 years old Polycrystalline Silicon Solar PV module Degradation.

Besides the results from maximum power determination experiment are evaluated with the correlation of module degradation factor given in the previous section. In order to calculate the module degradation factor, Isc and Voc at STC values has to be known however the values for Polycrystalline Silicon PV Module has not reachable from the datasheet. So, the module degradation factoris only calculated for 3 years old monocrystalline silicon PV module which shows the degradation of the module is 4.31%.

On the other hand, degradation rate of parameters for 3 years and 5 years' period of Monocrystalline and polycrystalline silicon PV module according to the degradation rate of parameters equation and yearly degradation rate of parameters equation explained in the degradation section of the thesis above. Both module have data sets from 2019 when the TSE experiments conducted, 2021 when the outdoor experiments conducted via PV200. Also the manufacturer datasheet values from 2016.

The decrease in the values of parameters cause by degradation electric characteristic of the module during time. The evaluation result in negative values of degradation rate of open circuit voltage of -4,70% between 2016 and 2019, -19,05% between 2016 and 2021 and also yearly degradation rate of open circuit voltage of -1,57% between 2016 and 2019, -3,81% between 2016 and 2021.

Table 3.9 : Monocrystalline Silicon PV Module Degradation.

Monocrystalline PV Module Degradation between 2016 and 2019				
	New product 2016	TSE experiment 01.04.2019	Degradation Rate(%)	Yearly Degradation Rate (%)
G (W/m^2)	1000	975,02		
T (℃)	25	25,50		
I_sc (A)	0,66	0,57	13,21	4,40
V_oc (V)	21,00	21,99	-4,70	-1,57
V_mp (V)	16,80	17,32	-3,10	-1,03
I_mp (A)	0,60	0,53	11,05	3,68
P_mp (W)	10,08	9,24	8,30	2,77
FF	0,7273	0,7340	-0,92	-0,31
Monocrystalline PV Module Degradation between 2016 and 2021				
	New product 2016	Recently Measured via PV200 2021	Degradation Rate(%)	Yearly Degradation Rate(%)
G (W/m^2)	1000	1000		
T (℃)	25	25		
I_sc (A)	0,66	0,49	25,76	5,15
V_oc (V)	21,00	25	-19,05	-3,81
V_mp (V)	16,80	19,6	-16,67	-3,33
I_mp (A)	0,60	0,43	28,33	5,67
P_mp (W)	10,08	8,43	16,39	3,28
FF	0,73	0,69	5,40	1,08
Monocrystalline PV Module Degradation between 2019 and 2021				
	TSE experiment 01.04.2019	Recently Measured via PV200 2021	Degradation Rate	Yearly Degradation Rate
G (W/m^2)	975,02	1000		
T (℃)	25,50	25		
I_sc (A)	0,57	0,49	14,46	7,23
V_oc (V)	21,99	25	-13,71	-6,85
V_mp (V)	17,32	19,6	-13,16	-6,58
I_mp (A)	0,53	0,43	19,43	9,71
P_mp (W)	9,24	8,43	8,83	4,41
FF	0,7340	0,69	6,26	3,13

Also evaluation result in negative values of degradation rate of voltage at maximum power point of -3,10% between 2016 and 2019, -16,67% between 2016 and 2021 and also yearly degradation rate of voltage at maximum power point of -1,03% between 2016 and 2019, -3,33% between 2016 and 2021. This results are because the open circuit votage value increased during time caused by the degradation of hotspot on the PV module. The degradation between 2019 and 2021 show similar results as if degradation caused by hotspot remains in existence.

Table 3.10 : Polycrystalline Silicon PV Module Degradation.

Polycrystalline PV Module between 2016 and 2019				
	New product 2016	TSE experiment 01.04.2019	Degradation Rate(%)	Yearly Degradation Rate(%)
G (W/m^2)	1000	1.068,54		
T (°C)	25	25,50		
I_sc (A)	Not available	0,40	-	-
V_oc (V)	Not available	22,44	-	-
V_mp (V)	15,60	11,85	24,06	8,02
I_mp (A)	0,46	0,27	41,28	13,76
P_mp (W)	7,18	3,20	55,41	18,47
FF	Not available	0,3592	-	-
Polycrystalline PV Module between 2016 and 2021				
	New product 2016	Recently Measured via PV200 2021	Degradation Rate(%)	Yearly Degradation Rate(%)
G (W/m^2)	1000	1000		
T (°C)	25	25		
I_sc (A)	Not available	0,36	-	-
V_oc (V)	Not available	27,2	-	-
V_mp (V)	15,60	14,5	7,05	1,41
I_mp (A)	0,46	0,27	41,30	8,26
P_mp (W)	7,18	3,92	45,44	9,09
FF	Not available	0,40	-	-
Polycrystalline PV Module between 2019 and 2021				
	TSE experiment 01.04.2019	Recently Measured via PV200 2021	Degradation Rate	Yearly Degradation Rate
G (W/m^2)	1068,54	1000,00		
T (°C)	25,50	25,00		
I_sc (A)	0,40	0,36	9,33	4,67
V_oc (V)	22,44	27,20	-21,23	-10,62
V_mp (V)	11,85	14,50	-22,40	-11,20
I_mp (A)	0,27	0,27	0,04	0,02
P_mp (W)	3,20	3,92	-22,35	-11,17
FF	0,36	0,40	-11,31	-5,66

By using the TSE experiment results, the PV modules within Zuhal Er’s laboratory examined via single diode model as given by the graphs below.

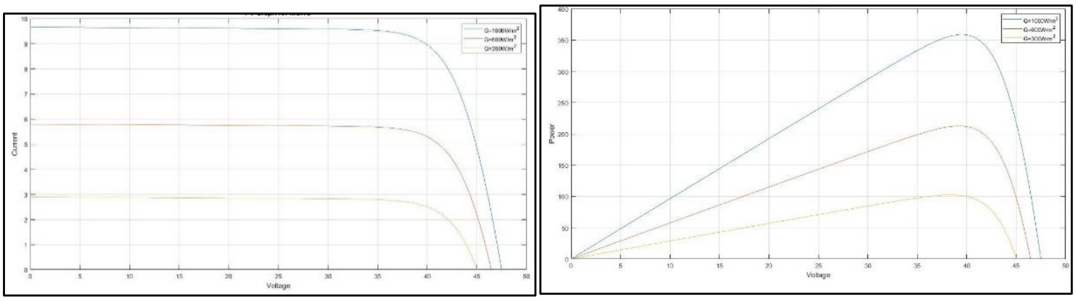

(a)

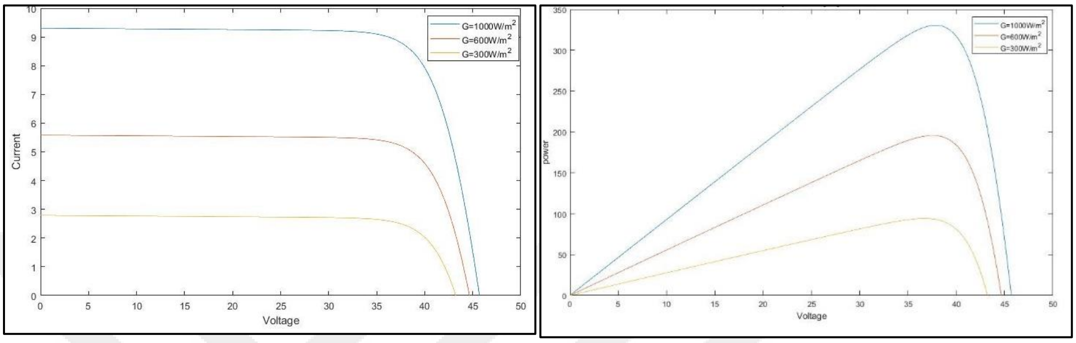

(b)

Figure 3.19 : Solar radiation dependence of **(a)** Monocrystalline PV **(b)** Performance figures of Polycrystalline PV**.**

For both monocrystalline and polycrystalline silicon PV module increase in the solar irradiance make rise in the Voc and Isc both for the ideal single diode model.

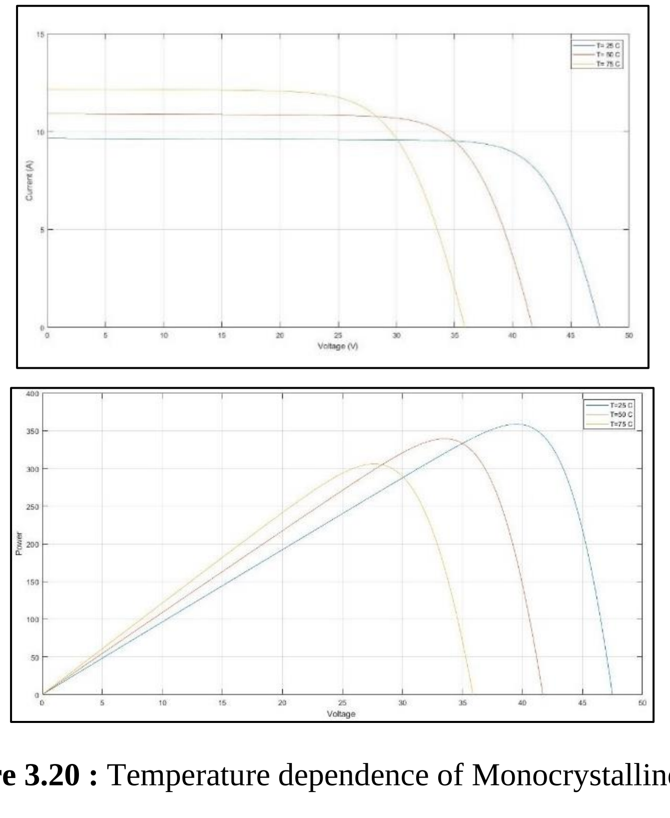

Figure 3.20 : Temperature dependence of Monocrystalline PV.

It is seen that by the increase of the temperature the Voc decreases meanwhile Isc increases. Besides maximum power point for the ideal single diode model is decline with the temperature increase. From those two set of results it is clearly seen that the maximum power point increases with the increase in the solar irradiance and decrease in the temperature.

Apart from PV modules, the performance evaluation is conducted for PV modules via experiments. The experiments conducted in the Bostanci district as stated in the previous section. The data received from the experiments consist of information such as air temperature, cloud opacity, global solar radiation, relative humidity, Arduino sensor values, current and voltage. These data will be evaluated due to the MATLAB code given in the appendix C for performance analysis to receive proper IV graphs due to the solar radiation changes. Besides, these data will be evaluated due to the MATLAB code given in the appendix D for extracting the unknown parameters.

The MATLAB results for A1.1. for the days 09.05.2020 and 10.05.2020 illustrated as I-V curve. The voltage and current results are colored according to the solar radiation value. However, the code should be improved to include other variables. Besides, for M1.2. and BA modules do not contain data for the days concerned. This is because of those days are within the research and development period of this Arduino study.

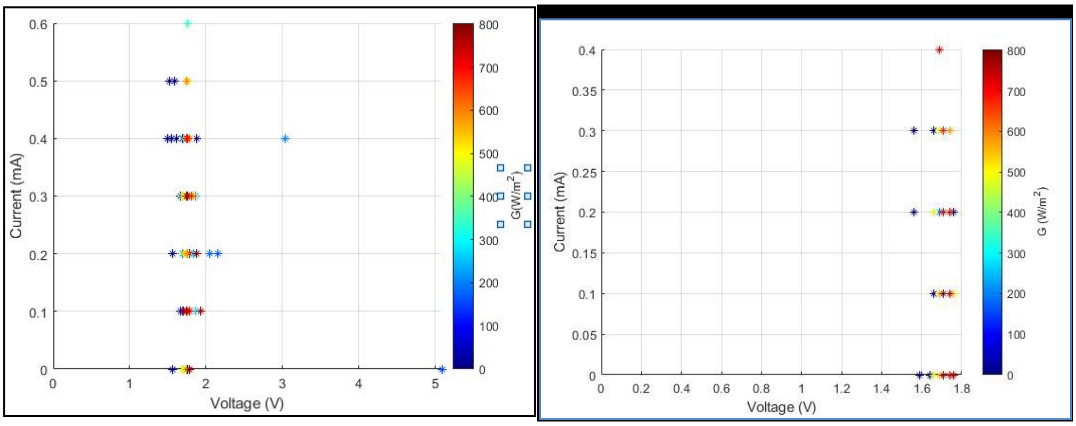

(a) (b)

Figure 3.21 : I-V curve of **(a)** A1.1. and **(b)**M1.1. modules at 09.05.2020 and 10.05.2020.

As it is seen from the graph above, the current values are in mA degree. The resolution bandwidth of the Arduino measurement device gives round values. So, different voltage values correspond to the same current output.

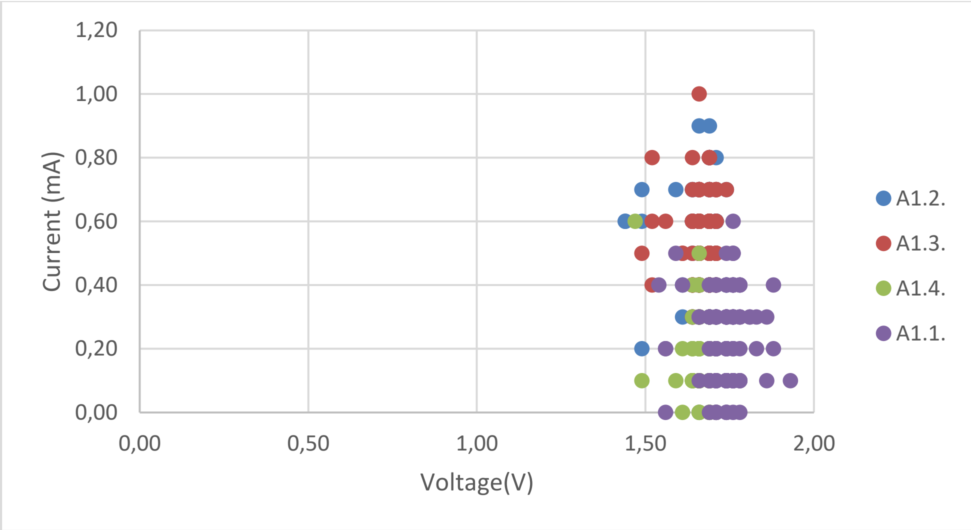

Figure 3.22 : I-V curve of Polycrystalline Modules.

On the other hand, to see the performance of the modules, the I-V graphs are generated within excel. The I-V graph for monocrystalline and polycrystalline silicon solar modules is given in the figure above for the days of 09.05.2020 and 10.05.2020. The modules do not receive the solar radiation from sunrise to sunset, so the current and voltage measurement do not give every voltage or current value.

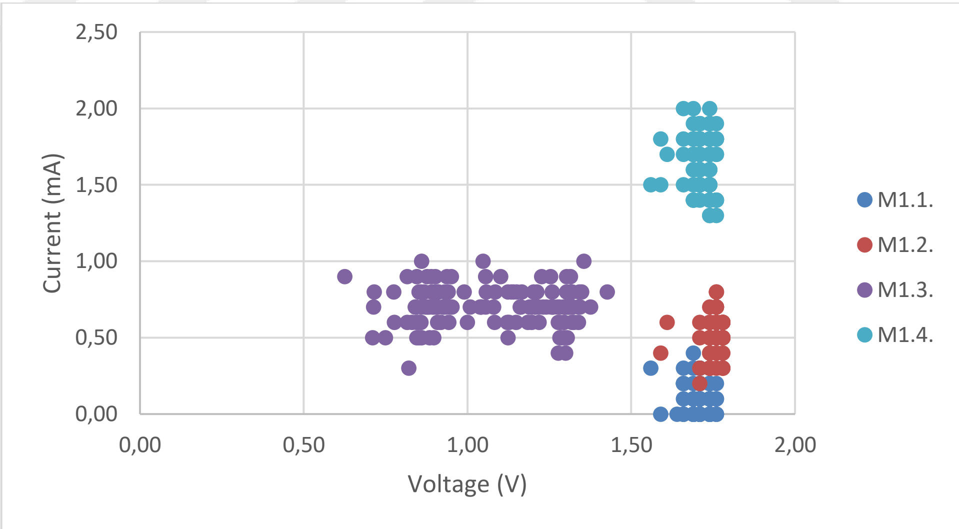

Figure 3.23 : I-V curve of Monocrystalline Modules.

Besides, all modules are bought from the same company and it is assumed that they are identical so the I-V results give almost the same values for the same solar radiation and temperature. However, this is not appropriate for M1.3. module as if that gives different results from others.

3.2 Nuclear Studies

The irradiation experiments are conducted at the research laboratory of Science and Letter Faculty of Suleyman Demirel University, Isparta and outdoor experiments are conducted at Istanbul as stated above.

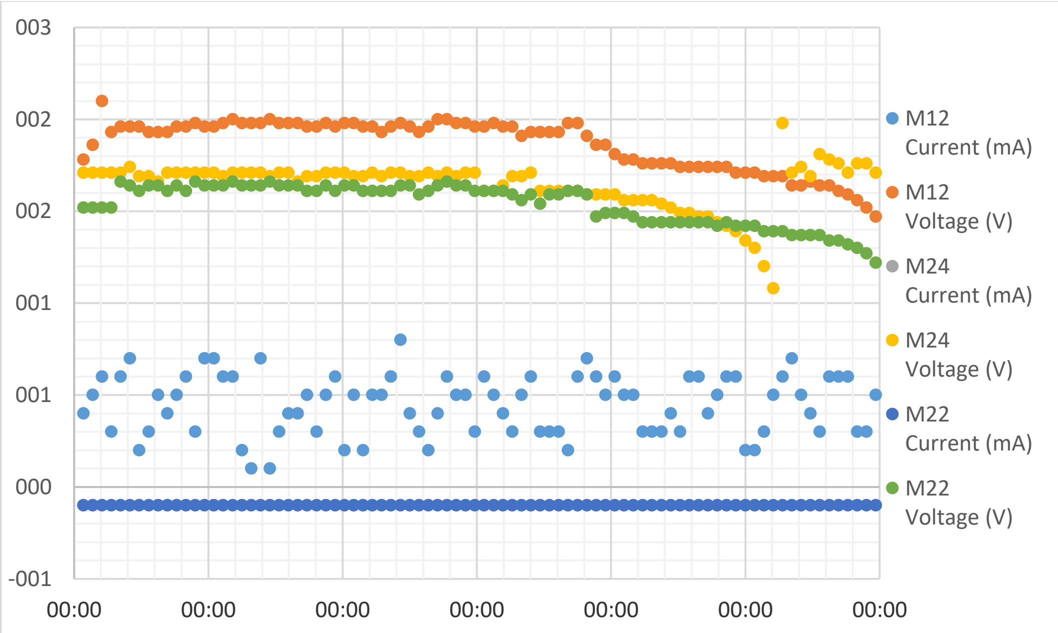

Figure 3.24 : M12 M22 and M24 at 12.10.2020.

The irradiated solar modules are evaluated as well. Likely in the previous section the current voltage data of the modules are collected via Arduino system. The results are given in the figure below. The current voltage data of monocrystalline M.1.2 named solar module have been collecting since May 2020. The M.2.2 is gamma irradiated monocrystalline solar module and M.2.4. is neutron irradiated monocrystalline solar module. The current measurent of M.2.2 and M.2.4 solar modules are the same and the voltage results are quite similar and lower than the M.1.2 solar module. The voltage data received from M.1.2 is near the open circuit voltage data as the measurement is done at October where the solar radiation week and the weather is cloudy. Besides, the current sensor used in this PhD thesis is two dimensional current sensor and for the current measurement of M.2.2 and M.2.4 result in negative values this shows the irradiated modules do not generate current

(a) **(b)** **(c)** **(d)**

Figure 3.25 : Photo of **(a)** M12, **(b)** M22, **(c)** back of M24 and **(d)** front of M24.

As it is seen from the above figure the loss of gloss is occurred on the front surface of M12 This is because the current voltage data of M1.2. have been collecting since May 2020 and so it is degraded because of the natural causes even the surface is cleaned periodically. Besides, in the irradiated modules there is also front and back surface deformation is occurred. More importantly, soldering cable to neutron irradaited modules is very diffucult.

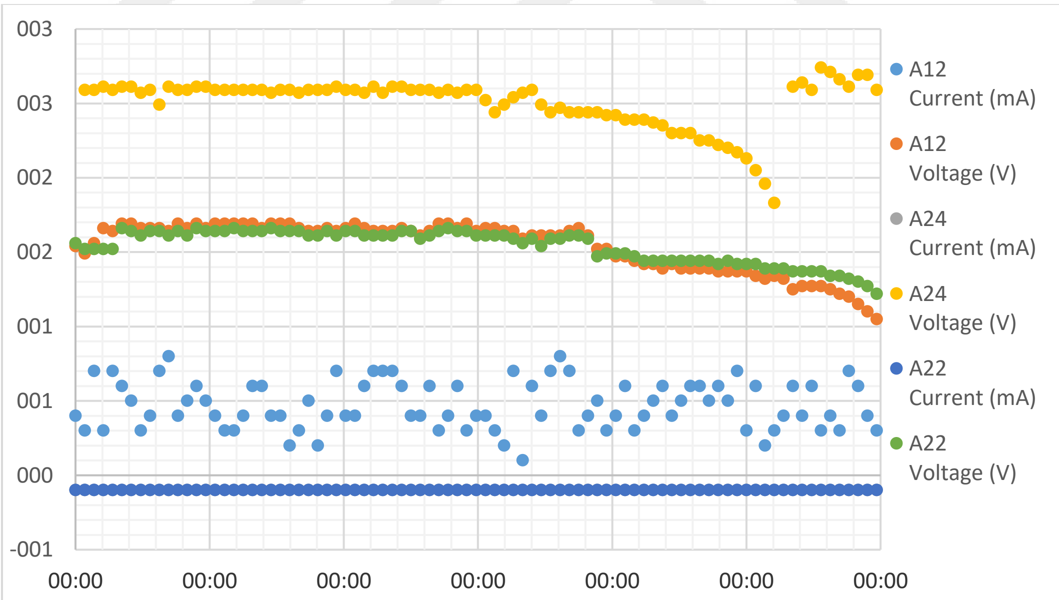

Figure 3.26 : A12 A22 and A24 at 12.10.2020.

Similar with the monocrystallime M.1.2 solar module, the current voltage data of polycrystalline A.1.2 named solar module have been collecting since May 2020. The measurement data illustrated is collected at 12th of October. The A.2.2 is gamma irradiated monocrystalline solar module and A.2.4. is neutron irradiated monocrystalline solar module. The current measurent of A.2.2 and A.2.4 solar modules are the same and the voltage results are quite similar and lower than the A.1.2 solar module.

(a) (b) (c) (d)

Figure 3.27 : Photo of **(a)** A12, **(b)** A22, **(c)** back of A24 and **(d)** front of A24.

Besides, the current sensor used in this PhD thesis is two dimensional current sensor and for the current measurement of A.2.2 and A.2.4 result in negative values this shows the irradiated modules do not generate current. Eventhough the loss of gloss occurred on the front surface of A.1.2 is not obvious and much as M1.2. the front surface is deformed. Besides, in the irradiated modules there is also front and back surface deformation is occurred. More importantly, soldering cable to neutron irradiated modules is very diffucult.

The A2.2, A2.3, M.2.2 and M.2.3 are gamma irradiated polycrystalline and monocrystalline solar modules and A2.4, A2.5, M.2.4 and M.2.5 are neutron irradiated polycrystalline and monocrystalline solar modules are evaluated for longer period of time. The current measurent of solar modules are the same and the voltage results are quite similar and lower than the T.P. and T.M. solar modules. The voltage data received is near the open circuit voltage data as the measurement is done at October where the solar radiation week and the weather is cloudy.

Besides, the current sensor used in this PhD thesis is two dimensional current sensor and for the current measurement of M.2.2 and M.2.4 result in negative values this shows the irradiated modules do not generate current.

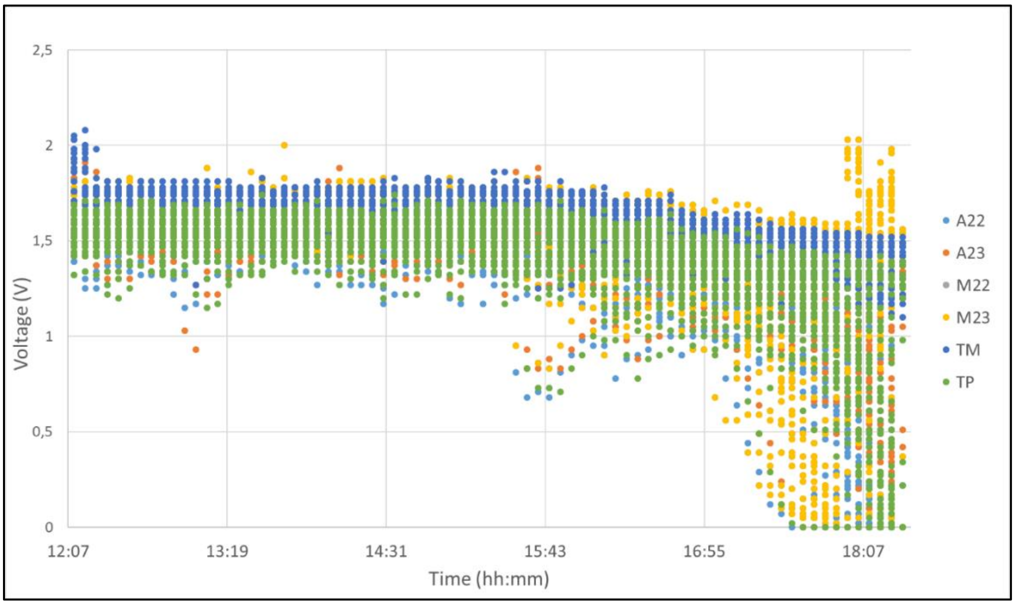

(a)

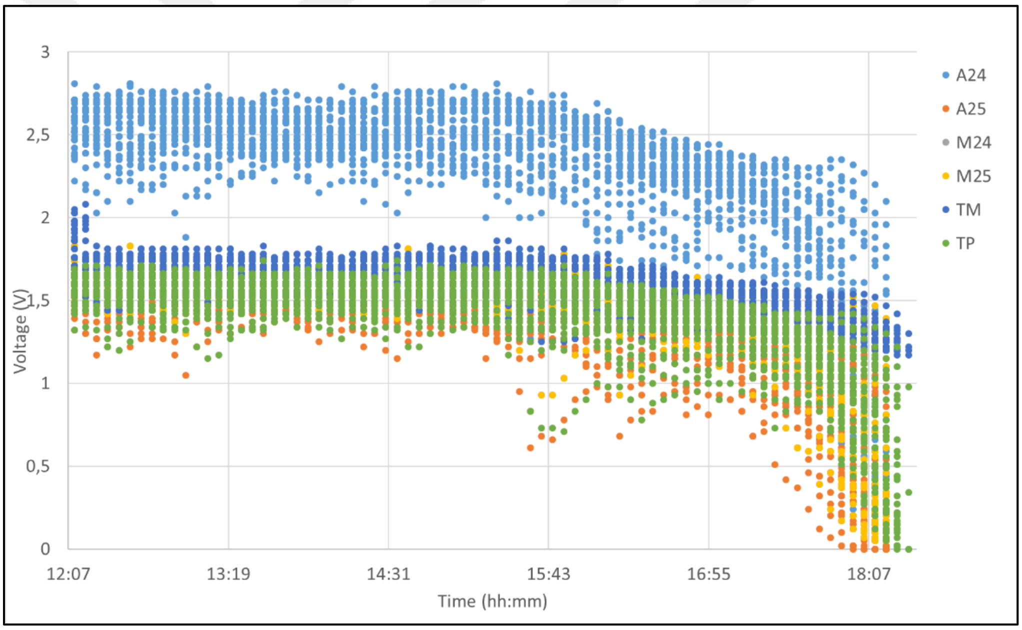

(b)

Figure 3.28 : (a) Gamma and **(b)** Neutron irradiated modules' voltage – time graph.

The A.2.2 is gamma irradiated monocrystalline solar module and A.2.4. is neutron irradiated monocrystalline solar module. The current measurent of A.2.2 and A.2.4 solar modules are the same and the voltage results are quite similar and lower than the T.P. solar module. Similarly, The M.2.2 is gamma irradiated monocrystalline solar module and M.2.4. is neutron irradiated monocrystalline solar module. The current measurent of M.2.2 and M.2.4 solar modules are the same and the voltage results are quite similar and lower than the T.A. solar module.

4. CONCLUSION

During and by the termination of this PhD thesis, the results are shared with the scientific and governmental communities by conferences and articles. So that, the scientific knowledge develops for further studies. The main objectives of this thesis to examine the theory behind the PV technology, performance evaluation of PV modules, degradation due to environmental and nuclear causes and so contribute new knowledge to literature due to experimental and theoretical conclusions of this thesis.

This thesis is explained under eight major sections; theory behind pv cell/module/panel, radioactivity, irradiation and efficiency of solar module, degradation, theoretical performance evaluation of cell/module/panel with subsections of parameter identification for photovoltaic models, simplified explicit method, slope method, combination of simplified explicit method and slope method, seven parameter double diode model, computational studies with regard to theoretical evaluations, experimental performance evaluation of cell/module/panel with subsections of Arduino studies, PV200 and Fluke studies, TSE studies, neutron and gamma studies, result and discussion section with subsections of performance and degradation studies, nuclear studies, and the last section conclusion.

To begin with, the experimental studies during this PhD thesis should be defined as experimental and theoretical study were compared and evaluated together throughout the thesis. The experimental studies within this thesis conducted for two modules that are 10W monocrystalline and 7W polycrystalline photovoltaic modules within the Zuhal ER's Laboratory at ITU Faculty of Arts and Sciences, with Seaward PV200 Solar PV Test Equipment, Seaward Solar Survey 200R and Fluke Ti90_9Hz Thermal Imager. Besides, maximum power determination experiments for two modules that are 10W monocrystalline and 7W polycrystalline photovoltaic modules are done at Turkish Standards Institution (TSE), Ankara at 2019 under the standard IEC 61215: Crystalline silicon terrestrial photovoltaic (PV) Modules-Design qualification and type approval. Apart from 10 W and 7W modules, the experimental study is conducted for also 0,15W modules. The study is conducted by collecting electrical data of 10 monocrystalline and polycrystalline solar module 5,2x2,7cm with 1,5V 100mA via Arduino sets and environmental data by CAMS online database. The experimental and theoretical studies compared for performance evaluation and degradation examination due to environmental and nuclear causes. The nuclear experiments are conducted by the help of Assoc. Prof. Kadir Gunoglu, at the research laboratory of Science and Letter Faculty of Suleyman Demirel University, Isparta, specials thanks to Prof. Dr. Iskender Akkurt.

One of the main objectives of this thesis is to model the PV module. As explained in the theory behind the PV technology part, PV cell's so the modules and panel's equivalent electric circuit design consist of resistances that correspond to losses in PV and one direction diode that correspond to pn junction. In order to model performance and degradation, the data is reached from the literature and the data of the existing PV module within the 3s-1t Solar Search Science and Technology Laboratory at ITU Faculty of Arts and Sciences. In one model there is one diode that are called single diode models which is mostly studied, and in other model there is two diodes that is called double diode model which is rarely studied. Four different models are investigated. The three of those models are single diode model that considers only manufacturer datasheets consist of key electric characteristics such as open circuit voltage, short circuit current, current and voltage at maximum power point, temperature coefficients, efficiencies. First two models do not consider the extraction of unknown parameters that are diode ideality factor, series resistance, shunt resistance, saturation current. However, those two model compared aspect of if the module temperature is directly equal to the ambient temperature and if the module temperature is affected by the ambient temperature. Under stable solar radiation, the increase in the ambient temperature result in the decrease in the open circuit voltage in both model meanwhile the increase in the ambient temperature result in increase and decrease in short circuit voltage for single diode model that not considers temperature effect on module temperature and single diode model that considers temperature effect on module temperature respectively. Besides, the change in the solar radiation and ambient temperature does not affect the open circuit voltage and short circuit current does not change due to in the single diode model that not considers temperature effect on module temperature, while those two electrical parameters have dependence in the solar irradiation and ambient temperature in the single diode model that considers temperature effect on module temperature. The yearly impact of those two model is also evaluated and it is seen that the change in the module temperature has high impact on the module maximum power output in the single diode model that considers temperature effect on module temperature and have significant changes during the year under different seasons meanwhile in the single diode model that not considers temperature effect on module temperature model the module maximum power output has slight differences almost retained the same level. The relation between the PV module performance and the solar irradiation and ambient temperature of those two models is seen under this thesis. Another purpose of the performance evaluation is to compare the efficiencies of monocrystalline and polycrystalline silicon PV modules. The comparison is done under single diode model that considers temperature effect on module temperature model. The yearly trend is similar for both type of PV modules. Even though the size and the parasitic resistances taken same for both modules, the monocrystalline silicon PV module has higher efficiency which is because of multiplication of open circuit voltage and short circuit current is greater than polycrystalline silicon PV module. Besides the results from TSE experiments of the PV modules within Zuhal Er’s laboratory examined via single diode model. For both monocrystalline and polycrystalline silicon PV module increase in the solar irradiance make rise in the Voc and Isc both for the ideal single diode model. It is seen that by the increase of the temperature the Voc decreases meanwhile Isc increases. Besides maximum power point for the ideal single diode model is decline with the temperature increase. From those two set of results it is clearly seen that the maximum power point increases with the increase in the solar irradiance and decrease in the temperature. The other two considers extraction of unknown parameters. The model evaluation is conducted for standard test conditions and outdoor conditions. The performance evaluation is conducted within computational studies via MATLAB and Simulink. The results of these studies and comparisons showed that double diode model has more reliable results compared with the experimental results. Meanwhile, considering solar radiation and temperature effect on PV performance cannot be ignored. Besides, the extraction of unknown parameter is necessary for modelling which are extracted by several methods such as slope method which the current voltage data is necessary as the slope at open circuit voltage point represents shunt resistance and slope at short circuit current point represents series resistance, simplified explicit method which the manufacturer data is necessary or combined method of slope and simplified explicit method. The best results in other words the results have the best agreement with the experimental results received from PV200 device is the seven parameter double diode model consist of both slope and simplified explicit method. The seven unknown parameters are series resistance, shunt resistance, first diode's saturation current and diode ideality factor, second diode's saturation current and diode ideality factor, photogenerated current. The double diode seven parameter model by slope and simplified explicit method with comparing both new theoretical and experimental evaluation results shared the scientific and governmental communities with this PhD thesis.

Besides, the other performance experimental study is conducted by collecting electrical data of 10 monocrystalline and polycrystalline solar module 5,2x2,7cm with 1,5V 100mA via Arduino sets and environmental data by CAMS online database. The modules do not receive the solar radiation from sunrise to sunset, so the current and voltage measurement do not give every voltage or current value. Besides, all modules are bought from the same company and it is assumed that they are identical so the I-V results give almost the same values for the same solar radiation and temperature.

The other objective of this thesis is to examine the PV degradation. Therefore, theory behind the degradation mechanisms such as discoloration, corrosion, hot point, delamination is studied and the causes and effects of degradation evaluated. Besides, the efficiencies for both monocrystalline and polycrystalline silicon PV module is evaluated with the degradation rate theoretically. The initial efficiencies for modules are calculated via single diode model that considers temperature effect on module temperature model and with respect to the manufacturer datasheet values that the company provide. As the degradation rate of polycrystalline silicon PV's is higher, the efficiency loss over 25 years is more compared to monocrystalline silicon PV. The reason is the effect of the number of layers. As increase in the layer number, the factors causing degradation increase in other words the increase in the series resistance. Not only theoretical but also experimentally degradation is evaluated. Besides, degradation is evaluated experimentally as well via Seaward PV200 Solar PV Test Equipment, Seaward Solar Survey 200R and Fluke Ti90_9Hz Thermal Imager. The data received via conducted TSE experiments at 2019 and the PV200 device experiments at 2021. Besides, the initial values of two modules that are 10W monocrystalline and 7W polycrystalline photovoltaic modules within the Zuhal ER's Laboratory at ITU Faculty of Arts and Sciences, are received from manufacturer datasheet at 2016. The degradation rate and yearly degradation rate is deduced for both modules and between years 2016-2019, 2016-2021 and 2019-2021 for key parameters such as short circuit current, open circuit voltage, current and voltage at maximum power point, maximum power, fill factor. It is seen that the decrease in the values of parameters cause by degradation electric characteristic of the module during time. However, the open circuit voltage value increased during time caused by the degradation of hotspot on the PV module. Besides after TSE experiments it is seen that 3 years old monocrystalline silicon solar pv module electrical characteristics shows that the short circuit current increased meanwhile the open circuit voltage and output power are decreased. As the short circuit current and open circuit voltage values for polycrystalline silicon pv module has not reachable from the datasheet, the only comparison is done for power output which shows maximum power output is decreased during 3 years. Besides the results from maximum power determination experiment are evaluated with the correlation of module degradation factor given in the previous section. In order to calculate the module degradation factor, short circuit current and open circuit voltage at standard test condition values has to be known however the values for polycrystalline silicon pv module has not reachable from the datasheet. So, the module degradation factors only calculated for 3 years old monocrystalline silicon PV module which shows the degradation of the module is 4.31 %.

On the other hand, the degradation caused by neutron and gamma irradiated solar modules. The nuclear experiments are conducted by the help of Assoc. Prof. Kadir Gunoglu, at the research laboratory of Science and Letter Faculty of Suleyman Demirel University, Isparta, specials thanks to Prof. Dr. Iskender Akkurt. After neutron gamma irradiation, the solar modules' electrical data is collected again the Arduino sets. The results showed that, the back and front surface of the modules that are gamma and neutron irradiated deformed and the electrical results are different from the modules that are not irradiated. The current measurement of neutron and gamma irradiated solar modules are the same and the voltage results are quite similar and lower than the not irradiated monocrystalline solar module. The voltage data received is near the open circuit voltage data as the measurement is done at October where the solar radiation weak and the weather is cloudy. Besides, the current sensor used in this PhD thesis is two dimensional current sensor and for the current measurement of neutron and gamma irradiated solar modules result in negative values this shows the irradiated modules do not generate current.

To sum, with this PhD thesis theory behind performance and degradation is evaluated under both experimental and theoretical studies. The experimental study conducted with 10W monocrystalline and 7W polycrystalline photovoltaic modules within the Zuhal ER’s Laboratory at ITU Faculty of Arts and Sciences, with Seaward PV200 Solar PV Test Equipment, Seaward Solar Survey 200R and Fluke Ti90_9Hz Thermal Imager. Besides, maximum power determination experiments for two modules that are 10W monocrystalline and 7W polycrystalline photovoltaic modules are done at Turkish Standards Institution (TSE). Also, electric data of 0,15W monocrystalline and polycrystalline solar module 5,2x2,7cm with 1,5V 100mA modules is collected via Arduino sets created within this thesis. The environmental data reviewed by CAMS online database as well. Besides, the effect of solar radiation (in W/m2) is examined as solar radiation is converted the electricity via PV modules. Apart from radiation the irradiation effects also examined. The gamma and neutron irradiation experiments conducted. The new results of experimental and theoretical results contributed to literature.

REFERENCES

[1] **IRENA.** (2021). *Renewable capacity statistics 2021*.

[2] **TEIAS.** (2021). *TEIAS - May 2021 Installed Power Report*.

[3] **TEIAS.** (2020). *TEIAS-May 2020 Installed Power Report*.

[4] **TEIAS.** (2019). *TEIAS-May 2019 Installed Power Report*.

[5] **Hernández-Callejo, L., Gallardo-Saavedra, S., & Alonso-Gómez, V.** (2019). A review of photovoltaic systems: Design, operation and maintenance. *Solar Energy*, *188*(June), 426–440. https://doi.org/10.1016/j.solener.2019.06.017

[6] **Boretti, A., & Castelletto, S.** (2020). Trends in performance factors of large photovoltaic solar plants. *Journal of Energy Storage, 30(*March), 101506. https://doi.org/10.1016/j.est.2020.101506

[7] **Ghosh, Santosh, & Yadav, R.** (2021). Future of photovoltaic technologies: A comprehensive review. *Sustainable Energy Technologies and Assessments*, *47*(April), 101410. https://doi.org/10.1016/j.seta.2021.101410

[8] **Er, Z., & Turna, I. B.** (2016). Future expectation of the photovoltaics role in compensating energy demand. *Acta Physica Polonica A, 129*(4). https://doi.org/10.12693/APhysPolA.129.865

[9] **Turna, I. B.** (2015). *NEW MODEL AND COMPERATIVE STUDY OF CORRELATION FACTORS WITH MONTHLY AVERAGE OF DAILY GLOBAL SOLAR RADIATION*. ISTANBUL TECHNICAL UNIVERSITY

[10] **Er, Z., Rouabah, Z., & Turna, I. B.** (2017). A Modal Study on the Estimation of Daily Global Solar Radiation from Sunshine Duration. *Acta Physica Polonica A*, *132*(3–II), 1070–1075. https://doi.org/10.12693/APhysPolA.132.1070

[11] **Er, Z., Derici, O., Turna, I. B., Karatas, B., Eroglu, M., & Alyanak, E.** (2018). The Cloudless Effect Evaluation for Hourly Irradiance in Turkey. *Acta Physica Polonica A*, *134*(1), 391–393. https://doi.org/10.12693/APhysPolA.134.391

[12] **Er, Zuhal, & Turna, I. B.** (2018). Solar radiation evaluation by t statistical analysis method for south and north region of Turkey. *Arabian Journal of Geosciences*, *11*(11), 249. https://doi.org/10.1007/s12517-018-3603-6

[13] **Ahmad, J. M., & Tiwari, G. N.** (2010). Solar Radiation Models - Review. *Journal of Energy and Environment*, *1*(3), 513–532. Retrieved from http://ijee.ieefoundation.org/vol2/public_html/ijeeindex/vol2/issue4/IJEE_03_v2n4.pdf

[14] **Yao, W., Li, Z., Wang, Y., Jiang, F., & Hu, L.** (2014). Evaluation of global solar radiation models for Shanghai, China. *Energy Conversion and Management*, *84*(AUGUST 2014), 597–612. https://doi.org/10.1016/j.enconman.2014.04.017

[15] **Besharat, F., Dehghan, A. A., & Faghih, A. R.** (2013). Empirical models for estimating global solar radiation: A review and case study. Renewable and Sustainable Energy Reviews, *21*, 798–821. https://doi.org/10.1016/j.rser.2012.12.043

[16] **Jordan, Dirk C., Silverman, T. J., Wohlgemuth, J. H., Kurtz, S. R., & VanSant, K. T.** (2017). Photovoltaic failure and degradation modes. Progress in Photovoltaics: Research and Applications, *25*(4), 318–326. https://doi.org/10.1002/pip.2866

[17] **Kumar, M., & Kumar, A.** (2017). Performance assessment and degradation analysis of solar photovoltaic technologies: A review. Renewable and Sustainable Energy Reviews, *78*(March), 554–587. https://doi.org/10.1016/j.rser.2017.04.083

[18] **Dhoke, A., Sharma, R., & Saha, T. K.** (2018). PV module degradation analysis and impact on settings of overcurrent protection devices. Solar Energy, *160* (December 2017), 360–367. https://doi.org/10.1016/j.solener.2017.12.013

[19] **Er, Zuhal, Rouabah, Z., Kizilkan, G., & Orken, A. T.** (2018). Standards and Testing Experiments for a Photovoltaic Module. *European Journal of Science and Technology*, (January), 12–15.

[20] **Massi Pavan, A., Mellit, A., & Lughi, V.** (2014). Explicit empirical model for general photovoltaic devices: Experimental validation at maximum power point. Solar Energy, *101*, 105–116. https://doi.org/10.1016/j.solener.2013.12.024

[21] **Villalva, M. G., Gazoli, J. R., & Filho, E. R.** (2009). Modeling and circuit-based simulation of photovoltaic arrays. 2009 Brazilian Power Electronics Conference, *24*(5), 1244–1254. https://doi.org/10.1109/COBEP.2009.5347680

[22] **Lakehal, B., & Dendouga, A.** (2018). Parameter Extraction of Schottky Solar Cell in Wide Temperature Range Using Genetic Algorithms. Journal of Nano- and Electronic Physics, *10*(6), 06046-1-06046–4. https://doi.org/10.21272/jnep.10(6).06046

[23] **Chen, Y., Wang, X., Li, D., Hong, R., & Shen, H.** (2011). Parameters extraction from commercial solar cells I–V characteristics and shunt analysis. Applied Energy, *88*(6), 2239–2244. https://doi.org/10.1016/j.apenergy.2010.12.048

[24] **Yordanov, G. H., & Midtgard, O.-M.** (2011). Physically-consistent parameterization in the modeling of solar photovoltaic devices. 2011 IEEE Trondheim PowerTech, 1–4. https://doi.org/10.1109/PTC.2011.6019232

[25] **Zhang, Yunpeng, Gao, S., & Gu, T.** (2017). Prediction of I-V characteristics for a PV panel by combining single diode model and explicit analytical model. Solar Energy, *144*, 349–355. https://doi.org/10.1016/j.solener.2017.01.043

[26] **Pindado, S., & Cubas, J.** (2017). Simple mathematical approach to solar cell/panel behavior based on datasheet information. Renewable Energy, *103*, 729–738. https://doi.org/10.1016/j.renene.2016.11.007

[27] **Karmalkar, S., & Saleem, H.** (2011). The power law J-V model of an illuminated solar cell. *Solar Energy Materials and Solar Cells*, *95*(4), 1076–1084. https://doi.org/10.1016/j.solmat.2010.12.005

[28] **Liu, L., Liu, W., Zhang, X., & Ingenhoff, J.** (2018). An novel explicit model for photovoltaic I-V characteristic prediction. Preprints, (August). https://doi.org/10.20944/preprints201808.0248.v1

[29] **El Tayyan, A. A.** (2015). An approach to extract the parameters of solar cells from their illuminated I - V curves using the Lambert W function. Turkish Journal of Physics, *39*(1), 1–15. https://doi.org/10.3906/fiz-1309-7

[30] **Khezzar R., Zereg M., K. A.** (2018). Comparative Study of Mathematical Methods for Parameters Calculation of Current-Voltage Characteristic of Photovoltaic Module. International Journal of Mechanical Engineering and Technology, *9*(11), 1251–1261.

[31] **Ishaque, K., Salam, Z., & Taheri, H.** (2011). Simple, fast and accurate two-diode model for photovoltaic modules. Solar Energy Materials and Solar Cells, *95*(2), 586–594. https://doi.org/10.1016/j.solmat.2010.09.023

[32] **Karmalkar, S., & Haneefa, S.** (2008). A Physically Based Explicit J– V Model of a Solar Cell for Simple Design Calculations. IEEE Electron Device Letters, *29*(5), 449–451. https://doi.org/10.1109/LED.2008.920466

[33] **Saloux, E., Teyssedou, A., & Sorin, M.** (2011). Explicit model of photovoltaic panels to determine voltages and currents at the maximum power point. Solar Energy, *85*(5), 713–722. https://doi.org/10.1016/j.solener.2010.12.022

[34] **Das, A. K.** (2011). An explicit J–V model of a solar cell for simple fill factor calculation. Solar Energy, *85*(9), 1906–1909. https://doi.org/10.1016/j.solener.2011.04.030

[35] **Boutana, N., Mellit, A., Lughi, V., & Massi Pavan, A.** (2017). Assessment of implicit and explicit models for different photovoltaic modules technologies. Energy, *122*, 128–143. https://doi.org/10.1016/j.energy.2017.01.073

[36] **Ibrahim, H., & Anani, N.** (2017a). Evaluation of Analytical Methods for Parameter Extraction of PV modules. Energy Procedia, *134*, 69–78. https://doi.org/10.1016/j.egypro.2017.09.601

[37] **Toprak, A., Şükür KILIÇ, H., Toprak, A., & Kepceoğlu, A.** (2016). GÜNEŞ PİLİNİN TEK DİYOT Rs MODEL PARAMETRELERİNİN HESAPLANMASI VE I-V İLE P-V KARAKTERİSTİKLERİNİN

İNCELENMESİ EXTRACTION OF SOLAR CELL SINGLE DIODE Rs MODEL PARAMETERS AND STUDY OF I-V AND P-V CHARACTERISTICS. Journal of Social and Technical Researches, *12*, 13–22.

[38] **Ghani, F., Duke, M., & Carson, J.** (2013). Numerical calculation of series and shunt resistance of a photovoltaic cell using the Lambert W-function: Experimental evaluation. *Solar Energy*, *87*(1), 246–253. https://doi.org/10.1016/j.solener.2012.11.002

[39] **Chellaswamy, C., & Ramesh, R.** (2016). Parameter extraction of solar cell models based on adaptive differential evolution algorithm. *Renewable Energy*, *97*, 823–837. https://doi.org/10.1016/j.renene.2016.06.024

[40] **Laudani, A., Lozito, G. M., Mancilla-David, F., Riganti-Fulginei, F., & Salvini, A.** (2015). An improved method for SRC parameter estimation for the CEC PV module model. *Solar Energy*, *120*, 525–535. https://doi.org/10.1016/j.solener.2015.08.003

[41] **Rhouma, M. B. H., Gastli, A., Ben Brahim, L., Touati, F., & Benammar, M.** (2017). A simple method for extracting the parameters of the PV cell single-diode model. *Renewable Energy*, *113*, 885–894. https://doi.org/10.1016/j.renene.2017.06.064

[42] **Gao, X., Cui, Y., Hu, J., Xu, G., & Yu, Y.** (2016). Lambert W-function based exact representation for double diode model of solar cells: Comparison on fitness and parameter extraction. *Energy Conversion and Management*, *127*, 443–460. https://doi.org/10.1016/j.enconman.2016.09.005

[43] **Ma, T., Yang, H., & Lu, L.** (2014). Development of a model to simulate the performance characteristics of crystalline silicon photovoltaic modules/strings/arrays. *Solar Energy*, *100*, 31–41. https://doi.org/10.1016/j.solener.2013.12.003

[44] **Siddiqui, M. U., & Abido, M.** (2013). Parameter estimation for five- and seven-parameter photovoltaic electrical models using evolutionary algorithms. *Applied Soft Computing*, *13*(12), 4608–4621. https://doi.org/10.1016/j.asoc.2013.07.005

[45] **Kichou, S., Silvestre, S., Guglielminotti, L., Mora-López, L., & Muñoz-Cerón, E.** (2016). Comparison of two PV array models for the simulation of PV systems using five different algorithms for the parameters identification. *Renewable Energy*, *99*, 270–279. https://doi.org/10.1016/j.renene.2016.07.002

[46] **Toledo, F. J., & Blanes, J. M.** (2016). Analytical and quasi-explicit four arbitrary point method for extraction of solar cell single-diode model parameters. *Renewable Energy*, *92*, 346–356. https://doi.org/10.1016/j.renene.2016.02.012

[47] **Lin, P., Cheng, S., Yeh, W., Chen, Z., & Wu, L.** (2017). Parameters extraction of solar cell models using a modified simplified swarm optimization algorithm. *Solar Energy*, *144*, 594–603. https://doi.org/10.1016/j.solener.2017.01.064

[48] **Khanna, V., Das, B. K., Vandana, Singh, P. K., Sharma, P., & Jain, S. K.** (2016). Statistical analysis and engineering fit models for two-diode model parameters of large area silicon solar cells. *Solar Energy*, *136*, 401–411. https://doi.org/10.1016/j.solener.2016.07.018

[49] **Chen, Z., Wu, L., Lin, P., Wu, Y., & Cheng, S.** (2016). Parameters identification of photovoltaic models using hybrid adaptive Nelder-Mead simplex algorithm based on eagle strategy. *Applied Energy*, *182*, 47–57. https://doi.org/10.1016/j.apenergy.2016.08.083

[50] **Yu, K., Liang, J. J., Qu, B. Y., Chen, X., & Wang, H.** (2017). Parameters identification of photovoltaic models using an improved JAYA optimization algorithm. *Energy Conversion and Management*, *150*, 742–753. https://doi.org/10.1016/j.enconman.2017.08.063

[51] **Oliva, D., Abd El Aziz, M., & Ella Hassanien, A**. (2017). Parameter estimation of photovoltaic cells using an improved chaotic whale optimization algorithm. *Applied Energy*, *200*, 141–154. https://doi.org/10.1016/j.apenergy.2017.05.029

[52] **Bai, J., Liu, S., Hao, Y., Zhang, Z., Jiang, M., & Zhang, Y.** (2014). Development of a new compound method to extract the five parameters of PV modules. *Energy Conversion and Management*, *79*, 294–303. https://doi.org/10.1016/j.enconman.2013.12.041

[53] **Cubas, J., Pindado, S., & Victoria, M.** (2014). On the analytical approach for modeling photovoltaic systems behavior. *Journal of Power Sources*, *247*, 467–474. https://doi.org/10.1016/j.jpowsour.2013.09.008

[54] **Taşçıoğlu, A., Taşkın, O., & Vardar, A.** (2016). A Power Case Study for Monocrystalline and Polycrystalline Solar Panels in Bursa City, Turkey. *International Journal of Photoenergy*, *2016*, 1–7. https://doi.org/10.1155/2016/7324138

[55] **Diantoro, M., Suprayogi, T., Hidayat, A., Taufiq, A., Fuad, A., & Suryana, R.** (2018). Shockley's Equation Fit Analyses for Solar Cell Parameters from I-V Curves. *International Journal of Photoenergy*, *2018*, 1–7. https://doi.org/10.1155/2018/9214820

[56] **Gao, X., Cui, Y., Hu, J., Xu, G., Wang, Z., Qu, J., & Wang, H.** (2018). Parameter extraction of solar cell models using improved shuffled complex evolution algorithm. *Energy Conversion and Management*, *157*(December 2017), 460–479. https://doi.org/10.1016/j.enconman.2017.12.033

[57] **Meng, Z., Zhao, Y., Tang, S., & Sun, Y.** (2020). An efficient datasheet-based parameters extraction method for two-diode photovoltaic cell and cells model. *Renewable Energy*, *153*, 1174–1182. https://doi.org/10.1016/j.renene.2020.02.084

[58] **Chegaar, M., Ouennoughi, Z., & Hoffmann, A.** (2001). A new method for evaluating illuminated solar cell parameters. *Solid-State Electronics*, *45*(2), 293–296. https://doi.org/10.1016/S0038-1101(00)00277-X

[59] **Jain, A.** (2004). Exact analytical solutions of the parameters of real solar cells using Lambert W-function. *Solar Energy Materials and Solar Cells*, *81*(2), 269–277. https://doi.org/10.1016/j.solmat.2003.11.018

[60] **Jain, A., Sharma, S., & Kapoor, A.** (2006). Solar cell array parameters using Lambert W-function. *Solar Energy Materials and Solar Cells*, *90*(1), 25–31. https://doi.org/10.1016/j.solmat.2005.01.007

[61] **Chegaar, M., Azzouzi, G., & Mialhe, P.** (2006). Simple parameter extraction method for illuminated solar cells. *Solid-State Electronics*, *50*(7–8), 1234–1237. https://doi.org/10.1016/j.sse.2006.05.020

[62] **Celik, A. N., & Acikgoz, N.** (2007). Modelling and experimental verification of the operating current of mono-crystalline photovoltaic modules using four- and five-parameter models. *Applied Energy*, *84*(1), 1–15. https://doi.org/10.1016/j.apenergy.2006.04.007

[63] **Bayhan, H., & Kavasoglu, A. S.** (2007). Exact analytical solution of the diode ideality factor of a pn junction device using Lambert W-function model. *Turkish Journal of Physics*, *31*(1), 7–10. https://doi.org/10.3906/tar-1104-33

[64] **Sera, D., Teodorescu, R., & Rodriguez, P.** (2007). PV panel model based on datasheet values. *2007 IEEE International Symposium on Industrial Electronics*, (July), 2392–2396. https://doi.org/10.1109/ISIE.2007.4374981

[65] **Jung, W., & Guziewicz, M.** (2009). Schottky diode parameters extraction using Lambert W function. *Materials Science and Engineering B: Solid-State Materials for Advanced Technology*, *165*(1–2), 57–59. https://doi.org/10.1016/j.mseb.2009.02.013

[66] **Alfaramawi, K.** (2010). Numerical simulation of the ideality factor of non-ideal n-Si/p-diamond heterojunction diodes. *Digest Journal of Nanomaterials and Biostructures*, *5*(4), 933–937.

[67] **Sandrolini, L., Artioli, M., & Reggiani, U.** (2010). Numerical method for the extraction of photovoltaic module double-diode model parameters through cluster analysis. *Applied Energy*, *87*(2), 442–451. https://doi.org/10.1016/j.apenergy.2009.07.022

[68] **Ishaque, K., & Salam, Z.** (2011). An improved modeling method to determine the model parameters of photovoltaic (PV) modules using differential evolution (DE). *Solar Energy*, *85*(9), 2349–2359. https://doi.org/10.1016/j.solener.2011.06.025

[69] **Lo Brano, V., & Ciulla, G.** (2013). An efficient analytical approach for obtaining a five parameters model of photovoltaic modules using only reference data. *Applied Energy*, *111*, 894–903. https://doi.org/10.1016/j.apenergy.2013.06.046

[70] **Meyer, E. L.** (2017). Extraction of Saturation Current and Ideality Factor from Measuring V oc and I sc of Photovoltaic Modules. *International Journal of Photoenergy*, *2017*, 1–9. https://doi.org/10.1155/2017/8479487

[71] **Fares, M. A., Atik, L., Bachir, G., & Aillerie, M.** (2017). Photovoltaic panels characterization and experimental testing. *Energy Procedia*, *119*, 945–952. https://doi.org/10.1016/j.egypro.2017.07.127

[72] **Ibrahim, H., & Anani, N.** (2017b). Variations of PV module parameters with irradiance and temperature. *Energy Procedia*, *134*, 276–285. https://doi.org/10.1016/j.egypro.2017.09.617

[73] **Liu, L., Liu, W., Zhang, X., & Ingenhoff, J.** (2019). Research on the novel explicit model for photovoltaic I-V characteristic of the single diode model under different splitting spectrum. *Results in Physics*, *12*(December 2018), 662–672. https://doi.org/10.1016/j.rinp.2018.12.021

[74] **Orioli, A., & Di Gangi, A**. (2019). A procedure to evaluate the seven parameters of the two-diode model for photovoltaic modules. *Renewable Energy*, *139*, 582–599. https://doi.org/10.1016/j.renene.2019.02.122

[75] **Wei, D., Wei, M., Cai, H., Zhang, X., & Chen, L.** (2020). Parameters extraction method of PV model based on key points of I-V curve. *Energy Conversion and Management*, *209*(November 2019), 112656. https://doi.org/10.1016/j.enconman.2020.112656

[76] **Mora Segado, P., Carretero, J., & Sidrach-de-Cardona, M.** (2015). Models to predict the operating temperature of different photovoltaic modules in outdoor conditions. *Progress in Photovoltaics: Research and Applications*, *23*(10), 1267–1282. https://doi.org/10.1002/pip.2549

[77] **Rizi, M. T., & Abadi, M. H. S.** (2016). A New Approach for Modeling of Photovoltaic Cell / Module / Array Based-on Matlab. *Physics Journal*, *2*(1), 23–24.

[78] **Jordan, D. C., & Kurtz, S. R.** (2013). Photovoltaic Degradation Rates-an Analytical Review. *Progress in Photovoltaics: Research and Applications*, *21*(1), 12–29. https://doi.org/10.1002/pip.1182

[79] **Dhoke, A., & Mengede, A.** (2017). Degradation analysis of PV modules operating in Australian environment. *2017 Australasian Universities Power Engineering Conference (AUPEC)*, *2017-Novem*, 1–5. https://doi.org/10.1109/AUPEC.2017.8282420

[80] **Barnes, C. E.** (1969). Thermal and Injection Annealing of Neutron-Irradiated p-Type Silicon between 76°K and 300°K. *IEEE Transactions on Nuclear Science*, *16*(6), 28–32. https://doi.org/10.1109/TNS.1969.4325501

[81] **Bilinski, J. R., Brooks, E. H., Cocca, U., & Maier, R. J.** (1963a). Proton-Neutron Damage Correlation in Semiconductors. *IEEE Transactions on Nuclear Science*, *10*(3), 20–26. https://doi.org/10.1109/TNS.1963.4323282

[82] **Korde, R., Ojha, A., Braasch, R., & English, T. C.** (1989). The effect of neutron irradiation on silicon photodiodes. *IEEE Transactions on Nuclear Science*, *36*(6), 2169–2175. Retrieved from https://linkinghub.elsevier.com/retrieve/pii/0022311568901712

[83] **Stofel, E. J., Stewart, T. B., & Ornelas, J. R.** (1969). Neutron damage to silicon solar cells. *IEEE Transactions on Nuclear Science*, *NS-16*(5), 97–105. https://doi.org/10.1109/TNS.1969.4325481

[84] **Ghosh, S., & Sargent, G. A.** (1971). The observation of damage regions produced in silicon solar cells by neutron irradiation. *Materials Research Bulletin*, *6*(6), 441–449. https://doi.org/10.1016/0025-5408(71)90021-3

[85] **Akkurt, I., Akyildirim, H., Özdemir, A. F., & Aldemir, D. A.** (2010). Neutron irradiation effects on I-V characteristics of Au/n-GaAs Schottky diodes. *Radiation Measurements*, *45*(10), 1381–1383. https://doi.org/10.1016/j.radmeas.2010.06.040

[86] **Games Paternò, G. M., Robbiano, V., Santarelli, L., Zampetti, A., Cazzaniga, C., Garcìa Sakai, V., & Cacialli, F.** (2019). Perovskite solar cell resilience to fast neutrons. *Sustainable Energy and Fuels*, *3*(10), 2561–2566. https://doi.org/10.1039/c9se00102f

[87] **Guseynov, N. A., Olikh, Y. M., & Askerov, S. G.** (2007). Ultrasonic treatment restores the photoelectric parameters of silicon solar cells degraded under the action of 60Co gamma radiation. *Technical Physics Letters*, *33*(1), 18–21. https://doi.org/10.1134/S1063785007010063

[88] **Tobnaghi, Davud Mostafa, Rahnamaei, A., & Vajdi, M.** (2014). Experimental study of gamma radiation effects on the electrical characteristics of silicon solar cells. *International Journal of Electrochemical Science*, *9*(6), 2824–2831.

[89] **Tobnaghi, D. M., & Madatov, R.** (2014). Recovery in the electrical parameters of the aging silicon solar cells by annealing. *Journal of Optoelectronics and Advanced Materials*, *16*(5–6), 764–768.

[90] **Tobnaghi, Davud Mostafa, Madatov, R., & Banki, T.** (2014). Effect of gamma radiation on the aged mono-crystalline silicon Solar cells. *Journal of Applied Science and Agriculture*, *9 (3)*(March), 903–907.

[91] **Tobnaghi, Davud Mostafa.** (2017). Experimental study on the variation of degraded silicon solar cells parameters. *Journal of Engineering Science and Technology*, *12*(9), 2528–2535.

[92] **Radosavljević, R. L., & Vasić, A. I.** (2012). Effects of radiation on solar cells as photovoltaic generators. *Nuclear Technology and Radiation Protection*, *27*(1), 28–32. https://doi.org/10.2298/NTRP1201028R

[93] **Nikolić, D., Vasić-Milovanović, A., Obrenović, M., & Dolićanin, E.** (2015). Effects of successive gamma and neutron irradiation on solar cells. *Journal of Optoelectronics and Advanced Materials*, *17*(3–4), 351–356.

[94] **Nikolić, Dejan, & Vasić-Milovanović, A.** (2016). Comparative study of gamma and neutron irradiation effects on the silicon solar cells parameters. *FME Transactions*, *44*(1), 99–104. https://doi.org/10.5937/fmet1601099N

[95] **Nikolić, Dejan.** (2019). Photodiodes, phototransistors and solar cells behaviour in environment with gamma and neutron radiation: literature review

and experiments. *Zbornik Radova Univerziteta Sinergija*, *19*(4), 90–95. https://doi.org/10.7251/zrsng1801090n

[96] **Horiuchi, N., Nozaki, T., & Chiba, A.** (2000). Improvement in electrical performance of radiation-damaged silicon solar cells by annealing. *Nuclear Instruments and Methods in Physics Research, Section A: Accelerators, Spectrometers, Detectors and Associated Equipment*, *443*(1), 186–193. https://doi.org/10.1016/S0168-9002(99)01013-X

[97] **Usami, A.** (1973). Predicted effects of gamma and neutron irradiation on silicon solar cells. *Opto-Electronics*, *5*(3), 223–236. https://doi.org/10.1007/BF01421787

[98] **Junga, F. A., & Enslow, G. M.** (1959). Radiation Effects in Silicon Solar Cells. *IRE Transactions on Nuclear Science*, *6*(2), 49–53. https://doi.org/10.1109/TNS2.1959.4315679

[99] **Simić, B., Nikolić, D., Stanković, K., Timotijević, L., & Stanković, S.** (2013). Damage Induced by Neutron Radiation on Output Characteristics of Solar Cells, Photodiodes, and Phototransistors. *International Journal of Photoenergy*, *2013*, 1–6. https://doi.org/10.1155/2013/582819

[100] **Perný, M., Šály, V., Mikolášek, M., Vary, M., Packa, J., & Huran, J.** (2016). The influence of Xe-Ions irradiation on c-Si/a-SiC photovoltaic device. *Proceedings of International Conference DEMISEE 2016: Diagnostic of Electrical Machines and Insulating Systems in Electrical Engineering*, 11–15. https://doi.org/10.1109/DEMISEE.2016.7530477

[101] **Zhang, Yanqing, Wu, Y., Zhao, H., Sun, C., Xiao, J., Geng, H., … Wang, Y.** (2016). Degradation behavior of electrical properties of inverted metamorphic tri-junction solar cells under 1 MeV electron irradiation. *Solar Energy Materials and Solar Cells*, *157*, 861–866. https://doi.org/10.1016/j.solmat.2016.08.006

[102] **Aierken, A., Fang, L., Heini, M., Zhang, Q. M., Li, Z. H., Zhao, X. F., … Sun, Q.** (2018). Effects of proton irradiation on upright metamorphic GaInP/GaInAs/Ge triple junction solar cells. *Solar Energy Materials and Solar Cells*, *185*(November 2017), 36–44. https://doi.org/10.1016/j.solmat.2018.04.035

[103] **Marius, P., Eugenia, P., Paul, G., & Viorel, B.** (2013). *Weather modelling and forecasting of PV system operation* (2013 ed.). England, United Kingdom: Springer London Ltd.

[104] **Di Piazza, M. C., & Vitale, G.** (2012). Photovoltaic Sources: Modeling and Emulation. In *Green Energy and Technology*. https://doi.org/10.2174/97816080528511120101

[105] **Smets, A.** (2018). *Solar Energy*.

[106] **URL-1** <https://www.circuitlab.com/> date retrieved 16.11.2020

[107] **URL-2** <https://www.pveducation.org/pvcdrom/ solar-cell-operation/ iv-curve> date retrieved 16.11.2020

[108] **URL-3** <https://www.pveducation.org/pvcdrom/solar-cell-operation/fill-factor> date retrieved 16.11.2020

[109] **Luque, A., & Hegedus, S.** (Eds.). (n.d.). *Handbook of photovoltaic science and engineering: Tüm Kaynaklar*. Retrieved from http://eds.a.ebscohost.com/eds/detail/detail?vid=1&sid=b9f31ce3-707d-498a-a50d-e1c6a16a7726%40sdc-v-sessmgr03&bdata=Jmxhbmc9dHImc2l0ZT1lZHMtbGl2ZQ%3D%3D#AN=itu.b1219705&db=cat01696a

[110] **Shockley, W., & Queisser, H. J.** (1961). Detailed balance limit of efficiency of p-n junction solar cells. *Journal of Applied Physics, 32*(3), 510–519. https://doi.org/10.1063/1.1736034

[111] **Kirk, P. A.** (2015). *Solar Photovoltaic Cells Photons to Electricity*. Academic Press, Elsevier.

[112] **Afework, B., Hanania, J., Stenhouse, K., & Donev, J.** (2018). Energy Education - Radioactive vs irradiated. Retrieved June 11, 2021, from https://energyeducation.ca/encyclopedia/Radioactive_vs_irradiated#cite_note-2

[113] **URL-4** < https://webstore.iec.ch/publication/21886> date retrieved 16.11.2020

[114] **Munoz, M. A., Alonso-García, M. C., Vela, N., & Chenlo, F.** (2011). Early degradation of silicon PV modules and guaranty conditions. *Solar Energy*, *85*(9), 2264–2274. https://doi.org/10.1016/j.solener.2011.06.011

[115] **Kaplanis, S., & Kaplani, E.** (2011). Energy performance and degradation over 20 years performance of BP c-Si PV modules. *Simulation Modelling Practice and Theory*, *19*(4), 1201–1211. https://doi.org/10.1016/j.simpat.2010.07.009

[116] **Nehme, B., M'Sirdi, N. K., Akiki, T., & Naamane, A.** (2014). Contribution to the Modeling of Ageing Effects in PV Cells and Modules. *Energy Procedia*, *62*, 565–575. https://doi.org/10.1016/j.egypro.2014.12.418

[117] **Yedidi, K. R.** (2013). *Failure and Degradation Modes of PV modules in a Hot Dry Climate: Results after 16 years of field exposure*. ARIZONA STATE UNIVERSITY.

[118] **Jordan, D., & Kurtz, S.** (2017). Photovoltaic module stability and reliability. In *The Performance of Photovoltaic (PV) Systems* (pp. 71–101). https://doi.org/10.1016/B978-1-78242-336-2.00003-3

[119] **Ndiaye, A., Charki, A., Kobi, A., Kébé, C. M. F., Ndiaye, P. A., & Sambou, V.** (2013). Degradations of silicon photovoltaic modules: A literature review. *Solar Energy*, *96*, 140–151. https://doi.org/10.1016/j.solener.2013.07.005

[120] **Köntges, M., Kurtz, S., Packard, C. E., Jahn, U., Berger, K., Kato, K., … Van Iseghem, M.** (2014). Review of Failures of Photovoltaic Modules - IEA-PVPS T13-01:2014. In *IEA-Photovoltaic Power Systems Programme*.

[121] **Huang, C., & Wang, L.** (2018). Simulation study on the degradation process of photovoltaic modules. *Energy Conversion and Management*, *165*(March), 236–243. https://doi.org/10.1016/j.enconman.2018.03.056

[122] **Saadsaoud, M., Ahmed, A. H., Er, Z., & Rouabah, Z.** (2017). Experimental Study of Degradation Modes and Their Effects on Reliability of Photovoltaic Modules after 12 Years of Field Operation in the Steppe Region. *Acta Physica Polonica A*, *132*(3–II), 930–935. https://doi.org/10.12693/APhysPolA.132.930

[123] **The MathWorks**, I. (2013). *Getting Started Guide R 2013 b*. 95.

[124] **Mathworks**, C. (2019). *Mathematics R 2019 a*.

[125] **DLR, Armines, & Transvalor**. (2018). *User ' s Guide to the CAMS Radiation Service (CRS) Status December 2018*. (December), 1–74.

[126] **Schroedter-Homscheidt, M.** (2016). The Copernicus Atmosphere Monitoring Service (CAMS) Radiation Service in a nutshell. *22nd SolarPACES Conference 2016*, (2015). https://doi.org/10.5194/amt-6-2403-2013.

[127] **URL-5** <http://www.soda-pro.com/web-services/radiation/cams-radiation-service > date retrieved 12.06.2020

[128] **Çobanoğlu, B.** (2017). *Derinlemesine Arduino* (First Ed.). Abaküs.

[129] **Recktenwald, G.** (2012). *Voltage Dividers and Potentiometers*. 1–8. Retrieved from http://web.cecs.pdx.edu/~eas199/A/topics/circuits/pot_voltage_divider.pdf

[130] **El Hammoumi, A., Motahhir, S., Chalh, A., El Ghzizal, A., & Derouich, A.** (2018). Low-cost virtual instrumentation of PV panel characteristics using Excel and Arduino in comparison with traditional instrumentation. *Renewables: Wind, Water, and Solar*, *5*(1), 3. https://doi.org/10.1186/s40807-018-0049-0

[131] **Texas Instruments.** (2015). INA219-Datasheet. *Texas Instruments*, *38*. https://doi.org/10.1180/claymin.2013.048.4.05

[132] **Texas Instruments**. (2011). *INA219: CURRENT / POWER MONITOR with I2C^{TM} Interface*. (7), 1–29.

[133] **URL-6** <https://en.wikipedia.org/wiki/Serial_communication> date retrieved 16.11.2020

[134] **URL-7** <https://www.arduino.cc/en/reference/SPI> date retrieved 16.11.2020

[135] **URL-8** <https://www.projehocam.com/arduino-spi-haberlesme/> date retrieved 16.11.2020

[136] **URL-9** <https://www.sdcard.org/developers/sd-standard-overview/> date retrieved 16.11.2020

[137] **Liu, T.** (2016). Digital Humidity and Temperature sensor. *Adfruit*, 1–5.

[138] **URL-10** <https://www.seaward.com/gb/support/download/300> date retrieved 16.11.2020

[139] **URL-11** < https://www.netes.com.tr/netes/dosyalar/dosya/ E808FA2AF4F661C 05048984E8F1798E8.pdf > date retrieved 16.11.2020

[140] **URL-12 <**https://www.seaward.com/gb/support/download/371> date retrieved 16.11.2020

[141] **URL-13 <**https://www.seaward-groupusa.com/downloads/solar_pv200_210 _manual_v1.5.pdf > date retrieved 16.11. 2020

[142] **URL-14 <** https://www.fluke-direct.com/pdfs/cache/www.fluke-direct.com/ ti90-9hz/datasheet/ti90-9hz-datasheet.pdf> date retrieved 16.11. 2020

[143] **Jahn, U., Herz, M., & Rheinland, T.** (2018). Review on Infrared (IR) and Electroluminescence (EL) imaging for photovoltaic field applications. In *IEA-Photovoltaic Power Systems Programme*.

[144] **FLIR System**. (2011). Thermal Imaging Guidebook for building and renewable energy applications. *Guide Book*, 68.

[145] **URL-15 <** https://www.iec.ch/understanding-standards > date retrieved 16.11. 2020

[146] **URL-16 <** https://www.iso.org/about-us.html> date retrieved 16.11. 2020

[147] **URL-17 <** https://www.tse.org.tr/Hakkimizda> date retrieved 16.11. 2020

[148] **International Electrotechnical Commission,** & IEC. (2005). *IEC 61215: Crytalline silicon terrestrial photovoltaic (PV) modules - Design qualification and type approval*.

[149] **Vega-carrillo, H. R., Manzanares-acuña, E., Hernández-dávila, V. M., Gallego, E., & Lorente, A.** (2006). Neutron Shielding for a 252 Cf Source. *First American IRPA Congress 2006*, 1–9.

[150] **Bilinski, J. R., Brooks, E. H., Cocca, U., & Maier, R. J.** (1963b). Proton-neutron damage equivalence in Si and Ge semiconductors. *IEEE Transactions on Nuclear Science*, *NS-10*(5), 71–86. https://doi.org/10.1109/TNS.1963.4323307

[151] **Vinay, K. M., Santosh, K., Chun, C., Asokan, K., Ashish, K., Shobha, V., … Krishnaveni, S.** (2018). *C tat onsInCrossRef*. *132*(2017), 10854.

[152] **Of, F.,** Irradiation, N., Interaction, O. N. D. A., Silicon, I. N., & Cells, S. (2010). *SOLID MATTER ON DYNAMIC ACOUSTO-DEFECT INTERACTION*. 769–775.

[153] **Othmer, S., & Curtis, O. L.** (1973). SCANNING ELECTRON MICROSCOPE MEASUREMENTS OF DIFFUSION LENGTH IN NEUTRON-IRRADIATED SILICON. *IEEE Transactions on Nuclear Science*, *20*(6), 204–208. https://doi.org/10.1109/TNS.1973.4327394

[154] **URL-18 <** http://www.yegm.gov.tr/MyCalculator> date retrieved 16.11. 2020

[155] **Turkish State Meteorological Service.** (2018). *Turkey Temperature Statistics*.

[156] **Turkish State Meteorological Service**. (2018). *Turkey Daily Sunshine Duration Statistics*.

APPENDICES

APPENDIX A: Literature Review
APPENDIX B: Arduino Code for Electrical and Weather Measurement
APPENDIX C: MATLAB Code for Performance Analysis
APPENDIX D: MATLAB Code for Combined Method

APPENDIX A: Literature Review

Table A.1 : Literature review

Ref	Details
[58]	Experimental Study; received from Photowatt - PWP 201 PV Module form of 36 series connected polycrystalline solar cells and RTC France silicon solar cell. Theoretical Study; I-V of each solar device used and extracted parameters compared with parameters in the literature. Numerical method used.
[59]	Experimenrat study; two solar cell used.Theoretical Study; Lambert W function method used. For Computational study; Maple Software.
[60]	Experimental data received; R_s, R_sh, I_ph, I_o, A are received from other.Theoretical analysis; series connected solar cells and parallel connected solar cells evaluated both seperately and together.Solar cell array 18 parallel strings with 324 cells in series per string. Lambert W function method used. For Computational study; Maple Software.
[61]	Experimental Study; Silicon Solar Cell, Silicon Solar Module, Plastic solar cell are used.Theoretical Study; I-V data is used. Simple parameter extraction method used.
[62]	Experimental Study; I-V data receive from measurement of existing PV system (120 W of mono-crystalline photovoltaic module). Solar radiation and temperature received. Theoretical Study; Manufacturer Datasheet and Calcuted I-V of existing PV module. Analytical method used. T&G dependent
[63]	Experimental Study; I-V data of Cu(In, Ga)Se2 solar cell in dark at 300 K temperature are received from the previous studies in the literature. Theoretical Study; resistance and saturation current data in dark at 300 K temperature are received from the previous studies in the literature. Lambert W function method used. T dependent

Table A.1 (continued) : Literature review

Ref	Details
[64]	Theoretical Study; Manufacturer datasheer used. T&G dependent
[32]	Explicit method used.
[65]	Experimental Study; received from; Current and voltage data of Au-GaAs (Gold-Gallium Arsenide) Schottky diodes Current and voltage data of Ir-4H SiC (Iridium-Silicon Carbide) Schottky diodes. Theoretical Study; I-V of each diode used. Lambert W function method used. Computational Study; Mathematica Software
[21]	Experimental Study; received from Solarex MSX60 solar panel and Kyocera KC200GT solar panel.Theoretical Study;Two Simulations; Based on single diode and two resistances, Based on numerically solving the I–V equation of one current source. Numerical method used. Computational Study; Matlab/Simulink.
[66]	Experimental data received from literatrue.n-Si/p-diamond heterojunction diode. Theoretical study; Simulation of ideality factor with regard to the change in current and temperature. I-V data of diode used. Numerical method used. T dependent.
[67]	Experimental Study; 6 identical monocrystalline PV module. Theoretical Study; I-V of each 6 identical monocrystalline PV module (each has 72 solar cells and 150W peak power) and Meteoreological Data. Numerical method used. Computational Study; LabView software.
[68]	Experimental Study; received from Multi-crystalline, mono-crystalline and thin-film Pv modules. Theoretical Study; computation of model parameters at any G and T using the manufacturer's data sheet used. T&G dependent.
[34]	Explicit method used.
[31]	Iterative method used.

Table A.1 (continued) : Literature review

Ref	Details
[69]	Experimental Study; received from literature.Theoretical Study; Manufacturer datasheet and I-V data of Kyocera KC175GHT-2, Sanyo HIT240HDE-4 and 5 anonymous PV panels of TÜV Rheinland PTL recieved from online free database. Analytic method used. T&G dependent. Computational Study; Free online database PHOTON database, Free online database Solar Advisor Model (SAM) database.
[38]	Lambert W function method used.
[43]	Experimental Study; received from 22 kWp grid-connected PV system. Theoretical Study; I-V of each module and meteoreological data used. T&G dependent. Simplified explicit method. Computational Study; Matlab, INSEL simulation software, PVsyst simulation software.
[53]	Analytic method used.
[40]	Experimental Study; received from PV module Sanyo HITN230SE10. Theoretical Study; Manufacturer Datasheet used. T&G dependent
[39]	Experimental Study; received from Mono-crystalline (SM55), Multi-crystalline (KC 200GT), multicrystalline and monocrystalline solar cells and modules.
[48]	Experimental Study; received from 82 numbers of large area (~154.8 cm2 area) single crystalline silicon solar cells. Theoretical Study; measured radaited I-V characteristic of 82 solar cell samples.
[45]	Experimental Study; received from PV grid-connected systems (PVGCS). The arrays of the PVGCS are of PV module technologies: Crystalline silicon, amorphous silicon and micromorph silicon. Theoretical Study; Manufacturer Datasheet and Experimental I-V Points, Experimental I-V and P-V curves, current Vs time variation used. T&G dependent.
[37]	Simplified explicit method and slope method used.
[26]	Simplified explicit method used.
[42]	Lambert W function method used.
[47]	57-mm diameter commercial (R.T.C. France) silicon solar cell used. Calculated and Experimental data are compared.

Table A.1 (continued): Literature review

Ref	Details
[70]	Experiments conducted with 36-Cell Multicrystalline Si Module and Monocrystalline Si Cell. Theoretical analysis;I_o and A extracted by V_oc and I_sc values at different G. Theoretical analysis;Voc-Isc Method is used for extracting I_o and A, degradation and quality assessment. G dependent. For Computational study;PV simulation program-PVSIM
[35]	Experimental Study; conducted at the test facility at Italy. I-V data and meteorological data received by Module temperature sensor(type DLE 124 produced by LSI Lastem S.r.l), Air temperature sensor and Pyranometer. Data loggers (E-Log,MW8024-02/10 produced by LSI Lastem S.r.l.) are used to collect both electrical and meteorological data. Multicrystalline Silicon Module, Copper Indium Gallium Selenide Module, Cadmium Telluride Module. Theoretical Study; seven implicit and explicit models in the literature compared. Implicit model and explicit method used. T&G dependent.
[50]	Experimental Study; received from 57 mm diameter commercial RTC, France silicon solar cell (under 1000 W/m2 at 33 °C) and a solar modulenamed Photowatt-PWP201(under 1000 W/m2 at 45 °C) that consists of 36 polycrystalline silicon cells in series. Theoretical Study; Experimental & Manufacturer Datasheet used.
[71]	Theoretical Study; conducted for different climatic conditions. Computational Study; Matlab.
[41]	Experimental Study; received from Poly-crystalline silicon PV: PTL Solar. Theoretical Study; with the method works for incomplete curves and not require of Voc,Isc, Impp, Vmpp. T dependent. Method without any approximations or assumptions. Analytic method used.
[72]	Analytic method used.
[25]	Explicit method used.
[30]	Simplified explicit method, and slope method used.
[28]	Explicit method used.

Table A.1 (continued) : Literature review

Ref	Details
[73]	Monocrystalline silicon photovoltaic modules tested experimentally with different splitting films. In theoretical study, current-voltage data and the radiation spectrum is evaluated with three approximation. Explicit method used. G dependent.
[74]	Analytic method used..
[75]	Simplified explicit method, and slope method used.
[57]	T&G dependent.

APPENDIX B: Arduino Code for Electrical and Weather Measurement

```
#include <Wire.h>
#include <Adafruit_INA219.h>
#include "DHT.h"
#include <SPI.h>
#include <SD.h>
#define DHTPIN 2
#define DHTTYPE DHT22
DHT dht(DHTPIN, DHTTYPE);
Adafruit_INA219 ina219;
const int chipSelect = 4;
File myFile;
void setup(void) {
  uint32_t currentFrequency;
  Serial.begin(9600);
  Serial.print(F("DHT22 test!"));
  dht.begin();
    while (!Serial) {
    ;   }
  Serial.print("Initializing SD card...");
  if (!SD.begin(chipSelect)) {
    Serial.println("initialization failed!");
    while (1);
  }
  Serial.println("initialization done.");
  myFile = SD.open("deneme.txt", FILE_WRITE);
  if (myFile) {
    Serial.print("Writing to deneme.txt...");
    myFile.println("testing 1, 2, 3.");
    myFile.close();
    Serial.println("done!");
  }
  else {
    Serial.println("error opening deneme.txt");
  }
  myFile = SD.open("deneme.txt");
  if (myFile) {
    Serial.print("deneme.txt:");
    while (myFile.available()) {
      Serial.write(myFile.read());
    }
    myFile.close();
  }
  else {
    Serial.println("error opening deneme.txt");
  }
  while (!Serial) {
      delay(1);
  }
```

```
  Serial.println("CLEARDATA");
  Serial.println("LABEL,t,Humidity,   Temperature,PV   current(),PV   Voltage   (V), 
Shunt Voltage(mV), Bus Voltage(V),  Load Voltage (V), power (mW)");
  ina219.begin();
}
void loop(void) {
  float shuntvoltage=0;
  float busvoltage=0;
  float PVcurrent=0;
  float loadvoltage=0;
  float power_mW=0;
  float PVvoltage =0;
  float h = dht.readHumidity();
  float t = dht.readTemperature();
  float f = dht.readTemperature(true);
  PVvoltage = analogRead(A0) * 5.0 * 5.0 / 1023.0;
  PVcurrent = ina219.getCurrent_mA();
  shuntvoltage = ina219.getShuntVoltage_mV();
  busvoltage = ina219.getBusVoltage_V();
  power_mW = ina219.getPower_mW();
  loadvoltage = busvoltage + (shuntvoltage / 1000);
   if (isnan(h) || isnan(t) || isnan(f)) {
    Serial.println(F("Failed to read from DHT sensor!"));
    return;
}
  myFile = SD.open("deneme.txt", FILE_WRITE);
  if (myFile) {
    myFile.print(h);
    myFile.print(t);
    myFile.print(PVcurrent);
    myFile.print(PVvoltage);
    myFile.print(shuntvoltage);
    myFile.print(busvoltage);
    myFile.print(loadvoltage);
    myFile.println(power_mW);
    myFile.close();  }
  else {
    Serial.println("error opening deneme.txt");
}
  Serial.print("DATA,TIME,"); // PLX-DAQ command
  Serial.print(h);
  Serial.print(t);
  Serial.print(PVcurrent);
  Serial.print(PVvoltage);
  Serial.print(shuntvoltage);
  Serial.print(busvoltage);
  Serial.print(loadvoltage);
  Serial.print(power_mW);
   delay(300000); }
```

APPENDIX C : MATLAB Code for Performance Analysis

```
GeneralCode.m
%Imports excel to MATLAB using importfile function that is generated
previosuly.
A120200509_10=importfile('20200509_10_A1.xlsx');
%returns the components of A120200509_10.Date as individual
variables
[Y,MO,D,H,MI,S] = datevec(A120200509_10.Date);
%To split the data according to date. The data where the date is not
equal
%to 10 will be used. With idx, date is selected and data is ready to
split.
idx=D~=10;
%Whereever the idx is true, this will return the data.
myA1Voltage=A120200509_10.VoltageV(idx);
myA1Current=A120200509_10.CurrentmA(idx);
myA1Ghi=A120200509_10.Ghi(idx);
myA1AirTemp=A120200509_10.AirTemp(idx);
myA1CloudOpacity=A120200509_10.CloudOpacity(idx);
myA1RelativeHumidity=A120200509_10.RelativeHumidity(idx);
%Creates I-V curve with regard to the change of Global Solar
Radiation
%using createfigure function that is generated previosuly.
%Creating curve for both days 09.5.2020 and 10.5.2020
createfigure(A120200509_10.VoltageV, A120200509_10.CurrentmA,
A120200509_10.Ghi,[],A120200509_10.Ghi)
%Creating curve for only day 09.5.2020
createfigure(myA1Voltage, myA1Current, myA1Ghi,[],myA1Ghi)
%%%%%%%%%%%%%%%%%%%%%%%%%%%%%%%%%%%%%%%%%%%%%%%%%%%%%%%%%%%%%%%%%%%%
%%%%%%%%%%
Functions
Code for Import Data Function
functionGetPVdata = importfile(workbookFile, sheetName, dataLines)
%IMPORTFILE Import data from a spreadsheet
%  GETPVDATA = IMPORTFILE(FILE) reads data from the first worksheet
in
%  the Microsoft Excel spreadsheet file named FILE.  Returns the
data as
%  a table.
%
%  GETPVDATA = IMPORTFILE(FILE, SHEET) reads from the specified
%  worksheet.
%
%  GETPVDATA = IMPORTFILE(FILE, SHEET, DATALINES) reads from the
%  specified worksheet for the specified row interval(s). Specify
%  DATALINES as a positive scalar integer or a N-by-2 array of
positive
%  scalar integers for dis-contiguous row intervals.
%% Input handling
% If no sheet is specified, read first sheet
ifnargin == 1 || isempty(sheetName)
sheetName = 1;
end
% If row start and end points are not specified, define defaults
ifnargin<= 2
dataLines = [2, 1000];
end
%% Setup the Import Options and import the data
opts = spreadsheetImportOptions("NumVariables", 14);
% Specify sheet and range
```

```
opts.Sheet = sheetName;
opts.DataRange = "A" + dataLines(1, 1) + ":N" + dataLines(1, 2);

% Specify column names and types
opts.VariableNames = ["Date", "Var2", "CurrentmA", "VoltageV",
"Var5", "Var6", "Var7", "Var8", "AirTemp", "CloudOpacity", "Ghi",
"RelativeHumidity", "Var13", "WindSpeed10m"];
opts.SelectedVariableNames = ["Date", "CurrentmA", "VoltageV",
"AirTemp", "CloudOpacity", "Ghi", "RelativeHumidity",
"WindSpeed10m"];
opts.VariableTypes = ["datetime", "char", "double", "double",
"char", "char", "char", "char", "double", "double", "double",
"double", "char", "double"];

% Specify file level properties
opts.ImportErrorRule = "omitrow";
opts.MissingRule = "omitrow";

% Specify variable properties
opts = setvaropts(opts, ["Var2", "Var5", "Var6", "Var7", "Var8",
"Var13"], "WhitespaceRule", "preserve");
opts = setvaropts(opts, ["Var2", "Var5", "Var6", "Var7", "Var8",
"Var13"], "EmptyFieldRule", "auto");
opts = setvaropts(opts, "Date", "InputFormat", "");
opts = setvaropts(opts, ["CurrentmA", "VoltageV", "AirTemp",
"CloudOpacity", "Ghi", "RelativeHumidity", "WindSpeed10m"],
"TreatAsMissing", '');
% Import the data
GetPVdata = readtable(workbookFile, opts, "UseExcel", false);

foridx = 2:size(dataLines, 1)
opts.DataRange = "A" + dataLines(idx, 1) + ":N" + dataLines(idx, 2);
tb = readtable(workbookFile, opts, "UseExcel", false);
GetPVdata = [GetPVdata; tb]; %#ok<AGROW>
end
end
%%%%%%%%%%%%%%%%%%%%%%%%%%%%%%%%%%%%%%%%%%%%%%%%%%%%%%%%%%%%%%%%%%%%
%%%%%%%%%%
Code For Create Figure Function
functioncreatefigure(X1, Y1, Z1, S1, Ghi1)
%CREATEFIGURE(X1, Y1, Z1, S1, Ghi1)
%  createfigure function is conducted to make the visualization of
the data
%  automatic according to the customized characteristics.
%  X1:  scatter3 x
%  Y1:  scatter3 y
%  Z1:  scatter3 z
%  S1:  scatter3 s
%  GHI1:  scatter3 c
%  S1 is the size markers inside the figure
%  GHI1: The figure is colored by Ghi values.
%  Auto-generated by MATLAB on 10-Jun-2020 14:49:04
% Create figure
figure1 = figure('Color',...
    [0.941176474094391 0.941176474094391 0.941176474094391]);
colormap(jet);
% Create axes
axes1 = axes('Parent',figure1);
hold(axes1,'on');
% Create scatter3
scatter3(X1,Y1,Z1,S1,Ghi1,'Marker','*')
```

```
% Create zlabel
zlabel('GHI (W/m^2)');
% Create ylabel
ylabel('Current (mA)');
% Create xlabel
xlabel('Voltage (V)');
% Uncomment the following line to preserve the X-limits of the axes
% xlim(axes1,[0 1.8]);
view(axes1,[-37.5 30]);
grid(axes1,'on');
% Create colorbar
colorbar(axes1);
```

APPENDIX D : MATLAB Code for Combined Method

```
% Combined method of Slope and Simplified Explicit Method %
% Step 1,2 & 3:
% Step 1: Getting IV data from Excel and Drawing I-V graph
% Step 2: Determination of Sampling Points(Numeric
Method):(I_sc,0),(I_a,V_a), (I_b,V_b), (I_c,V_c),
% Step 3: Determination of R_sho and R_Cso by SLOPE METHOD (Numeric
Method) [filename, path] = uigetfile('*.*','Select
data.','MultiSelect', 'off');
 data = xlsread(fullfile(path, filename));
 V = data(:,1);
 I = data(:,2);
 plot(V,I)
 hold on
%%Slope At (0,V_oc) for R_so
ft=fittype('a1*x1+b1','coefficients',{'a1','b1'},'indep','x1');
 [f,gof,output] = fit(V(20:22),I(20:22),ft);

 c = coeffvalues(f);
fv = V(14:22);
fy = c(1)*fv+c(2);

%%Slope At (I_sc,0) for R_sho
 ft1=fittype('a2*x2+b2','coefficients', {'a2', 'b2'}, 'indep',
'x2');
 [f1,gof1,output1]=fit(V(1:3),I(1:3),ft1);

 c1=coeffvalues(f1);
 fv1=V(1:20);
 fy1=c1(1)*fv1+c1(2);

%%Slope At (I_c,V_c)=(I(15),V(15)) for R_Co
 ft2=fittype('a3*x3+b3','coefficients', {'a3', 'b3'}, 'indep',
'x3');
 [f2,gof2,output2]=fit(V(15:17),I(15:17),ft2);

 c2=coeffvalues(f2);
 fv2=V(13:17);
 fy2=c2(1)*fv2+c2(2);

 plot(fv,fy)
plot(fv1, fy1)
plot(fv2, fy2)

yazi = ['$$f_Voc= $$' num2str(c(1)) '$$*X+$$' num2str(c(2))];
text(6.5,1.1, yazi ,'Interpreter','latex','fontsize',12);

yazi1=['$$f_Isc= $$' num2str(c1(1)) '$$*X+$$' num2str(c1(2))];
text(2,0.9,yazi1,'Interpreter','latex','fontsize',12);

yazi2=['$$f_Ic= $$' num2str(c2(1)) '$$*X+$$' num2str(c2(2))];
text(4,0.8,yazi2,'Interpreter','latex','fontsize',12);

xlabel('Voltage')
ylabel('Current')

%%%%%%%%%%%%%%%%%%%%%%%%%%%%%%%%%%%%%%%%%%
% Determination of R_sho, R_soslope and R_Cso
```

```
% Slope at (0,Voc);
slope_Voc=c(1);
% Slope at (Isc,0);
slope_Isc=c1(1);
% Slope at (Ic,Vc);
slope_Ic=c2(1);

R_soslope=-1*slope_Voc;
R_sho=-1/slope_Isc;
R_Cso=-1/slope_Ic;

%%%%%%%%%%%%%%%%%%%%%%%%%%%%%%%%%%%%%%%%%%
% Determination of Constant Parameters
q=1.602176487*10^-19;
k=1.3806504*10^-23;
T_celsius=45;
T=T_celsius+273;
N_s=36;
N_p=1;
V_oc=V(22);
I_sc=I(1);
I_a=I(5);
I_b=I(10);
I_c=I(15);
V_a=V(5);
V_b=V(10);
V_c=V(15);
%%%%%%%%%%%%%%%%%%%%%%%%%%%%%%%%%%%%%%%%%%
%Step 4: Ideality Factor (A) Calculation %
ideality_a=-log((I_sc-I_a-(V_a/R_sho))/(I_sc-I_b-
(V_b/R_sho)))/R_sho;
ideality_b=-log((I_sc-I_a-(V_a/R_sho))/(I_sc-I_b-
(V_b/R_sho)))*(I_sc-I_c-(V_c/R_sho))-(I_a-I_b)+((V_a-V_b+(I_a-
I_b)*R_Cso)/R_sho);
ideality_c=(V_a-V_b+(I_a-I_b)*R_Cso)*(I_sc-I_c-(V_c/R_sho));

A=(q/(k*T))*((-ideality_b-sqrt((ideality_b*ideality_b)-
(4*ideality_a*ideality_c)))/(2*ideality_a));

%%%%%%%%%%%%%%%%%%%%%%%%%%%%%%%%%%%%%%%%%%%%%%%
%Step 5: Series Resistance (R_s) Calculation %
R_s=(R_Cso-(((A*k*T)/q)/(I_sc-I_c-
(V_c/R_sho)+(((A*k*T)/q)/R_sho))));

%%%%%%%%%%%%%%%%%%%%%%%%%%%%%%%%%%%%%%%%%%%%%%%
%%Step 6: Saturation Current(I_o) Calculation %
I_o=(I_sc-I_a-(V_a/R_sho))*exp((V_a+(I_a*R_s))/((A*k*T)/q));

%%%%%%%%%%%%%%%%%%%%%%%%%%%%%%%%%%%%%%%%%%%%%%
%Step 7: Shunt Resistance (R_sh) Calculation %
R_sh=(1/((1/(R_sho-R_s))-
((I_o/((A*k*T)/q))*exp((R_s*I_sc)/((A*k*T)/q)))));

%%%%%%%%%%%%%%%%%%%%%%%%%%%%%%%%%%%%%%%%%%%%%%
%Step 8: Photocurrent(I_ph) Calculation %
I_ph=I_o*(exp(V_oc/((A*k*T)/q))-1)+(V_oc/R_s);
```

CURRICULUM VITAE

Name Surname : İnal Begüm TURNA DEMİREL

EDUCATION :

- **B.Sc.** : 2013, Istanbul Technical University, Faculty of Science and Literature, Physics Engineering
- **M.Sc.** : 2015, Istanbul Technical University, Faculty of Science and Literature, Physics Engineering

PROFESSIONAL EXPERIENCE AND REWARDS:

- 2009, İstanbul Technical University, Faculty of Mechanical Engineering, (Internship)
- 2011, TUBITAK UME, Laboratory Assistant (Internship)
- 2012, İstanbul Technical University, Faculty of Science and Literature, Physics Laboratory Assistant
- 2014, Arçelik Intellectual Property Right Department, Project Engineer
- 2016-2018, Sim Çelik Industry and Trade INC, Project Engineer
- Until 2019, Beykoz University, Lecturer
- 2021, Completed Doctorate at Istanbul Technical University

PUBLICATIONS, PRESENTATIONS AND PATENTS ON THE THESIS:

- ER, Z., DERICI O., **TURNA, I.B.**, KARATAS B., EROGLU, M., ALYANAK, E., 2018. Acta Physica Polonica A, Vol.134,(1), The Cloudless Effect Evaluation for Hourly Irradiance in Turkey, DOI: 10.12693/APhysPolA.134.391

- **TURNA, I.B.**, ER, Z., Solar Radiation Evaluation by t-Statistical Analysis Method for South and North Region of Turkey, International Conference on Computational and Experimental Science and Engineering (ICCESEN), Antalya, October 2017

- ER, Z., **TURNA, I.B.**, 2018. Solar Radiation Evaluation by t-Statistical Analysis Method for South and North Region of Turkey. (June 2018) Arabian Journal of Geosciences 11(11):249, DOI:10.1007/s12517-018-3603-6

- ER, Z., ROUABAH, Z., **TURNA, I.B.**, 2017. A Modal Study on the Estimation of Daily Global Solar Radiation from Sunshine Duration. (September 2017) Acta Physica Polonica A, Vol.132,(3-II), DOI:10.12693/APhysPolA.132.1070

- Güneş Radyasyonu Tahmini ve PV Panellerin Bozulma Modlarının Bir Uygulama Çalışması, Proje Yürütücüsü; ER Zuhal, Proje Personeli; **TURNA İnal Begüm**, 2019-halen devam ediyor, İTÜ Bilimsel Araştırma Projesi (ULUSAL)

- YAKISAN H.M., KARATAS B., **TURNA I.B**., YORULMAZ B.Y., ER Z., Evaluation of the IR temperature measuring unit for the PV surface, International Eurasion Conference on Science, Engineering and Technology (EurasianSciEnTech 2018)
- ULUDAĞ E.C., **TURNA I.B.**, ER Z., New PV Panel Construction and Analysis for Little Boat, 2nd International Conference on Energy Research (ENRES 2019)
- **TURNA, I.B**., ER, Z., Monokristal PV Modülünün İşletme Performansının MATLAB / Simulink ile Tahminine İlişkin Simülasyon Çalışması, 2nd International Conference on Sustainable Science and Technology (ICSuSaT-2019) 05-07July 2019, ISTANBUL-TURKEY,
- **TURNA, I.B.**, ER, Z., Energy Balance Between the PV System And Sun Radiation, ULIBTK'19 22th Congress of Thermal Sciences and Technology, 11-14 September 2019, KOCAELI

OTHER PUBLICATIONS, PRESENTATIONS AND PATENTS:

- ER, Z., **TURNA, I.B.**, 2015: Future Expectation of PVs Roel in Compensating Energy Demand. International Advances in Applied Physics and Material Science Congress & Exhibition, April 16-19, 2015 Oludeniz, Turkey.
- ER, Z., Rouabah, Z., and **TURNA, I.B.**, A Modal Study on The Estimation of Daily Global Solar Radiation from Sunshine Duration, International Conference on Computational and Experimental Science and Engineering (ICCESEN), Antalya, October 2016
- ER, Z., **TURNA, I.B.**, Future Expectation of Photovoltaics Role in Compensating Energy Demand. (April 2016) Acta Physica Polonica A, Vol.129,(4), doi:10.12693/AphysPolA.129.865
- **TURNA, I.B.**, Theoretical Investigation of Organic Light Emitting Diodes, 11.National Lighting Congress, İstanbul, 21-22 October 2017
- Solar Simülasyon ve Hesaplama, Proje Yürütücüsü; ER Zuhal, Proje Personeli; **TURNA İnal Begüm**, 2013-2015, İTÜ Bilimsel Araştırma Projesi (ULUSAL)
- **TURNA, I.B.**, ER, Z., RMS and MB Error Methods for Solar Radiation Analysis South Region of Turkey, International Conference on Computational and Experimental Science and Engineering (ICCESEN), Antalya, October 2017